FORMATION OF PALLADIUM NANOFILMS USING ELECTROCHEMICAL ATOMIC LAYER DEPOSITION (E-ALD): GROWTH OPTIMIZATION AND INVESTIGATIONS OF HYDROGEN SORPTION/DESORPTION PROPERTIES

by

LEAH BULLARD SHERIDAN

(Under the Direction of John L. Stickney)

ABSTRACT

This dissertation discusses the layer-by-layer formation of Pd nanofilms on polycrystalline Au and Au(111) electrodes by electrochemical atomic layer deposition (E-ALD) using surface limited redox replacement (SLRR). E-ALD is a deposition technique that relies on surface limited reactions to form smooth, conformal films with controlled thickness. In SLRR, underpotential deposition (UPD) is used to form an atomic layer of one metal to act as a sacrificial layer, which is subsequently exchanged at open circuit for a more noble metal. In these studies, an atomic layer of Cu or Pb was deposited by UPD, followed by galvanic exchange in a Pd ion solution, resulting in a layer of Pd. That cycle was then repeated until achieving the desired film thickness. Films were characterized using coulometry, electron probe microanalysis (EPMA), cyclic voltammetry (CV), X-ray diffraction (XRD) and in-situ scanning tunneling microscopy (STM). The addition of Pd^{2+} complexing agents and their effect on the resulting deposits was studied. EPMA results showed improved film uniformity and suggested an SLRR mechanism dominated by indirect electron transfer from the Cu_{UPD} atom to the Pd ion

through the electrode, rather than a direct electron transfer from atom to ion. The optimized Pd nanofilms on Au(111) were used as a platform for studying the hydrogen sorption (adsorption and absorption) and desorption properties of Pd as a function of film thickness. CV revealed that hydrogen adsorption is strongly influenced by the underlying Au, as well as film thickness for deposits below 5 cycles. No hydrogen absorption occurs for thinner films, while it increases with the number of E-ALD cycles for films formed with 3 cycles or more.

Since Pd is often used as a material in hydrogen storage and sensing devices, the kinetics for hydrogen sorption/desorption from Pd are of critical importance. Varying amounts of Rh have been deposited on Pd nanofilms by direct electrodeposition and E-ALD. CV of these films indicates enhanced kinetics for hydrogen absorption and desorption in the presence of Rh, with the greatest enhancement observed for Rh deposited at 0 V for 60 s.

INDEX WORDS: UPD, ALD, E-ALD, SLRR, Pd, Rh, EPMA, STM, XRD, cyclic voltammetry, electrodeposition, nanofilm, hydrogen absorption, hydrogen adsorption, underpotential deposition, electrochemical atomic layer deposition, surface limited redox replacement

FORMATION OF PALLADIUM NANOFILMS USING ELECTROCHEMICAL ATOMIC LAYER DEPOSITION (E-ALD): GROWTH OPTIMIZATION AND INVESTIGATIONS OF HYDROGEN SORPTION/DESORPTION PROPERTIES

by

LEAH BULLARD SHERIDAN

BS, University of Arkansas, 2005

A Dissertation Submitted to the Graduate Faculty of The University of Georgia in Partial Fulfillment of the Requirements for the Degree

DOCTOR OF PHILOSOPHY

ATHENS, GEORGIA

2013

FORMATION OF PALLADIUM NANOFILMS USING ELECTROCHEMICAL ATOMIC LAYER DEPOSITION (E-ALD): GROWTH OPTIMIZATION AND INVESTIGATIONS OF HYDROGEN SORPTION/DESORPTION PROPERTIES

by

LEAH B. SHERIDAN

Major Professor: John L. Stickney

Committee: I. Jonathon Amster
Jason Locklin

Electronic Version Approved:

Maureen Grasso
Dean of the Graduate School
The University of Georgia
May 2013

DEDICATION

I would like to dedicate this dissertation to my amazing parents, Roy and Karen Bullard, and my wonderful husband, Derek Sheridan. It was their continual encouragement, support, patience and love that made this achievement possible.

ACKNOWLEDGEMENTS

I would like to thank my advisor, Professor John L. Stickney, for his valuable advice, support, and enthusiasm. He was approachable, but he also continually challenged me to ensure I reached my full potential as a scientist. He always had his students' best interest in mind and for that I am grateful. I would like to thank my committee members, Professor Jonathan I. Amster and Jason Locklin, for their support and advice, as well as our collaborator, Dr. David B. Robinson, for his encouragement and willingness to discuss research and offer advice at any time throughout the last 2 years. Finally, I would like to thank all of the current and former Stickney group members, including Dr. Wayne Suggs, for being great co-workers that were always available to listen, make suggestions or even get their hands dirty if necessary.

TABLE OF CONTENTS

Page

CHAPTER 1

INTRODUCTION AND LITERATURE REVIEW

Thin films are an important part of today's technology, found in numerous applications from electronics and energy storage/conversion devices to gas and biomedical sensors. Palladium is well known for its high catalytic activity[1, 2] and its ability to selectively and reversibly absorb up to 900 times its volume in hydrogen[3, 4]. Consequently, Pd thin films have been used in fuel cells[5-8], hydrogen sensors and hydrogen storage devices[9-14].

There are currently numerous applications for both thin films and nanofilms which require controlled film growth. A variety of techniques are available, including different types of physical vapor deposition (PVD), chemical vapor deposition (CVD), molecular beam epitaxy (MBE) and electrodeposition.[15] Atomic layer deposition (ALD) is yet another option for forming such films. ALD involves the formation of conformal nanofilms with atomic level control using layer-by-layer deposition of a material and is achieved under vacuum, typically at temperatures above 100 $^{\circ}$C.[16, 17]

ALD is based on gas phase surface limited reactions (SLRs), for which deposition is limited to the top layer of a deposit and stops once the surface is covered, resulting in formation of an atomic layer. An atomic layer is defined as a monolayer (ML) or less that is no more than one atom thick. A ML, which is a unit of coverage, is defined as one adsorbate per substrate surface atom. Electrochemical atomic layer deposition (E-ALD) is the electrochemical analog of ALD and follows the same principles, but instead of

using gas phase SLRs, solution based electrochemical SLRs provide the basis for formation of conformal nanofilms.[18]

The SLRs used in E-ALD take advantage of underpotential deposition (UPD). UPD is driven by the free energy of formation of a surface compound or alloy and involves the electrodeposition of one element on another, at a potential prior to, or "under," that needed to deposit the element on itself.[19-21] In E-ALD, atomic layer deposition is divided into a sequence of steps, such as introduction of a solution, a change in potential, rinse, etc. The series of steps required to deposit the atomic layer constitute a cycle and deposit thickness is based on the number of cycles performed. The first E-ALD nanofilms formed were II-VI compound semiconductors,[22] after which E-ALD was quickly extended to the formation of III-V[23] and IV-VI[24] semiconductor nanofilms and superlattice nanofilms[25, 26], as well as nanoclusters[18, 27], nanowires and more complex materials such as $CuInSe_2$.[28]

Around a decade ago surface limited redox replacement (SLRR) was developed by Brankovic et al.[29], Mrozek et al.[30], Vasilic and Dimitrov,[31] and Kim et al.[32] SLRR made it possible to expand the applications of E-ALD to include formation of metal nanofilms. An SLRR cycle begins with deposition of a less noble "sacrificial" metal, via UPD, that is then exchanged for a more noble metal at open circuit by redox replacement. Redox replacement, often referred to as galvanic exchange, involves oxidation of the less noble sacrificial metal, which supplies electrons for reducing a more noble metal ion to its metallic state. The amount of noble metal that can be deposited is limited by the amount of sacrificial metal (i.e. an atomic layer). This cycle is then repeated any number of times to grow nanofilms of the desired thickness.[33-35] At

present, SLRR has been used to form nanofilms of Cu,[33, 34, 36, 37] Ag[38], Ru,[35] Pt[29, 30, 39, 40]and Pt/Ru[41], using various experimental configurations ranging from one-cell to an automated flow cell system.

Adzic´ and co-workers[29] were the first to report Pd SLRR. They found that one replacement of Cu_{UPD} resulted in a nearly uniform Pd ML on Au(111). Soon after, Weaver and coworkers[30] reported the formation of Pd SERS-active substrates by exchanging either Pb_{UPD} or Cu_{UPD} for Pd on roughened Au. This method has been used more recently to form bimetallic CuPd particles on graphite[42], a single ML of Pd on IrCo nanoparticles[27] and nanoporous Au film electrodes covered by a ML of Pd.[43]

Due to the unique ability of Pd to absorb large quantities of hydrogen, the reactions between Pd and hydrogen have been studied extensively. Pd forms a surface limited hydride by adsorption, a bulk hydride by absorption and is a catalyst for hydrogen gas evolution. Low concentrations of absorbed hydrogen exist in an FCC α-phase Pd hydride, while higher concentrations exist in an FCC β-phase with an increased lattice constant.[4] The kinetics of hydrogen absorption and desorption are crucial to the development of improved materials for hydrogen sensing and storage.

The mechanism and kinetics of hydrogen absorption is complex and, despite numerous studies, remains a subject of debate.[44-47] However, there are several reports that the high stability of the surface hydride acts as a barrier to hydrogen transport into the bulk under certain conditions.[46-48] Lasia and coworkers have suggested a two-part absorption mechanism that includes fast, direct absorption and slower, indirect absorption that proceeds through the surface hydride.[49, 50] In order to study these reactions electrochemically, very thin Pd films are required. Otherwise, the features for

absorption/desorption will overlap with those for adsorption/desorption, making the two processes indiscernible.[51]

Greeley and Mavrikakis[52] recently reported theoretical modeling of near-surface Pd alloys, or submonolayers of alloy elements at or just below the Pd surface, which predict that some of these materials will have an adsorbed surface hydride with lower energetics, making it energetically equivalent to the bulk state, enabling improved transport of hydrogen between them. This work, in addition to experimental reports of Pd-rich, Pd-Rh bulk alloys with improved absorption/desorption kinetics, suggests that a Rh-modified Pd electrode may experience enhanced kinetics for hydrogen absorption and desorption.[53, 54] Rh-modified E-ALD Pd nanofilms offer a unique platform for the study of hydrogen sorption and desorption properties of palladium as a function of Pd thickness.

This dissertation describes the formation of Pd nanofilms on polycrystalline Au and Au(111) by E-ALD using SLRR, as depicted by the schematic in Figure 1.1. All deposits were formed using an automated electrochemical flow cell deposition system[18, 55, 56] (Electrochemical ALD L.C.) based on a single variable speed pump, 5 valves, 5 solution reservoirs, a potentiostat and an electrochemical flow cell. "Sequencer" E-ALD control software allowed programming of the deposition cycles (Electrochemical ALD L.C.). The flow cell, illustrated in Figure 1.2, included an imbedded Au wire auxiliary electrode in the top face of the flow cell cavity, with the Au working electrode as the bottom face and a Ag/AgCl (3 M KCl) reference electrode (Bioanalytical Systems, Inc.), housed downstream in an external compartment. Incorporation of the Au(111) disc into the flow cell required additional hardware and a

different flow cell design was used for electrochemical scanning tunneling microscopy (EC-STM) of the Au(111) bead (see Chapter 4).

Chapters 2 and 3 discuss the development and optimization of an E-ALD cycle for Pd nanofilm formation. Initially, Pb_{UPD} was used as the sacrificial metal for Pd SLRR, but it proved to be problematic due to its incorporation into the Pd deposit. Cu_{UPD} was examined as an alternative and results indicated essentially pure Pd nanofilms could be formed, making Cu_{UPD} an ideal sacrificial metal for Pd deposition. Preliminary results showed differential deposition of Pd across the Au electrode surface with excess Pd near the flow cell ingress. These results suggested that the SLRR mechanism was not a direct exchange of electrons from a sacrificial metal atom to a depositing metal ion, but rather an indirect mechanism involving transfer of electrons through the electrode. The hypothesis was that a reduction in exchange rate relative to the timescale for introduction of Pd^{2+} solution uniformly across the electrode could prevent differential deposition. This scenario should afford homogeneous Pd^{2+} activity throughout the cell before the exchange has proceeded significantly, thereby promoting uniform deposition. The addition of a Pd^{2+} complexing agent (either EDTA or Cl^-) to decrease the rate of exchange by lowering the availability of free Pd^{2+} ions was studied. Appropriate concentrations of EDTA and chloride, relative to Pd^{2+} concentration, proved effective at improving film homogeneity. However, EDTA produced films that were only a 1/3 as thick as those formed using the Cl^- complex, making Cl^- the more suitable option. These films were characterized using electron probe microanalysis (EPMA) to determine film composition and X-ray diffraction (XRD) to verify crystallinity and structure. The E-ALD process was monitored by time-potential-current plots and coulometry was used to

calculate the exchange efficiency between Cu and Pd. CV provided characterization of Pd film surface chemistry.

The optimized Pd deposition cycle was then utilized in the formation of Pd nanofilms on Au(111) and is the subject of Chapter 4. The resulting deposits were characterized similarly to those formed on polycrystalline Au. In addition, EC-STM of the first 3 E-ALD cycles was used to probe the growth mechanism and showed constant surface morphology from cycle to cycle and the presence of monoatomic steps, which indicated layer-by-layer growth. CVs were used to characterize the formation of Pd surface hydride (adsorption/desorption) and bulk Pd hydride (adsorption/desorption) as a function of deposit thickness. The results revealed the extreme sensitivity of hydrogen adsorption to the underlying Au and Pd film thickness. The charges for adsorption and absorption were measured and compared to other reports in the literature. Lastly, an electrochemical annealing procedure was developed to improve the surface order of the films.

The final topic of this dissertation, presented in Chapter 5, focuses on the electrodeposition of Rh onto Pd nanofilms on Au and the hydrogen sorption/desorption properties of the resulting films. Rh was deposited by direct electrodeposition and E-ALD using SLRR of Cu_{UPD}. CV was used to investigate the effects of the Rh overlayers on the interactions of hydrogen with Pd. The Rh coverage was dependent on the method of deposition and its variables (i.e. potential, time, number of E-ALD cycles). For all Rh coverages studied here, the Rh overlayer was found to enhance the kinetics for hydrogen absorption and desorption into and out of the underlying Pd nanofilm.

References

1. Schwartz, M., *Encyclopedia and Handbook of Materials, Parts and Finishes, Second Edition*. 2002, New York: CRC Press.
2. Adams, B.D. and A.C. Chen, *The role of palladium in a hydrogen economy.* Materials Today, 2011. **14**(6): p. 282-289.
3. Barton, J.C., W.F.N. Leitch, and F.A. Lewis, *Kinetics of Desorption and Oxidation of Hydrogen Contained in Hydrided Palladium Immersed in Aqueous Solutions* Transactions of the Faraday Society, 1963. **59**(485): p. 1208.
4. Dullaghan, J.A.A.a.C.A., *Electrodeposition of Palladium and Palladium Alloys*, in *Modern Electroplating*, M.S.a.M. Paunovic, Editor. 2000, John Wiley & Sons, Inc.: New York. p. 483-554.
5. Lai, B.K., K. Kerman, and S. Ramanathan, *Methane-fueled thin film micro-solid oxide fuel cells with nanoporous palladium anodes.* Journal of Power Sources, 2011. **196**(15): p. 6299-6304.
6. Kang, S., et al., *Low intermediate temperature ceramic fuel cell with Y-doped BaZrO(3) electrolyte and thin film Pd anode on porous substrate.* Electrochemistry Communications, 2011. **13**(4): p. 374-377.
7. Zhang, J.T., et al., *Facile fabrication and unexpected electrocatalytic activity of palladium thin films with hierarchical architectures.* Journal of Physical Chemistry C, 2008. **112**(36): p. 13970-13975.
8. Arroyo-Ramirez, L., et al., *Palladium Nanoshell Catalysts Synthesis on Highly Ordered Pyrolytic Graphite for Oxygen Reduction Reaction.* Acs Applied Materials & Interfaces, 2012. **4**(4): p. 2018-2024.

9. Randler, R.J., et al., *Electrochemical copper deposition on Au(100): a combined in situ STM and in situ surface X-ray diffraction study.* Surface Science, 2000. **447**(1-3): p. 187-200.

10. Noh, J.S., J.M. Lee, and W. Lee, *Low-Dimensional Palladium Nanostructures for Fast and Reliable Hydrogen Gas Detection.* Sensors, 2011. **11**(1): p. 825-851.

11. Niessen, R.A.H., P. Vermeulen, and P.H.L. Notten, *The electrochemistry of Pd-coated MgySc(1-y) thin film electrodes: A thermodynamic and kinetic study.* Electrochimica Acta, 2006. **51**(12): p. 2427-2436.

12. Tan, Z.P., et al., *Thermodynamics, kinetics and microstructural evolution during hydrogenation of iron-doped magnesium thin films.* International Journal of Hydrogen Energy, 2011. **36**(16): p. 9702-9713.

13. Yoon, J.-H., B.-J. Kim, and J.-S. Kim, *Design and fabrication of micro hydrogen gas sensors using palladium thin film.* Materials Chemistry and Physics, 2012. **133**(2-3): p. 987-991.

14. Zeng, X.Q., et al., *Hydrogen responses of ultrathin Pd films and nanowire networks with a Ti buffer layer.* Journal of Materials Science, 2012. **47**(18): p. 6647-6651.

15. Barlow, F., Elshabini-Riad, Aicha, Brown, R., *Film Deposition Techniques and Processes*, in *Thin Film Technology Handbook*, F. Barlow, Elshabini-Riad, Aicha, Editor. 1997, McGraw-Hill: New York.

16. *Electrochemical Society Transactions*. Atomic Layer Deposition Applications 3, ed. A. Londergan, Elam, J.W., van der Straten, O., De Gendt, S. Bent, S.F., Kang, S.B. Vol. 11 no. 7. 2007, Pennington: The Electrochemical Society.

17. George, S.M., *Atomic Layer Deposition: An Overview.* Chemical Reviews, 2010. **110**(1): p. 111-131.

18. Stickney, J.L., *Electrochemical Atomic Layer Epitaxy (EC-ALE): Nanoscale Control in the Electrodeposition of Compound Semiconductors*, in *Advances in Electrochemical Science and Engineering*, R.C.A.a.D.M. Kolb, Editor. 2002, Wiley-VCH: Weinheim.

19. Adzic, R.R., *Electrocatalytic Properties of the Surfaces Modified by Foreign Metal Adatoms* Advances in Electrochemistry and Electrochemical Engineering, ed. H.G.a.C.W. Tobias. Vol. 13. 1984, New York: Wiley-Interscience. 159-260.

20. Herrero, E., L.J. Buller, and H.D. Abruna, *Underpotential deposition at single crystal surfaces of Au, Pt, Ag and other materials.* Chemical Reviews, 2001. **101**(7): p. 1897-1930.

21. Kolb, D.M., *Advances in Electrochemistry and Electrochemical Engineering*, ed. H.G.a.C.W. Tobias. Vol. 11. 1978, New York: John Wiley. 125.

22. Gregory, B.W. and J.L. Stickney, *Electrochemical Atomic Layer Epitaxy (Ecale).* Journal of Electroanalytical Chemistry, 1991. **300**(1-2): p. 543-561.

23. Wade, T.L., et al., *Electrodeposition of InAs.* Electrochemical and Solid State Letters, 1999. **2**(12): p. 616-618.

24. Banga, D.O., et al., *Formation of PbTe nanofilms by electrochemical atomic layer deposition (ALD).* Electrochimica Acta, 2008. **53**(23): p. 6988-6994.

25. Wade, T.L., et al., *Electrochemical formation of a III-V compound semiconductor superlattice: InAs/InSb.* Journal of Electroanalytical Chemistry, 2001. **500**(1-2): p. 322-332.

26. Vaidyanathan, R., et al., *Preliminary studies in the electrodeposition of PbSe/PbTe superlattice thin films via electrochemical atomic layer deposition (ALD).* Langmuir, 2006. **22**(25): p. 10590-10595.

27. Cavallini, M., et al., *Two-dimensional self-organization of CdS ultra thin films by confined electrochemical atomic layer epitaxy growth.* Journal of Physical Chemistry C, 2007. **111**(3): p. 1061-1064.

28. Banga, D., et al., *Electrodeposition of CuInSe2 (CIS) via Electrochemical Atomic Layer Deposition (E-ALD).* Langmuir, 2012. **28**(5): p. 3024-3031.

29. Brankovic, S.R., J.X. Wang, and R.R. Adzic, *Metal monolayer deposition by replacement of metal adlayers on electrode surfaces.* Surface Science, 2001. **474**(1-3): p. L173-L179.

30. Mrozek, M.F., Y. Xie, and M.J. Weaver, *Surface-enhanced Raman scattering on uniform platinum-group overlayers: Preparation by redox replacement of underpotential-deposited metals on gold.* Analytical Chemistry, 2001. **73**(24): p. 5953-5960.

31. Vasilic, R. and N. Dimitrov, *Epitaxial growth by monolayer-restricted galvanic displacement.* Electrochemical and Solid State Letters, 2005. **8**(11): p. C173-C176.

32. Kim, Y.G., et al., *Platinum nanofilm formation by EC-ALE via redox replacement of UPD copper: Studies using in-situ scanning tunneling microscopy.* Journal of Physical Chemistry B, 2006. **110**(36): p. 17998-18006.

33. Thambidurai, C., et al., *E-ALD of Cu Nanofilms on Ru/Ta Wafers Using Surface Limited Redox Replacement.* Journal of the Electrochemical Society, 2010. **157**(8): p. D466-D471.

34. Thambidurai, C., et al., *Copper Nanofilm Formation by Electrochemical ALD.* Journal of the Electrochemical Society, 2009. **156**(8): p. D261-D268.

35. Thambidurai, C., Y.G. Kim, and J.L. Stickney, *Electrodeposition of Ru by atomic layer deposition (ALD).* Electrochimica Acta, 2008. **53**(21): p. 6157-6164.

36. Gebregziabiher, D.K., et al., *Electrochemical atomic layer deposition of copper nanofilms on ruthenium.* Journal of Crystal Growth, 2010. **312**(8): p. 1271-1276.

37. Viyannalage, L.T., R. Vasilic, and N. Dimitrov, *Epitaxial growth of Cu on Au(111) and Ag(111) by surface limited redox replacement - An electrochemical and STM study.* Journal of Physical Chemistry C, 2007. **111**(10): p. 4036-4041.

38. Vasilic, R., L.T. Viyannalage, and N. Dimitrov, *Epitaxial growth of Ag on Au(111) by galvanic displacement of Pb and Tl monolayers.* Journal of the Electrochemical Society, 2006. **153**(9): p. C648-C655.

39. Jayaraju, N., et al., *Electrochemical Atomic Layer Deposition (E-ALD) of Pt Nanofilms Using SLRR Cycles.* Journal of the Electrochemical Society, 2012. **159**(10): p. D616-D622.

40. Fayette, M., et al., *From Au to Pt via Surface Limited Redox Replacement of Pb UPD in One-Cell Configuration.* Langmuir, 2011. **27**(9): p. 5650-5658.

41. Jayaraju, N., *Electrochemical atomic layer deposition (E-ALD) of Pt and PtRu nanofilms*, in *Chemistry*. 2010, University of Georgia: Athens.

42. Ghodbane, O., L. Roue, and D. Belanger, *Study of the electroless deposition of Pd on Cu-modified graphite electrodes by metal exchange reaction.* Chemistry of Materials, 2008. **20**(10): p. 3495-3504.

43. Kiani, A. and E.N. Fard, *Fabrication of palladium coated nanoporous gold film electrode via underpotential deposition and spontaneous metal replacement: A low palladium loading electrode with electrocatalytic activity.* Electrochimica Acta, 2009. **54**(28): p. 7254-7259.

44. Zhao, Z., et al., *All-optical hydrogen-sensing materials based on tailored palladium alloy thin films.* Analytical Chemistry, 2004. **76**(21): p. 6321-6326.

45. Kulprathipanja, A., et al., *Pd and Pd-Cu membranes: inhibition of H-2 permeation by H2S.* Journal of Membrane Science, 2005. **254**(1-2): p. 49-62.

46. Delmelle, R. and J. Proost, *An in situ study of the hydriding kinetics of Pd thin films.* Physical Chemistry Chemical Physics, 2011. **13**(23): p. 11412-11421.

47. Matsumura, D., et al., *Fast and real-time observation of hydrogen absorption kinetics for palladium nanoparticles.* Journal of Alloys and Compounds, 2011. **509**: p. S849-S852.

48. Ward, T.L. and T. Dao, *Model of hydrogen permeation behavior in palladium membranes.* Journal of Membrane Science, 1999. **153**(2): p. 211-231.

49. Duncan, H. and A. Lasia, *Mechanism of hydrogen adsorption/ab sorption at thin Pd layers on Au(111).* Electrochimica Acta, 2007. **52**(21): p. 6195-6205.

50. Lasia, A., *On the mechanism of the hydrogen absorption reaction.* Journal of Electroanalytical Chemistry, 2006. **593**(1-2): p. 159-166.

51. Czerwinski, A., et al., *The study of hydrogen sorption in palladium limited volume electrodes (Pd-LVE) I. Acidic solutions.* Journal of Electroanalytical Chemistry, 1999. **471**(2): p. 190-195.

52. Greeley, J. and M. Mavrikakis, *Surface and subsurface hydrogen: Adsorption properties on transition metals and near-surface alloys.* Journal of Physical Chemistry B, 2005. **109**(8): p. 3460-3471.

53. Lukaszewski, M., K. Hubkowska, and A. Czerwinski, *Electrochemical absorption and oxidation of hydrogen on palladium alloys with platinum, gold and rhodium.* Physical Chemistry Chemical Physics, 2010. **12**(43): p. 14567-14572.

54. Zurowski, A., M. Lukaszewski, and A. Czerwinski, *Electrosorption of hydrogen into palladium-rhodium alloys.* Electrochimica Acta, 2006. **51**(15): p. 3112-3117.

55. Wade, T.L., T.A. Sorenson, and J.L. Stickney, *Interfacial Electrochemistry*, ed. A. Wieckowski. 1999, New York: Marcel Dekker.

56. Stickney, J.L., *Electrochemical atomic layer epitaxy*, in *Electroanalytical Chemistry, Vol 21*, A.J.B.a.I. Rubinstein, Editor. 1999, Marcel Dekker, Inc.: New York. p. 75-209.

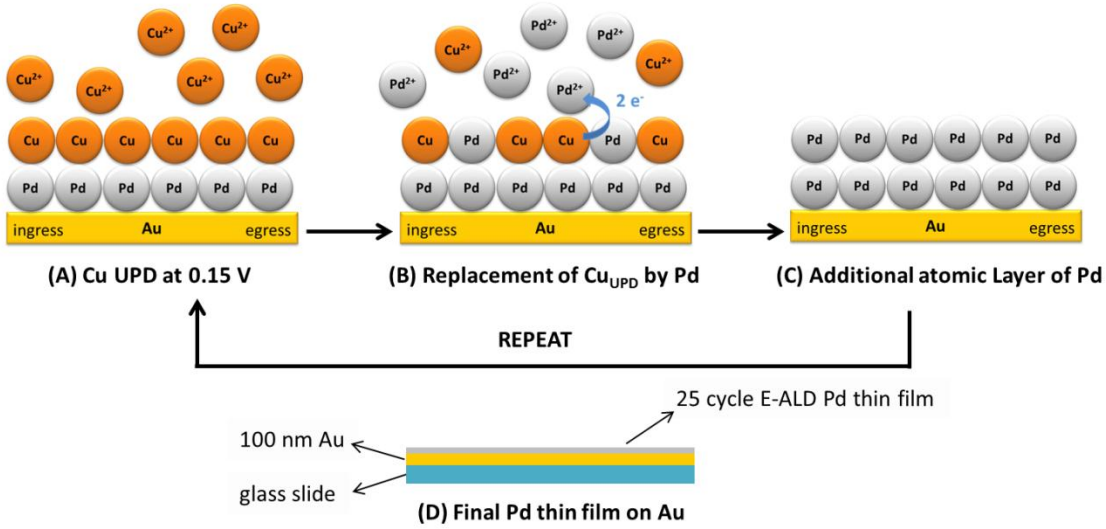

Figure 1.1 Cartoon of the formation of E-ALD Pd nanofilms using SLRR. Note that the 1st layer of Cu_{UPD} is deposited on Au and replaced by Pd ions to form the 1st Pd atomic layer.

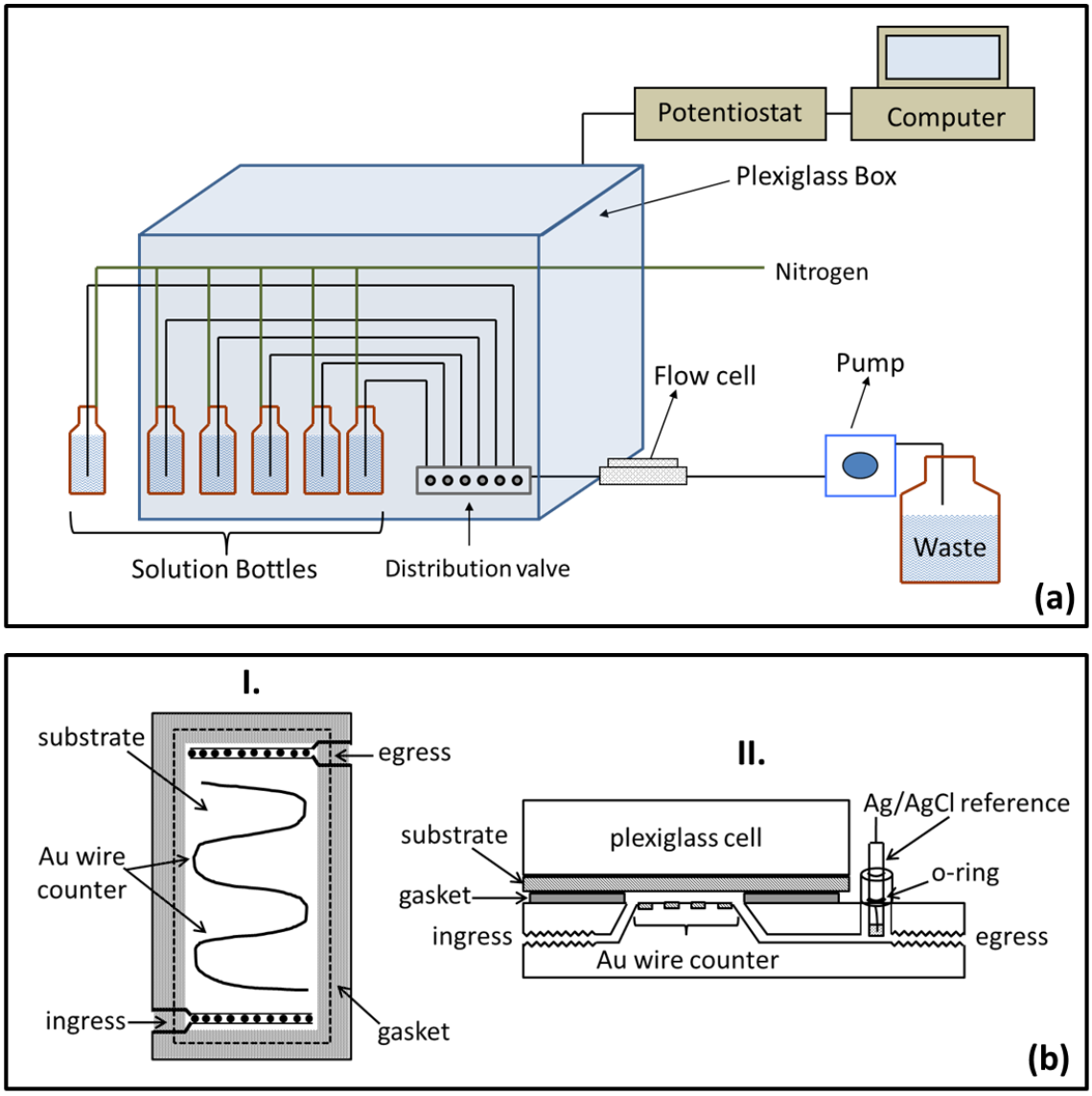

Figure 1.2 Schematics of the electrochemcial flow cell deposition system **(a)** and detailed views of the flow cell **(b)** used in formation of E-ALD films. **(b) I.** shows the top-down view of the flow cell, while **(b) II** shows the side view.

CHAPTER 2

ELECTROCHEMICAL ATOMIC LAYER DEPOSITION OF PALLADIUM NANOFILMS BY SURFACE LIMITED REDOX REPLACEMENT (SLRR), WITH EDTA COMPLEXATION[1]

[1] L. B. Sheridan, J. Czerniawski, N. Jayaraju, D. K. Gebregziabiher, J. L. Stickney, D. B. Robinson and M.P. Soriaga, *Electrocatalysis*, **3**, 96 (2012)

Reprinted here with permission of the publisher.

Abstract

Atomic-scale control in the formation of Pd thin films is being developed using electrochemical atomic layer deposition (E-ALD) via surface limited redox replacement (SLRR). Pd has unique hydrogen storage properties. To study hydrogen storage capacity, hydrogen charging and discharging kinetics and its catalytic properties at the nanoscale will require films with well-defined thickness, and structure. SLRR is the use of underpotential deposition (UPD) to form a sacrificial atomic layer of a less noble metal, such as Cu or Pb, and to exchange it at open circuit potential (OCP) for a more noble metal (Pd) via galvanic displacement. The deposits were grown using an automated electrochemical flow cell system which allowed sequential variation of solutions and potentials. Electron probe microanalysis (EPMA) revealed excess growth at the flow cell ingress, suggesting that the SLRR mechanism involved electron transfer from substrate to Pd^{2+} ions, rather than direct electron exchange from sacrificial metal atom(s) to Pd^{2+} ions. Ethylenediaminetetraacetic acid (EDTA) was used to slow the galvanic displacement by complexing the Pd^{2+}, in an attempt to form more uniform Pd deposits. The resulting films were more homogeneous and displayed the expected Pd voltammetry in H_2SO_4. The charge for UPD remained constant from cycle to cycle, indicating no roughening of the surface. Ways of optimizing complexing agent properties, as well as the flow cell design and deposition parameters are discussed.

Introduction

Palladium has unique properties, such as the reversible absorption of 900 times its volume in hydrogen at moderate temperatures and pressures[1], high catalytic activity, selectivity for a variety of reactions such as hydrogenation and dehydrogenation[2], and high hardness and nobility[3]. These are of great technological importance and have led to its widespread use in gas storage, catalysis and electronic applications. In recent years there has been considerable interest in the formation of thin Pd films for optical sensors[4, 5], catalysis, fuel cells[6-8], and hydrogen sensors[9]. Many applications today require the controlled growth of very thin metal films. A variety of techniques exist to form Pd thin films, such as: physical vapor deposition[10], electron beam evaporation[11], magnetron sputtering[12], and electrodeposition[13-15]. Electrodeposition is a classic technique for the deposition of metals on conducting substrates and offers the benefits of low cost, low temperature and low complexity.

Underpotential deposition (UPD) is electrodeposition of an atomic layer (AL) of an element at a potential prior to (under) that required to deposit the element on itself [16-20]. UPD is driven by the free energy of formation of a surface compound or alloy. UPD results in deposition of an AL of the element, where an AL is no more than one atom high, with a coverage (atoms/cm^2) of less than a monolayer (ML). In this report a monolayer (ML) is defined as one adsorbate atom per substrate surface atom: for example, this is 1.378 x 10^{15} atoms/cm^2 (224 $\mu C/cm^2$) for a one electron process on a gold (111) single-crystal surface.

Atomic layer deposition (ALD) is a class of methods for the formation of materials one AL at a time, using surface limited reactions to promote the formation of

smooth, conformal deposits[21]. E-ALD is an electrochemical implementation of ALD: the combination of UPD and ALD, and has been used to deposit nanofilms of compound semiconductors and metals, as well as superlattices[22, 23], nanoclusters[22, 23], and nanowires. It is based on alternating potentials and solutions in a sequence of steps, referred to as a cycle. Each cycle results in deposition of a ML or less of the material and the numbers of cycles determine the thickness.

Metal films were not initially grown using E-ALD, that is until the development of surface limited redox replacement (SLRR) by Brankovic et al.[24], Mrozek et al.[25], Vasilic and Dimitrov,[26] and Kim et al[27]. SLRR starts with deposition of an AL of a sacrificial metal (often Cu or Pb), via UPD. The cell solution is then exchanged for one containing salts of a more noble metal, such as Pd, Pt or Ru, at open circuit potential (OCP). Galvanic displacement occurs, limited by the presence of only an AL of the sacrificial element. That is, the nobler element is deposited while the more reactive, sacrificial, element is oxidized to a soluble ion. This cycle is then repeated to form nanofilms of metal [28-30]. The author's group has grown nanofilms of Cu,[28, 29, 31] Ru,[30] and Pt[32] using an automated flow-cell deposition systems. Dimitrov et al. [33] have also grown Pt thin films on Au and Pt substrates using up to 10 SLRR cycles, while Mkwizu et al.[34] have used SLRR to form Pt/Ru multilayer nanostructures on glassy carbon substrates. It has been pointed out by Goken et al. in a study of the stoichiometry of Pt to UPD Cu, on Au(111), that counterions have specific effects on the resulting deposits.[35] There are multiple factors which appear to influence how fast the displacement takes place, including concentration and oxidation state of the displacement precursor, pH, and the presence of complexing agents. Thambidurai et al. used a

complexing agent to lower the activity of Cu^{2+} ions during exchange for Pb, to improve deposit homogeneity in Cu films formed on Ru/Ta/Si wafers. Prior to the addition of the complexing agent, a Cu gradient was observed across the deposit, decreasing from ingress to egress of the flow cell. That work suggested the SLRR mechanism may not be electron transfer between ion and atom, but rather between substrate and ion. That is, electrons generated anywhere on the surface can move freely through a conducting substrate, reducing reactant ions wherever their activity is greatest. During solution exchange in the flow cell, the activity of the nobler ion precursor is initially significantly greater at the ingress, until the concentration becomes homogeneous through the cell[28]. More recently, Gokcen et al.[36] published a thorough kinetic study of submonolayer Pt SLRR on Au(111) and determined that the sacrificial metal, the concentration of Pt ions, and the anions present in the supporting electrolyte directly affect the overall kinetics for deposition. Those results appear consistent with the conclusions by Thambidurai et al.[28], as well as those presented in this report.

Pd SLRR was first reported by Adzic´ and co-workers[24], who found that a single replacement of Cu_{UPD} resulted in a near-uniform Pd monolayer on Au(111). Shortly thereafter, Weaver and coworkers[25] reported the formation of Pd SERS-active substrates by depositing Pd monolayers onto roughened Au by replacing either Pb_{UPD} or Cu_{UPD}. More recently this technique has been used to form a single monolayer of Pd on IrCo alloy[23] nanoparticles and in the formation of bimetallic CuPd particles on graphite.[37]

In this work we report the use of Pd SLRR as the surface limited process in the E-ALD formation of Pd nanofilms using an automated flow cell electrodeposition system.

Furthermore, this report examines the use of Pb and Cu as sacrificial elements and the incorporation of a complexing agent, EDTA. Deposits were formed with a range of EDTA concentrations. The elemental compositions and distributions across the substrates were characterized using electron probe microanalysis. Coulometry was used to monitor deposited amounts, and cyclic voltammetry (CV) to characterize the resulting Pd films.

Experimental

Au on glass films, 100 nm with a 5 nm Ti adhesion layer, were used as substrates. CVs indicated a predominantly Au (111) surface structure. The automated electrochemical flow cell deposition system[22, 38, 39], included a variable speed pump, 5 valve blocks, 5 solution reservoirs, potentiostat, electrochemical flow cell and "Sequencer" control software (Electrochemical ALD L.C.), specifically designed for E-ALD. The flow cell had a deposition area of 3.0 cm^2, and was of an older "V-cell" design. That is, the solution entered the flow channel from a tube at the base of a V shaped slot, designed to spread solution across the 1 cm wide channel. The cell employed an Au wire counter electrode, imbedded in the wall opposite the working electrode, and an external Ag/AgCl (3 M KCl) reference electrode (Bioanalytical Systems, Inc.). Prior to deposition, the Au substrates were cleaned by cycling between 1.4 V and -0.2 V in 0.1 M H_2SO_4, until the Au CV remained constant.

All solutions were prepared with 18 mΩ water from a Nanopure water filtration system (Barnstead). The Pd^{2+} ion solution was based on that used by Sanabria-Chinchilla et al. for the electrodeposition of ultrathin Pd films on Au(332) and Au(111) single crystals[40]; it consisted of 0.1 mM $PdCl_2$ (Aldrich, 99.999%), 0.6 mM HCl (Fisher

Scientific), and 0.1 M H_2SO_4 (Fischer Scientific). Upon dissolution, $PdCl_4^{2-}$ is formed, leaving the solution 0.4 mM in HCl, as well. Solutions containing ethylenediaminetetraacetic acid (EDTA) (J.T. Baker, 99.9%) were referred to by their ratio of $[Pd^{2+}]$/[EDTA], formed with Pd^{2+} concentrations between 0.1- 0.2 mM, and [EDTA] between 0.1 or 1 mM. All Pd solutions were adjusted to pH 1.8 using H_2SO_4. Sacrificial metal ion solutions were 1 mM $PbClO_4$ (Aldrich, 99.995%) in 0.1 M $NaClO_4$ (Fischer Scientific, HPLC grade), pH 4.8 and 0.1 mM $CuSO_4$ (J.T. Baker, 99.8%) in 0.1 M H_2SO_4, pH 1.4. The corresponding blank solutions were 0.1 M $NaClO_4$ and 0.1 M H_2SO_4, respectively. To reduce dissolved oxygen, nitrogen was bubbled through all solutions for an hour prior to electrochemical studies. Potentials are reported versus Ag/AgCl (3 M KCl). EPMA was performed using a JEOL 8600 wavelength-dispersive scanning electron microprobe. EPMA measurements had minimum detection limits (MDL), given in atomic % (at. %), of: 0.3 for Pd, 0.4 for Pb and 1 for Cu.

Results and Discussion

Figure 2.1 is a diagram of the set-up of the automated electrochemical flow cell deposition system. A scheme for a typical SLRR cycle is depicted in Figure 2.2. A Cu^{2+} ion solution was pumped into the cell for 16 sec at a flow rate of 11 mL/min and held for 8 s with the working electrode at an underpotential, resulting in formation of a Cu AL. The working electrode was then maintained at OCP, and the Cu^{2+} ion solution was replaced with the Pd^{2+} ion solution, allowing the displacement of Cu UPD for Pd. The potential was monitored during the exchange, until a pre-designated "stop potential" was reached. At that point, the cell was rinsed with the sulfuric acid blank solution, removing the remaining Pd^{2+} ions and any Cu^{2+} ions formed, completing the cycle. The cycle was

repeated to form nanofilms of Pd, where the thickness was a function of the number of cycles performed. Figure 2.3 displays current and potential time plots for two E-ALD cycles. Current and potential time data was collected and monitored for each cycle during the deposition of all Pd films, and used to help optimize the deposition cycles.

Sacrificial metal

Pb was initially chosen as the sacrificial metal because the ΔE between Pb_{UPD} and the Pd formal potential ($E^{o'}_{Pd}$) was 0.4 V larger than that for Cu_{UPD}[41-44]. Pb has been used successfully by the this group in SLRR cycles for the deposition of: Ru[30], Cu[28, 29, 31], and Pt[32]. In the present study, Pb_{UPD} was performed at -0.35 V, after examination of CVs and comparison with the literature.[45, 46] CVs of polycrystalline Au in the Pb^{2+} solution are displayed in Figure 2.4, and are typical for a polycrystalline surface[45]. Reduction current begins at 0.09 V during the negative scan, with the main Pb_{UPD} peak showing at -0.22 V. At -0.45 V a reduction feature for bulk Pb deposition appears, and displays hysteresis in the subsequent positive going scan, suggesting a nucleation and growth mechanism for the bulk Pb. Stripping bulk Pb occurs in a sharp peak at -0.43 V, followed by a broad peak at -0.38 V, felt to correspond to Pb oxidation from a Pb/Au alloy[47]. The "stop potential" is used to limit the OCP reached during the displacement step. When the stop potential was reached, the system rinsed the cell with blank to remove leftover Pd^{2+} ions and any Pb^{2+} produced. An ideal stop potential is one where the displacement is just completed: all the sacrificial metal has been oxidized. From earlier studies using Pb_{UPD} as the sacrificial AL[28], 0.0 V was chosen as all Pb had been oxidized by that potential.

A 25 cycle deposit, formed using Pb with a stop potential of 0.0 V, resulted in a Pd nanofilm contaminated with Pb. Figure 2.5 (solid line) shows the Pb/Pd ratio from EPMA, from ingress (0.25 cm) to egress (2.5 cm) of the flow cell. The Pb/Pd ratio was about 0.25, although lower at the egress. EPMA provided at. %, though based on a sample being a homogeneous alloy, rather than the Pd/Pb alloy coated Au substrate, which was actually characterized. The at. % of Pb and % of Pd serve as relative measures of their coverages, and provided accurate elemental ratios. Experience has shown that 25 E-ALD cycles of a metal should produce about 2-4 at. %, the other 96-98 at. % coming from the Au substrate (Fig. 6).

Two issues present themselves: why was Pb present and why was there more deposition near the ingress? Pb may be more stable alloyed with Pd than it was with Cu, Pt or Ru [30, 32], where the Pb sacrificial layers were removed above 0.0 V. As for the second issue, such deposition gradients have been observed for E-ALD deposits formed using SLRR cycles, when the rate of galvanic displacement was rapid compared with the time required to exchange solutions in the flow cell.

In an attempt to prevent Pb from building up in the deposit, a "stripping" step was added to the cycle. That is, once the OCP reached the stop potential, 0.0 V, blank solution was pumped through the cell. The potential was then set so as to oxidize any remaining Pb. The dashed line in Figure 2.5 displays the Pb/Pd ratio across the deposit when a stripping step at 0.45 V was used. A drop in the Pb/Pd ratio is evident at 1.75 cm, but Pb was still present, indicating that the stripping step was insufficient to remove the Pb.

Cu_{UPD} was then investigated as a sacrificial metal, having been used successfully in SLRR for Pt[24, 25], Ag[24], and Pd[23-25, 37]. The CVs of polycrystalline Au in

Cu^{2+} solution (Figure 2.7) agree well with the literature[46, 48]. Cu_{UPD} can be clearly seen in the inset, where two deposition features (~ 0.25 and 0.06 V) and their corresponding oxidation features (~ 0.11 and 0.25 V) are evident. Bulk Cu deposition begins at 0 V, and strips in the subsequent positive scan in multiple sharp peaks, suggesting some alloy formation[49, 50]. In the present study, Cu UPD was performed at 0.1 V, followed by displacement with the Pd^{2+} ion solution at OCP. A stop potential of 0.4 V was used, just lower than Pd oxidation. The dash-dot line in Figure 2.5 shows the Cu/Pd ratio from a 25 cycle deposit. Again some of the sacrificial metal (Cu) was entrained near the ingress, where the deposit was thicker (Figures 2.5 and 2.6). However there was no Cu near the egress, within the minimum detectible limit (MDL), suggesting that the Cu AL was completely removed there. Examination of Figures 2.5 and 2.6 indicates that Cu was only retained when excessive Pd deposition took place: where Pd was present at over the 4 at. % expected for a 25 cycle deposit. This suggests that deposition of more than a ML can trap (bury) Cu atoms. Although the Cu should not be stable at an OCP of 0.4 V, it is kinetically difficult to oxidize it from the surface once it is buried by Pd. This indicates that forming deposits with more than 1 ML/cycle could trap sacrificial metal.

That Cu is more easily stripped than Pb from Pd deposits is consistent with differences in the molar enthalpy of formation (ΔH_f) of Pd_xCu_y alloys[51, 52] versus Pd_xPb_y alloys[52, 53] (Table 1). Both Pd_xCu_y and Pd_xPb_y are formed exothermically, but the ΔH_f's for Pd_xPb_x are more than double those for Pb_xCu_y. Even though the ΔE for Pd and Pb_{UPD} are roughly double that for Pd and Cu_{UPD}, Table 1 shows the difference in enthalpies is a greater proportion.

Complexation of Pd^{2+}

Deposition gradients (Figures 2.5 and 2.6) have been observed previously in the SLRR formation of Cu[28]. It has been proposed that they are the result of fast kinetics for the displacement reaction, relative to the time it takes to fill the cell.[28] This would not affect the distribution of deposited Pd atoms if each depositing Pd^{2+} ion were to oxidize a specific sacrificial metal atom(s). The gradient in deposit thickness is evidence that the SLRR mechanism involves reduction of Pd^{2+} ions via electrons from the deposit rather than from individual atoms. Electrons move freely through the metallic substrate and deposited film, resulting in Pd^{2+} reduction where the ion's activity is highest. Deposition is greatest at the ingress, as that is where the Pd^{2+} ion solution first encounters the substrate. If exchange is faster than solution introduction, the sacrificial metal atoms anywhere on the surface can be oxidized, and the electrons conducted to the part of the electrode in contact with the highest Pd^{2+} activity.

Figure 2.3 indicates that it took approximately 10 s for the OCP to increase from 0.1 V to 0.3 V, a ΔE sufficient to oxidize the majority of the Cu UPD, while solution exchange, took approximately 20 s. Faster pumping for a shorter exchange time should result in a more homogeneous deposit, as would a cell design where the solution is introduced in a more homogeneous fashion. Alternatively, the exchange reaction could be slowed by complexation of the depositing ion: decreasing the free ion activity in solution. In the development of an SLRR cycle for the deposition of Cu by this group, complexation of the Cu^{2+} with citrate was used to slow the exchange, resulting in more homogeneous deposits.[28]

EDTA is a common complexing agent, with well characterized chemistry. It forms a strong 1:1 complex with Pd^{2+}, as it does with most metal ions.[54] The conditional complex formation constant ($K_f^{'}$) for Pd^{2+} ions and EDTA at pH 2 is 8×10^{12}, however, in the presence of chloride, a mixed Pd-EDTA-Cl complex is formed.[55, 56]

Voltammetry for Au electrodes in the $Pd(EDTA)^{2-}$ solutions is displayed in Figure 2.8. The peak potential for Pd reduction shifts from 0.57 V to 0.18 V as the $[Pd^{2+}]/[EDTA]$ ratio decreased, consistent with decreasing activity of free Pd^{2+} ions.

25 SLRR cycle deposits of Pd were formed with Cu_{UPD} as the sacrificial metal, using various $[Pd^{2+}]/[EDTA]$ ratios. Figure 2.9 displays the OCP during displacement for three different $[Pd^{2+}]/[EDTA]$ ratios. The time for the OCP to change from 0.1 V to 0.3 V was used as a measure of the kinetics for displacement (Figure 2.9); this was 10 s with no EDTA while it was 34.6 s for the $[Pd^{2+}]/[EDTA]$ ratio of 1. The intent was to decrease the kinetics for displacement, relative to the time for introduction of the Pd^{2+} solution into the cell (20 s). EPMA measurements were made from ingress to egress on the 25 cycle Pd films, and are shown in Figure 2.10. As noted in the experimental section, having used the V-cell for these studies, there was a point, 1 mm^2, where the solution impinges on the 3 cm^2 deposit. That point, the ingress, is generally where the highest Pd coverage was found. From the graphs in Figure 2.10 it might appear that there was an exponential decrease in coverage from the ingress to egress. However, that was not the case, as the coverage dropped rapidly within a mm of the ingress, and then only gently over the majority of the surface, towards the egress. The coverage at the ingress went from 24 at. % with no EDTA to 4 at. %, with $[Pd^{2+}]/[EDTA] = 1$. The EDTA did act to decrease the extensive deposition at the ingress, as expected, however the coverage over the rest of the

deposit was decreased as well, for $[Pd^{2+}]/[EDTA] = 1$. The film grown using $[Pd^{2+}] / [EDTA] = 0.1$ was not included in Figure 2.10, as no signal was detected above the MDL.

Ignoring the coverage at the ingress (on the left), deposits formed using solutions with no EDTA or with high $[Pd^{2+}] / [EDTA]$ ratios resulted in Pd at. % averaging near 4, as expected from previous studies of 25 cycle deposits of other metals and compounds. On the other hand, the $[Pd^{2+}] / [EDTA] = 1$ solution resulted in an average Pd at. % closer to 1.5, and disappeared when the ratio was 0.1. Overall, the $[Pd^{2+}] / [EDTA]$ ratio of 1 was chosen for deposits discussed subsequently in this paper, as it resulted in more homogeneous deposits, though suppressed deposition in general.

In SLRR, the amount deposited is controlled by the coverage of the sacrificial UPD layer. Examination of the Cu_{UPD} charges, provided in Figure 2.11, showed no significant variation for a 100 cycle Pd film formed with $[Pd^{2+}] / [EDTA]$ of 1. However, the resulting Pd coverages decreased when Pd^{2+} was complexed. From the potential vs time graphs in Figure 2.9, it was observed that the displacements were slower with EDTA present, resulting in an increased opportunity for parasitic reactions, such as the reduction of traces of O_2.

EDTA clearly results in complexation of the Pd^{2+} (Figure 2.10), but also limits the displacement reaction, resulting in thinner deposits. This may be a function of the lability of the EDTA complex, slowing the formation of free Pd^{2+} ions for the displacement. A more labile complexing agent might result in more homogeneous deposits without loss of thickness.

Figure 2.12 displays graphs of Pd at. % measured from ingress to egress for 50 cycle deposits using $[Pd^{2+}]$ / [EDTA] = 1, as a function of the stop potential. At each stop potential the average Pd at. %, discounting the ingress, was about 2. The coverages at the ingress were significantly higher, though they dropped with increasing stop potential. Higher stop potentials increase the amount of time EDTA and Pd^{2+} were in the cell (Figure 2.9), as well as allow the OCP to drift closer to the formal potential for Pd^{2+}/Pd in the EDTA solution (about 0.4 V). In general the OCP is a mixed potential, dependent on the relative activities for Pd and Cu in the deposit. An OCP less than the formal potential indicates the presences of some Cu in the deposit. These results suggest that the increased Pd at. % at the ingress may have something to do with the amount of Cu in the deposit. Given the design of the V-cell, an excess of deposition can occur at the ingress, where the inflow initially impinges on the substrate. Any excess Pd deposition increases the tendency to trap Cu at the ingress. The use of higher stop potentials decreases the amount of Cu left, which appears to decrease Pd buildup at the ingress (Figure 2.12).

Coulometry of Cu_{UPD} was used to follow film growth. From Figure 2.11, the charge for Cu_{UPD}, about 0.55 ML/cycle, was constant from cycle to cycle for 100 cycles, as expected for layer by layer growth in an ALD process. The lack of an increase in Cu_{UPD} with cycle # indicated that the deposit did not roughen. An important characteristic of layer by layer growth is a linear relationship between thickness and cycle # (Figure 2.13). The x-axis intercept was 8 cycles, rather than the expected 0, suggesting the exchange efficiency (% of the Cu_{UPD} electrons resulting in Pd deposition) was significantly less than 100% for the first few cycles. Such behavior is frequently seen for

gas phase ALD, and is referred to as an incubation or induction period, and is generally thought to be associated with barriers to nucleation of islands of the deposit.

Hydrogen storage properties

Figure 2.14 displays CVs of electrodes with various thicknesses of Pd, in 0.1 M H_2SO_4. Figure 2.14 (A) compares a 100 nm Pd film sputtered on Si to a 25 cycle E-ALD Pd film grown on Au (about 3 nm). Both show Pd oxidation beginning near 0.46 V, with oxide reduction at 0.4 V, as expected. For the 25 cycle E-ALD deposit (Figure 2.14 (A), solid line), no Au oxide reduction feature (0.9 V) was observed. The upper potential limit of the CV (1.3 V) was sufficient to oxidize Au, thus the lack of a reduction feature at 0.9 V confirms complete coverage of the Au by the Pd film.

In the negative scan, features corresponding to reductive hydrogen adsorption and then absorption start at 0 V, followed by oxidative desorption in the subsequent positive scan. The CV for the E-ALD film displays peaks corresponding to hydrogen adsorption (1) and its reversible oxidation (4), as well as initial absorption (2) and its reversible oxidation (3), consistent with previous work by Baldauf and Kolb.[13] These same features begin to overlap for the 100 nm sputtered film, with the peaks for reductive adsorption (1) and oxidative desorption (4) becoming shoulders on the primary features for hydrogen absorption and desorption (dotted curve). To clearly distinguish between adsorption and absorption requires Pd nanofilms[13, 57], nanoporous films[58] or nanoparticles[59] where the current for hydrogen absorption does not overwhelm that for adsorption. Figure 2.14 (B) displays the same CVs shown in (a), with the addition of the CV of bulk Pd, as a 0.5 mm diameter Pd wire (dashed line). Any features corresponding

to hydrogen adsorption and its oxidation are overwhelmed by the extensive hydrogen absorption and oxidation processes for bulk Pd.

Conclusion

This report describes studies of the formation of Pd nanofilms using E-ALD on Au electrodes. An automated electrochemical flow cell system was used to form deposits layer by layer using SLRR cycles. UPD of two metals, Pb and Cu, were investigated as the sacrificial layer for the SLRR cycles. EPMA results revealed that substantial amounts of Pb_{UPD} were incorporated into the dep*osit formed when it was used as a sacrificial metal, while essentially pure Pd films were formed when using Cu_{UPD}.

Preliminary results showed that excess Pd was deposited at the ingress, suggesting differential deposition across the substrate. This suggested that the SLRR mechanism was not strictly direct exchange of electrons between an atom of the sacrificial metal and an ion of the depositing metal. Rather, the deposition proceeded by transferring electrons from the sacrificial metal through the surface to reduce the depositing metal ions where their activity was highest. Studies using a complexing agent have shown that by slowing down the displacement reaction, a more homogeneous deposit could be formed. That is, it is important that the time to fill the cell be short compared to the time needed to complete the displacement. The addition of EDTA as a complexing agent was investigated, to slow the exchange reaction, allowing solution to be exchanged before all the sacrificial metal atoms were oxidized. Complexation of the Pd^{2+} is a classic method of decreasing the rate of reaction by decreasing the availability of free Pd^{2+} ions. Various $[Pd^{2+}]$/ [EDTA] ratios were investigated, with a ratio of 1 showing the best result in this study. Too much EDTA resulted in no deposit, while too little had little effect. Overall,

EDTA does not appear to be the optimal complexing agent for this application. It is expected that a more labile complexing agent would provide more flexibility in controlling the displacement kinetics vs. the rate of solution introduction.

Investigation of the dependence of the deposit distribution on the stop potential provided a surprise, in that the use of higher stop potentials resulted in more homogeneous deposits. It appears that the higher stop potentials allowed removal of the last traces of Cu from the deposit, and that those Cu traces were facilitating some excess deposition of Pd near the ingress.

Pd film thicknesses were linear with the number of cycles performed, after the first 8, indicating the expected layer-by-layer growth mechanism of ALD. The departure from linearity for the first 8 cycles suggests issues with nucleation, not expected for Pd on Au, possibly because of the presence of EDTA. CVs of a 25 cycle film indicate that the entire Au substrate was covered by Pd since no Au features were visible. The presences of well-defined hydrogen adsorption waves were consistent with the formation of a nanofilm of Pd.

Acknowledgements

Acknowledgment is made of the support of the National Science Foundation, Division of Materials Science, as well as Sandia National Laboratories, a multi-program laboratory managed and operated by Sandia Corporation, a wholly owned subsidiary of Lockheed Martin Corporation, for the U.S. Department of Energy's National Nuclear Security Administration under contract DE-AC04-94AL85000.

References

1. Barton, J.C., W.F.N. Leitch, and F.A. Lewis, *Kinetics of Desorption and Oxidation of Hydrogen Contained in Hydrided Palladium Immersed in Aqueous Solutions* Transactions of the Faraday Society, 1963. **59**(485): p. 1208.
2. Schwartz, M., *Encyclopedia and Handbook of Materials, Parts and Finishes, Second Edition*. 2002, New York: CRC Press.
3. Harper, C.A., *Electronic packaging and interconnection handbook*. 4th ed. 2005: McGraw-Hill
4. Avila, J.I., et al., *Optical properties of Pd thin films exposed to hydrogen studied by transmittance and reflectance spectroscopy.* Journal of Applied Physics, 2010. **107**(2).
5. T. J. Richardson, J.L.S., B. Farangis, and M. D. Rubin, *Mixed metal films with switchable optical properties.* Applied Physics Letters, 2002. **80**(8): p. 1349-1351.
6. Zhang, J.T., et al., *Facile fabrication and unexpected electrocatalytic activity of palladium thin films with hierarchical architectures.* Journal of Physical Chemistry C, 2008. **112**(36): p. 13970-13975.
7. Thotiyl, M.M.O., T.R. Kumar, and S. Sampath, *Pd Supported on Titanium Nitride for Efficient Ethanol Oxidation.* Journal of Physical Chemistry C, 2010. **114**(41): p. 17934-17941.
8. Sarapuu, A., et al., *Electroreduction of oxygen on gold-supported nanostructured palladium films in acid solutions.* Electrochimica Acta, 2010. **55**(22): p. 6768-6774.

9. Noh, J.S., J.M. Lee, and W. Lee, *Low-Dimensional Palladium Nanostructures for Fast and Reliable Hydrogen Gas Detection.* Sensors, 2011. **11**(1): p. 825-851.

10. Eyrich, M., et al., *Planar Au/TiO2 Model Catalysts: Fabrication, Characterization and Catalytic Activity.* Chemphyschem, 2010. **11**(7): p. 1430-1437.

11. Gu, G.R. and T. Ito, *Field emission characteristics of thin-metal-coated nano-sheet carbon films.* Applied Surface Science, 2011. **257**(7): p. 2455-2460.

12. Samuelsson, M., et al., *On the film density using high power impulse magnetron sputtering.* Surface & Coatings Technology, 2010. **205**(2): p. 591-596.

13. Baldauf, M. and D.M. Kolb, *A Hydrogen Adsorpiton and Absorption Study with Ultrathin Pd Overlayers on Au(111) and Au(100)* Electrochimica Acta, 1993. **38**(15): p. 2145-2153.

14. Takahasi, M., et al., *Orientation dependence of Pd growth on Au electrode surfaces.* Journal of Physics-Condensed Matter, 2010. **22**(47).

15. Czerwinski, A., S. Zamponi, and R. Marassi, *The Influence of Carbon-monoxide on Hydrogen Absorption by Thin-films of Palladium* Journal of Electroanalytical Chemistry, 1991. **304**(1-2): p. 233-239.

16. Magnussen, O.M., *Ordered anion adlayers on metal electrode surfaces.* Chemical Reviews, 2002. **102**(3): p. 679-725.

17. Herrero, E., L.J. Buller, and H.D. Abruna, *Underpotential Deposition at Single Crystal Electrodes Surfaces of Au, Pt, Ag and other Materials.* Chemical Reviews, 2001. **101**: p. 1897-1930.

18. Gewirth, A.A. and B.K. Niece, *Electrochemical applications of in situ scanning probe microscopy.* Chem. Rev., 1997. **97**: p. 1129-1162.

19. Adzic, R.R., *Electrocatalytic Properties of the Surfaces Modified by Foreign Metal Ad Atoms*, in *Advances in Electrochemistry and Electrochemical Engineering*, H. Gerishcher and C.W. Tobias, Editors. 1984, Wiley-Interscience: New York. p. 159.

20. Kolb, D.M., *Physical and Electrochemcial Properties of Metal Monolayers on Metallic Substrates*, in *Advances in Electrochemistry and Electrochemical Engineering*, H. Gerischer and C.W. Tobias, Editors. 1978, John Wiley: New York. p. 125.

21. George, S.M., *Atomic Layer Deposition: An Overview.* Chemical Reviews, 2010. **110**(1): p. 111-131.

22. Stickney, J.L., *Electrochemical Atomic Layer Epitaxy (EC-ALE): Nanoscale Control in the Electrodeposition of Compound Semiconductors*, in *Advances in Electrochemical Science and Engineering*, R.C.A.a.D.M. Kolb, Editor. 2002, Wiley-VCH: Weinheim.

23. Cavallini, M., et al., *Two-dimensional self-organization of CdS ultra thin films by confined electrochemical atomic layer epitaxy growth.* Journal of Physical Chemistry C, 2007. **111**(3): p. 1061-1064.

24. Brankovic, S.R., J.X. Wang, and R.R. Adzic, *Metal monolayer deposition by replacement of metal adlayers on electrode surfaces.* Surface Science, 2001. **474**(1-3): p. L173-L179.

25. Mrozek, M.F., Y. Xie, and M.J. Weaver, *Surface-enhanced Raman scattering on uniform platinum-group overlayers: Preparation by redox replacement of underpotential-deposited metals on gold.* Analytical Chemistry, 2001. **73**(24): p. 5953-5960.

26. Vasilic, R. and N. Dimitrov, *Epitaxial growth by monolayer-restricted galvanic displacement.* Electrochemical and Solid State Letters, 2005. **8**(11): p. C173-C176.

27. Kim, Y.G., et al., *Platinum nanofilm formation by EC-ALE via redox replacement of UPD copper: Studies using in-situ scanning tunneling microscopy.* Journal of Physical Chemistry B, 2006. **110**(36): p. 17998-18006.

28. Thambidurai, C., et al., *E-ALD of Cu Nanofilms on Ru/Ta Wafers Using Surface Limited Redox Replacement.* Journal of the Electrochemical Society, 2010. **157**(8): p. D466-D471.

29. Thambidurai, C., et al., *Copper Nanofilm Formation by Electrochemical ALD.* Journal of the Electrochemical Society, 2009. **156**(8): p. D261-D268.

30. Thambidurai, C., Y.G. Kim, and J.L. Stickney, *Electrodeposition of Ru by atomic layer deposition (ALD).* Electrochimica Acta, 2008. **53**(21): p. 6157-6164.

31. Gebregziabiher, D.K., et al., *Electrochemical atomic layer deposition of copper nanofilms on ruthenium.* Journal of Crystal Growth, 2010. **312**(8): p. 1271-1276.

32. Jayaraju, N., *Electrochemical atomic layer deposition (E-ALD) of Pt and PtRu nanofilms*, in *Chemistry*. 2010, University of Georgia: Athens.

33. Fayette, M., et al., *From Au to Pt via Surface Limited Redox Replacement of Pb UPD in One-Cell Configuration.* Langmuir, 2011. **27**(9): p. 5650-5658.

34. Mkwizu, T.S., M.K. Mathe, and I. Cukrowski, *Electrodeposition of Multilayered Bimetallic Nanoclusters of Ruthenium and Platinum via Surface-Limited Redox-Replacement Reactions for Electrocatalytic Applications.* Langmuir, 2010. **26**(1): p. 570-580.

35. Gokcen, D., S.E. Bae, and S.R. Brankovic, *Stoichiometry of Pt Submonolayer Deposition via Surface-Limited Redox Replacement Reaction.* Journal of the Electrochemical Society, 2010. **157**(11): p. D582-D587.

36. Gokcen, D., S.E. Bae, and S.R. Brankovic, *Reaction kinetics of metal deposition via surface limited red-ox replacement of underpotentially deposited metal monolayers.* Electrochimica Acta, 2011. **56**(16): p. 5545-5553.

37. Ghodbane, O., L. Roue, and D. Belanger, *Study of the electroless deposition of Pd on Cu-modified graphite electrodes by metal exchange reaction.* Chemistry of Materials, 2008. **20**(10): p. 3495-3504.

38. Wade, T.L., T.A. Sorenson, and J.L. Stickney, *Interfacial Electrochemistry*, ed. A. Wieckowski. 1999, New York: Marcel Dekker.

39. Stickney, J.L., *Electrochemical atomic layer epitaxy*, in *Electroanalytical Chemistry, Vol 21*, A.J.B.a.I. Rubinstein, Editor. 1999, Marcel Dekker, Inc.: New York. p. 75-209.

40. Sanabria-Chinchilla, J., et al., *Electrocatalytic hydrogenation and oxidation of aromatic compounds studied by ITEMS: Benzene and p-dihydroxybenzene at ultrathin Pd films electrodeposited on Au(hkl) surfaces.* Journal of Colloid and Interface Science, 2007. **314**(1): p. 152-159.

41. Adzic, R., E. Yeager, and B.D. Cahan, *Optical and Electrochemical Studies of Underpotential Deposition of Lead on Gold Evaporated and Single-crystals Electrodes* Journal of the Electrochemical Society, 1974. **121**(4): p. 474-484.

42. Chen, C.H., N. Washburn, and A.A. Gewirth, *In-situ Atomic-force Microscope Study of Pb Underpotential Deposition on Au(111) - Structural Properties of the Catalytically Active Phase.* Journal of Physical Chemistry, 1993. **97**(38): p. 9754-9760.

43. Engelsmann, K., W.J. Lorenz, and E. Schmidt, *Underpotential Deposition of Lead on Polycrystalline and Single-crysal Gold Surfaces. 2. Kinetics* Journal of Electroanalytical Chemistry, 1980. **114**(1): p. 11-24.

44. Hamelin, A., et al., *Surface Characterization by Underpotential Deposition - Lead on Gold Surfaces* Journal of Electroanalytical Chemistry, 1980. **113**(2): p. 293-300.

45. Banga, D.O., et al., *Formation of PbTe nanofilms by electrochemical atomic layer deposition (ALD).* Electrochimica Acta, 2008. **53**(23): p. 6988-6994.

46. Kim, J.Y., Y.G. Kim, and J.L. Stickney, *Cu nanofilm formation by electrochemical atomic layer deposition (ALD) in the presence of chloride ions.* Journal of Electroanalytical Chemistry, 2008. **621**(2): p. 205-213.

47. Green, M.P. and K.J. Hanson, *Alloy Formation in an Electrodeposited Monolayer* Surface Science, 1991. **259**(3): p. L743-L749.

48. Herrero, E., L.J. Buller, and H.D. Abruna, *Underpotential deposition at single crystal surfaces of Au, Pt, Ag and other materials.* Chemical Reviews, 2001. **101**(7): p. 1897-1930.

49. Randler, R.J., et al., *Electrochemical copper deposition on Au(100): a combined in situ STM and in situ surface X-ray diffraction study.* Surface Science, 2000. **447**(1-3): p. 187-200.

50. Hotlos, J., O.M. Magnussen, and R.J. Behm, *Effect of Trace Amounts of Cl- in Cu Underpotential Deposition on Au(111) in Perchlorate Solutions - An In-situ Scanning Tunneling Microscopy Study* Surface Science, 1995. **335**(1-3): p. 129-144.

51. Laurie, G.H. and J.N. Pratt, *Electronic Constitution + Partial Thermodynamic Properties of Liquid in Tin Plus Palladium Plus Silver Alloys* Transactions of the Faraday Society, 1964. **60**(5008): p. 1391-&.

52. de Boer, F.R., B oom, R., Mattens, W.C.M., Miedema, A.R., Niessen, A.K., *Cohesion in Metals: Transition Metal Alloys*, ed. F.R.a.P. de Boer, D.G. Vol. 1. 1988, Amsterdam: Elsevier Science Publishers B.V.

53. Lbibb, R., A. Chouiyakh, and R. Castanet, *Thermodynamic investigation of the Pd-Pb solid alloys.* Intermetallics, 1996. **4**(8): p. 589-592.

54. Macnevin, W.M. and O.H. Kriege, *Chelation of Platinum Group Metals - Spectrophotometric Determination of Palladium with Ethylenediaminetetraacetic Acid.* Analytical Chemistry, 1954. **26**(11): p. 1768-1770.

55. Kragten, J., *The stability constant of Pd-EDTA.* Talanta, 1978. **25**(4): p. 239-240.

56. Alimarin, I.P. and V.I. Shlenskaya, *The analytical chemistry of mixed ligand complexes.* Pure and Applied Chemistry, 1970. **21**(4): p. 461-478.

57. Gabrielli, C., et al., *Investigation of hydrogen adsorption and absorption in palladium thin films - II. Cyclic voltammetry*. Journal of the Electrochemical Society, 2004. **151**(11): p. A1937-A1942.

58. Bartlett, P.N., et al., *The preparation and characterisation of H-1-e palladium films with a regular hexagonal nanostructure formed by electrochemical deposition from lyotropic liquid crystalline phases.* Physical Chemistry Chemical Physics, 2002. **4**(15): p. 3835-3842.

59. Tateishi, N., et al., *Electrochemical properties of ultra-fine palladium particles for adsorption and absorption of hydrogen in an aqueous HClO4 solution.* Electrochimica Acta, 1991. **36**(7): p. 1235-1240.

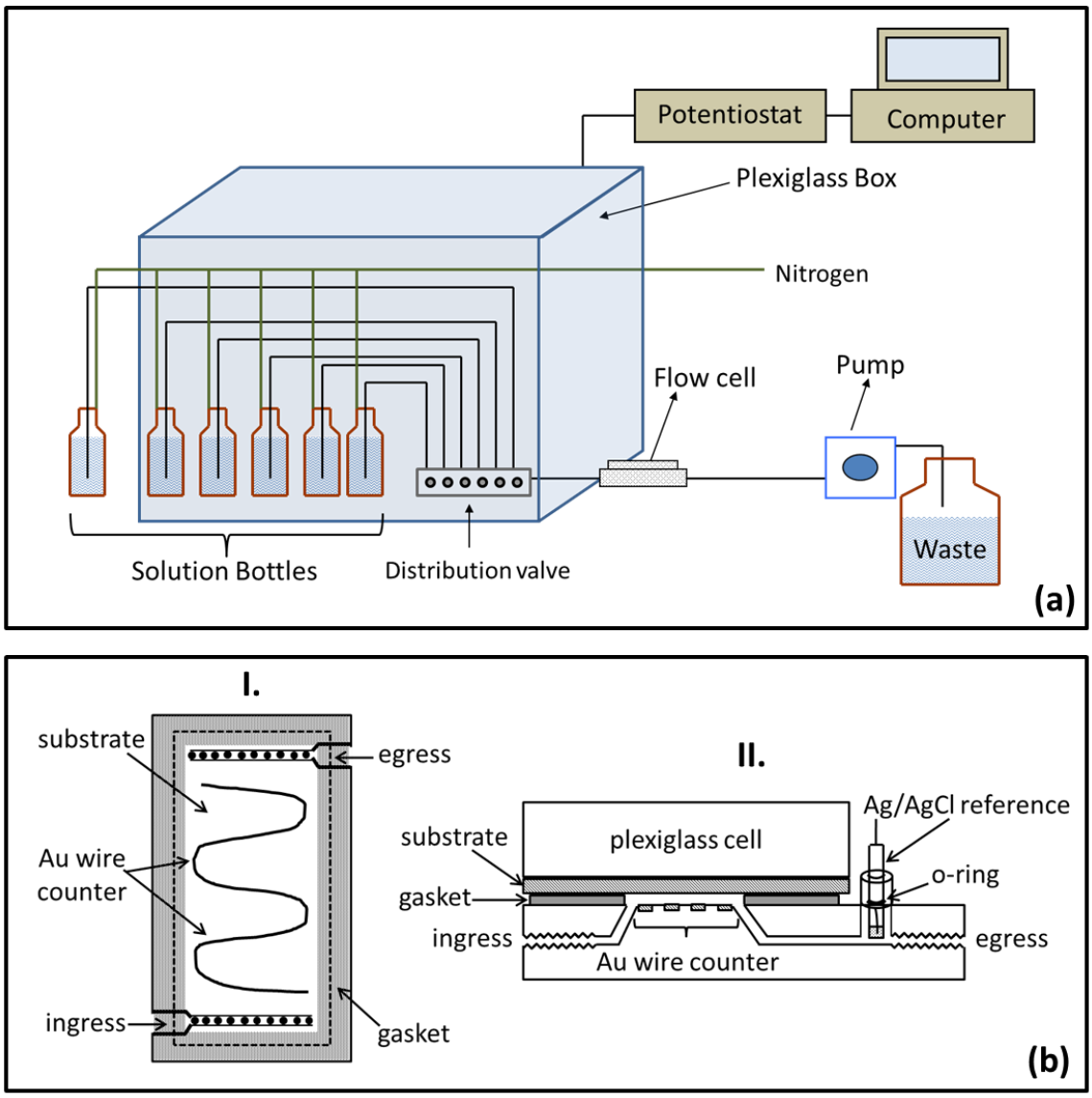

Figure 2.1 Diagrams of the experimental set-up, including the (a) automated electrochemical flow cell system and the (b) flow cell depicted from (I.) the top down and (II.) the side view.

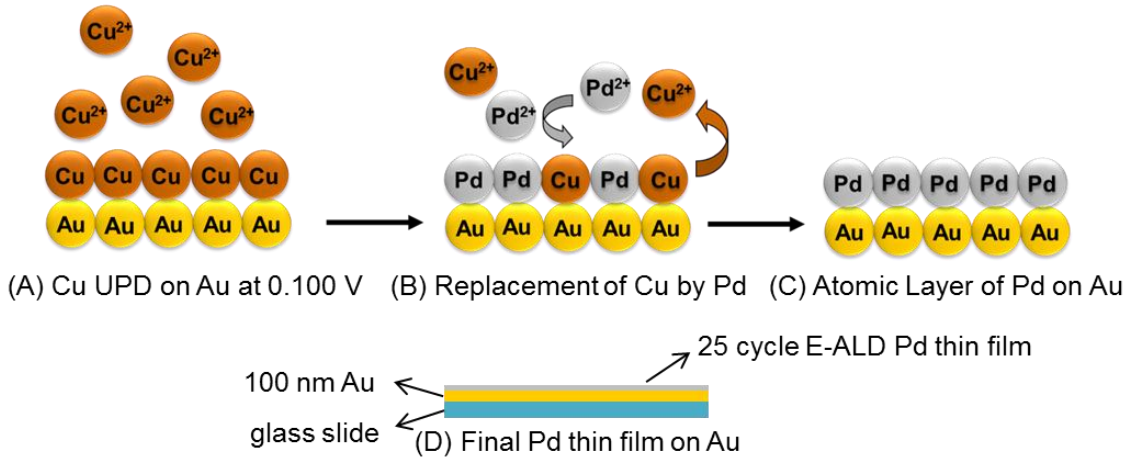

Figure 2.2 Cartoon of electrochemical ALD using a SLRR cycle for Pd film deposition on Au substrates.

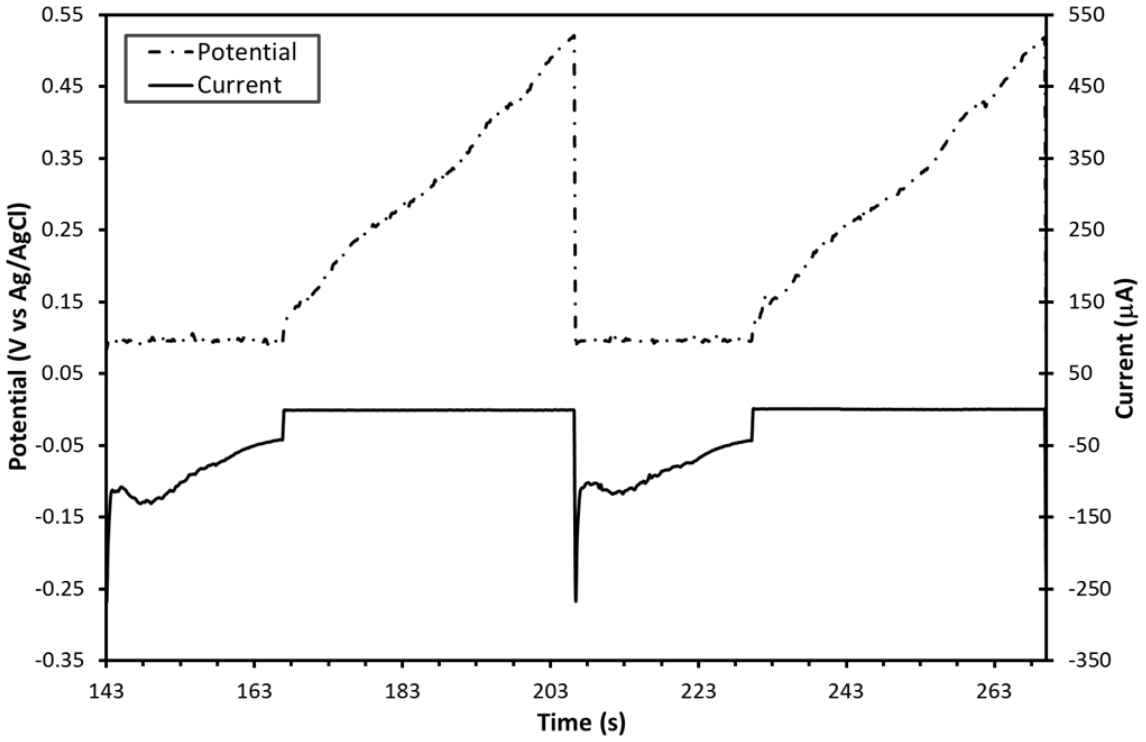

Figure 2.3 Time-Potential-Current graph displaying two Pd SLRR cycles. Cu was deposited at 0.10 V and replaced by Pd^{+2} ions until reaching an OCP of 0.40 V. The cell remained at open circuit during a 10 s blank rinse.

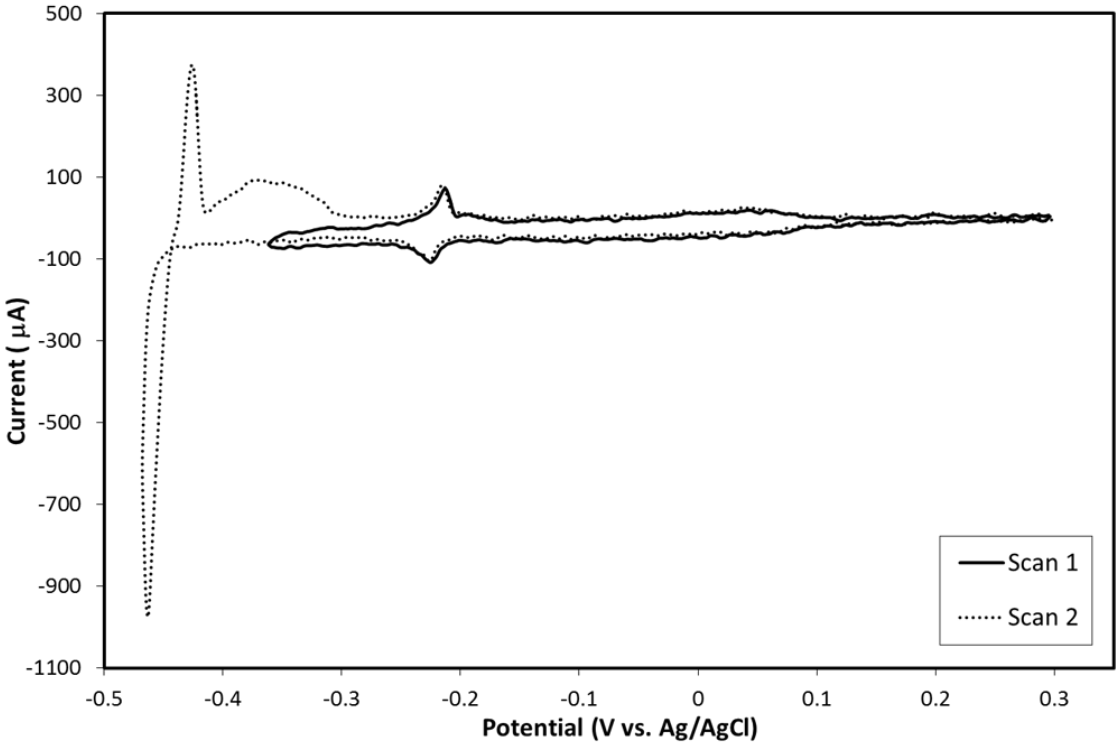

Figure 2.4 CVs of Au in 1 mM $PbClO_4$ and 0.1 M $NaClO_4$ at 10 mV/s.

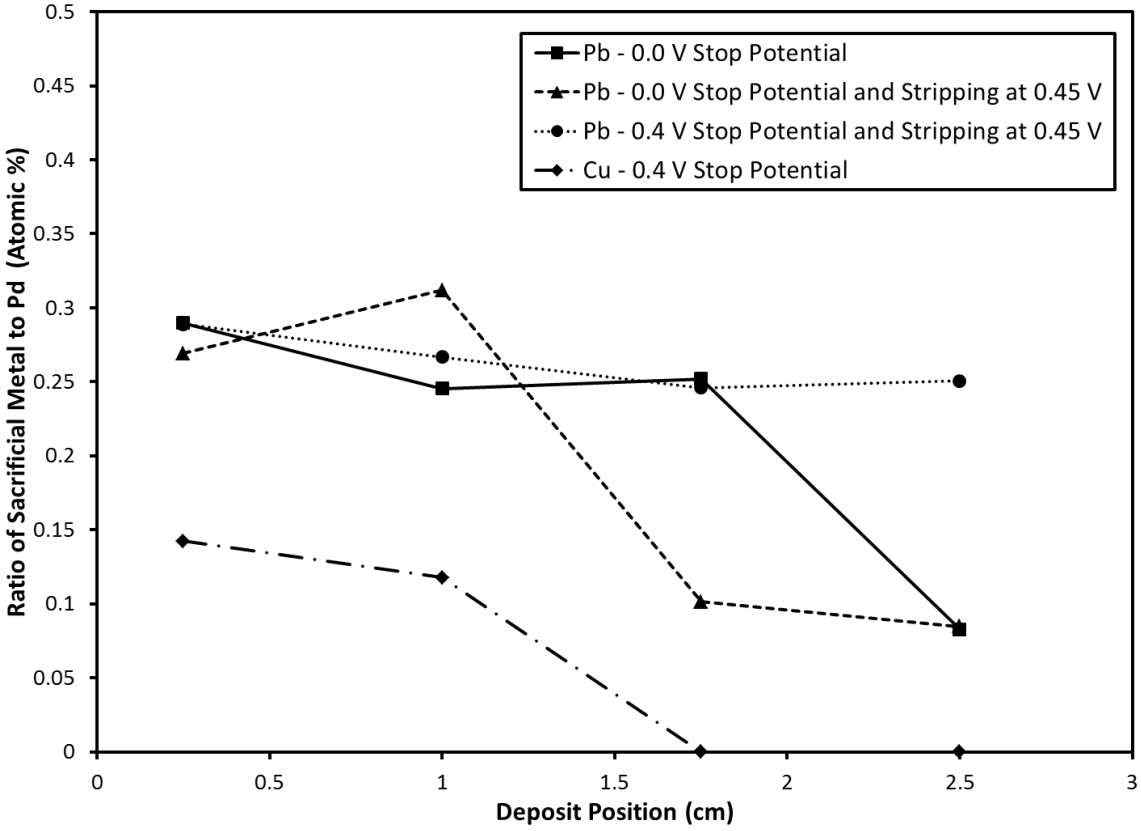

Figure 2.5 Ratio of Pb or Cu to Pd, determined by EPMA, versus deposit position for 25 cycle Pd E-ALD films formed by depositing Pb at -0.35 V or Cu at 0.10 V. Points were taken from the ingress (0.25 cm) to egress (2.5 cm).

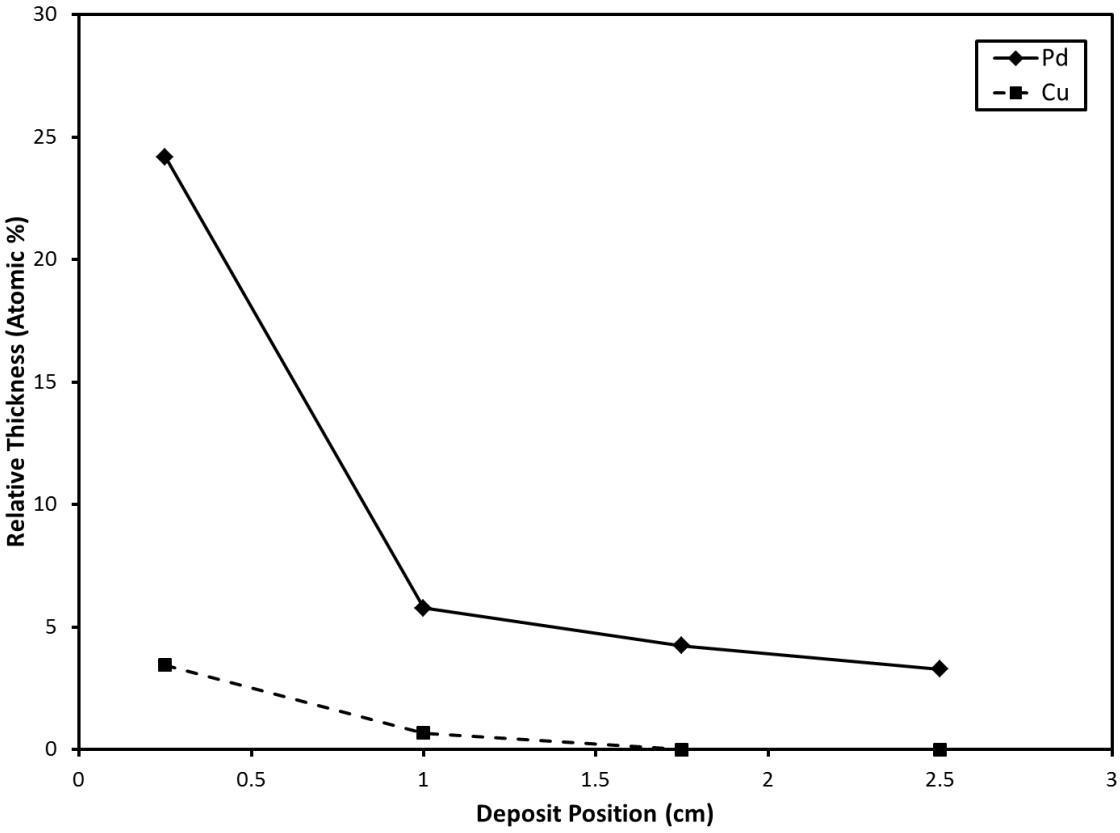

Figure 2.6 Relative Pd and Cu thickness, reported as atomic %, obtained from EPMA of a 25 cycle deposit formed using Cu deposited at 0.10 V and a 0.40 V stop potential. Points were taken from the ingress (0.25 cm) to egress (2.5 cm).

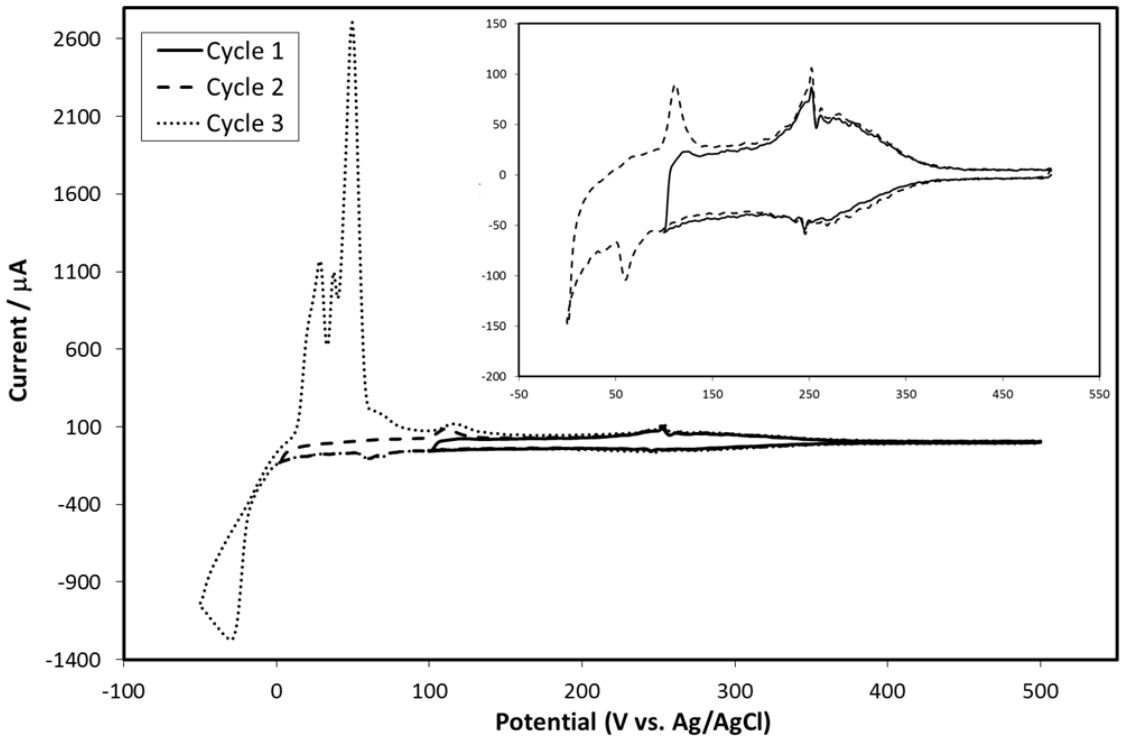

Figure 2.7 CVs of Au in 2 mM $CuSO_4$ and 0.1 M H_2SO_4 at 10 mV/s.

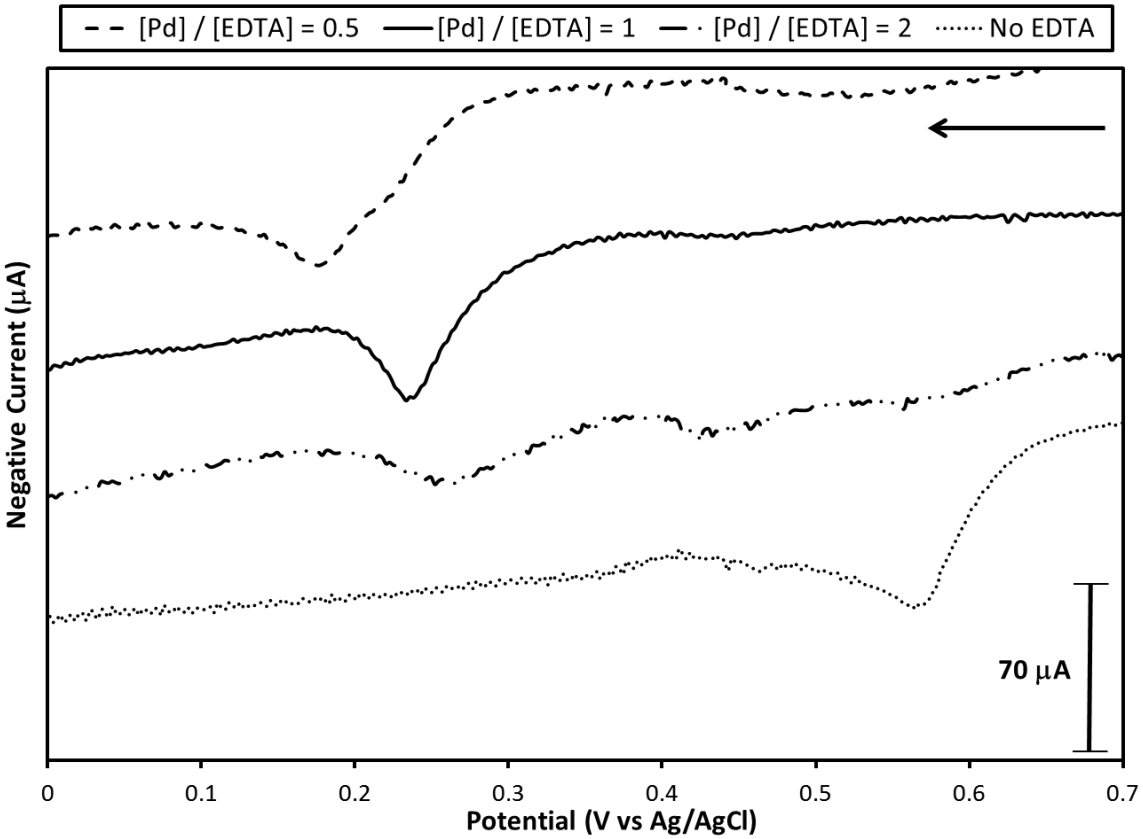

Figure 2.8 Reduction waves of CVs of polycrystalline Au in various Pd solutions at a scan rate of 10 mV/s.

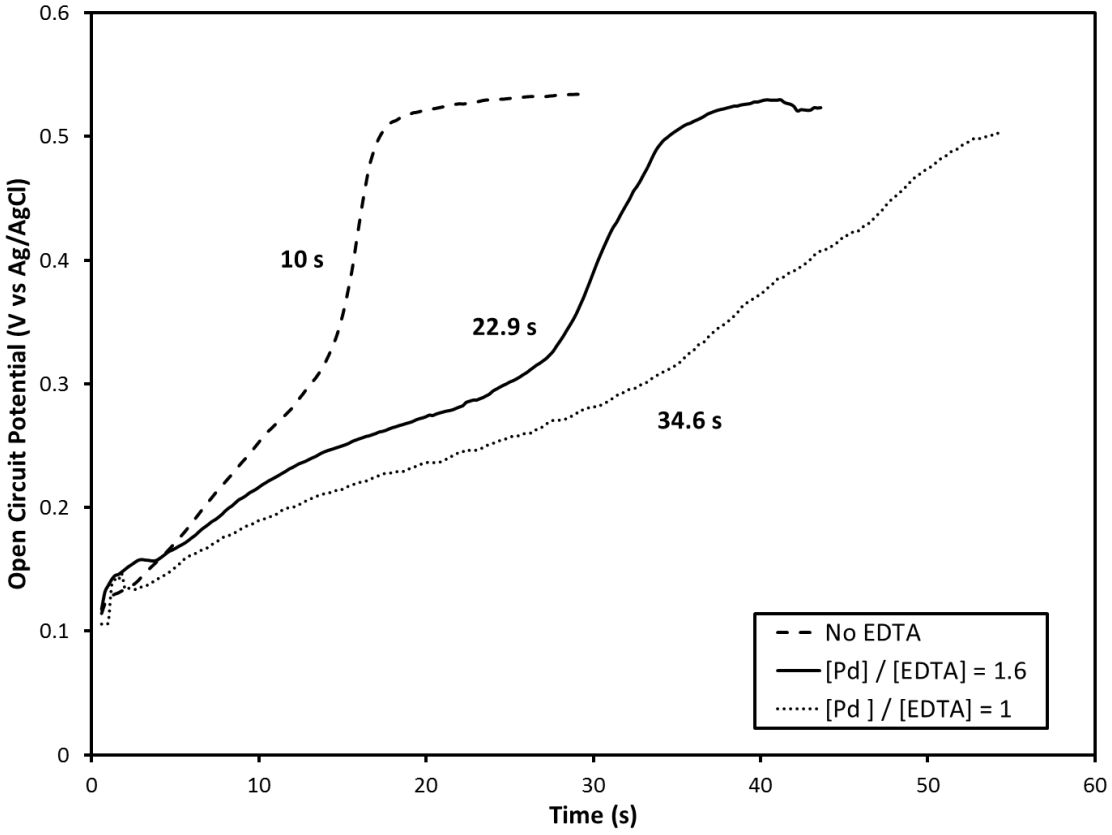

Figure 2.9 The OCP of the 14th cycle in 25 cycle deposits is plotted as a function of time where time 0 s is the start of the replacement reaction marked by the flowing of Pd solution. The times represent the average time needed for the OCP to shift from 0.1 V to 0.3 V. All films were grown using Cu deposited at 0.1 V and a 0.40 V stop potential.

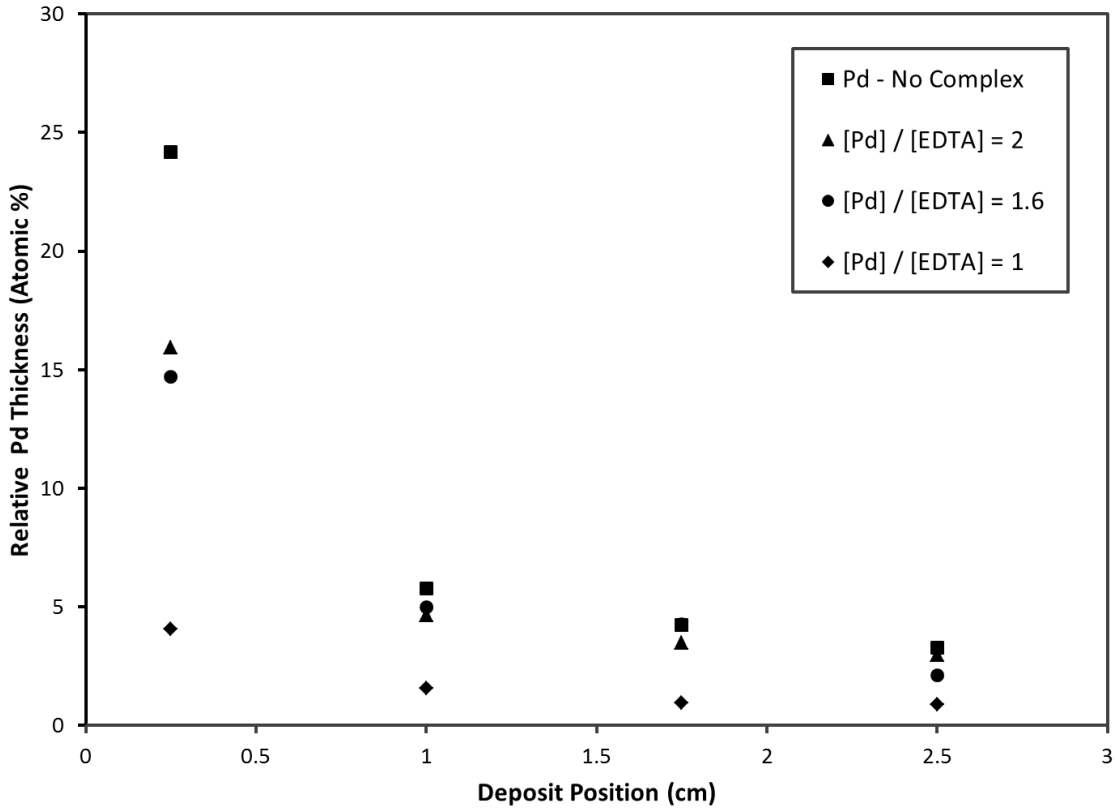

Figure 2.10 Relative atomic % was obtained from EPMA of 25 cycle films formed using Cu deposited at 0.10 V and a 0.40 V stop potential. Points were taken from the ingress (0.25 cm) to egress (2.5 cm).

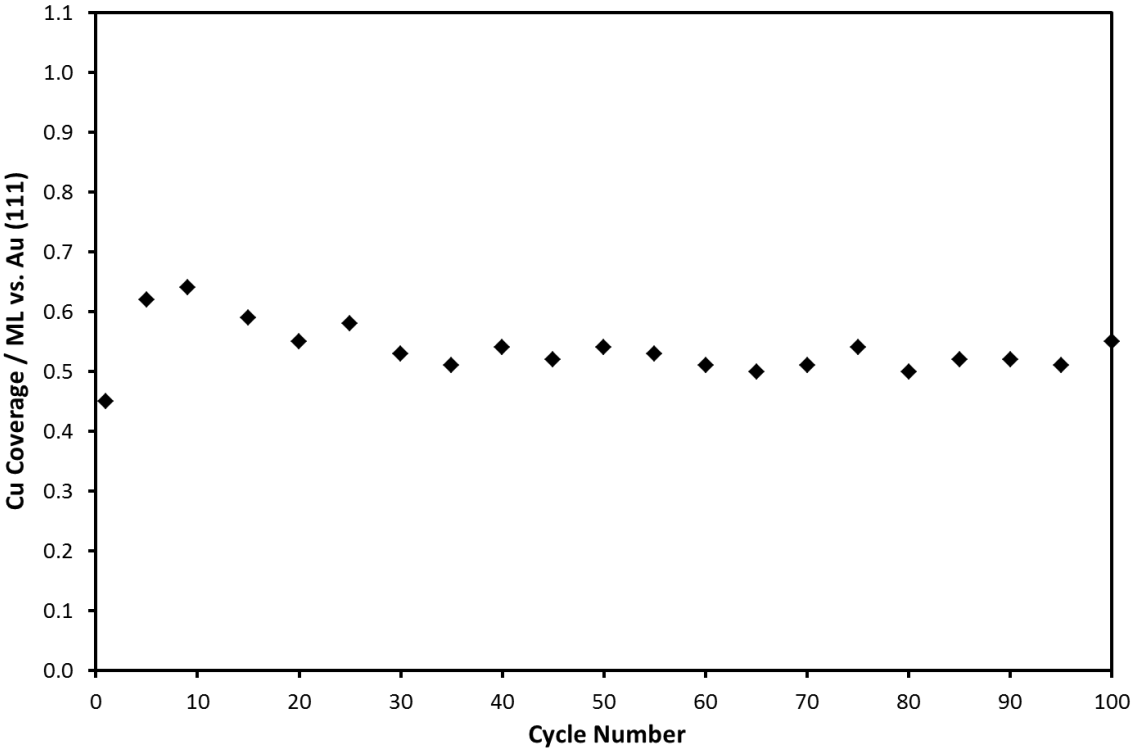

Figure 2.11 Cu coverage calculated from deposition current for every 10th cycle of a 100 cycle Pd E-ALD film. The film was formed using [Pd^{2+}] / [EDTA] of 1, a Cu deposition potential of 0.10 V and a stop potential of 0.40 V.

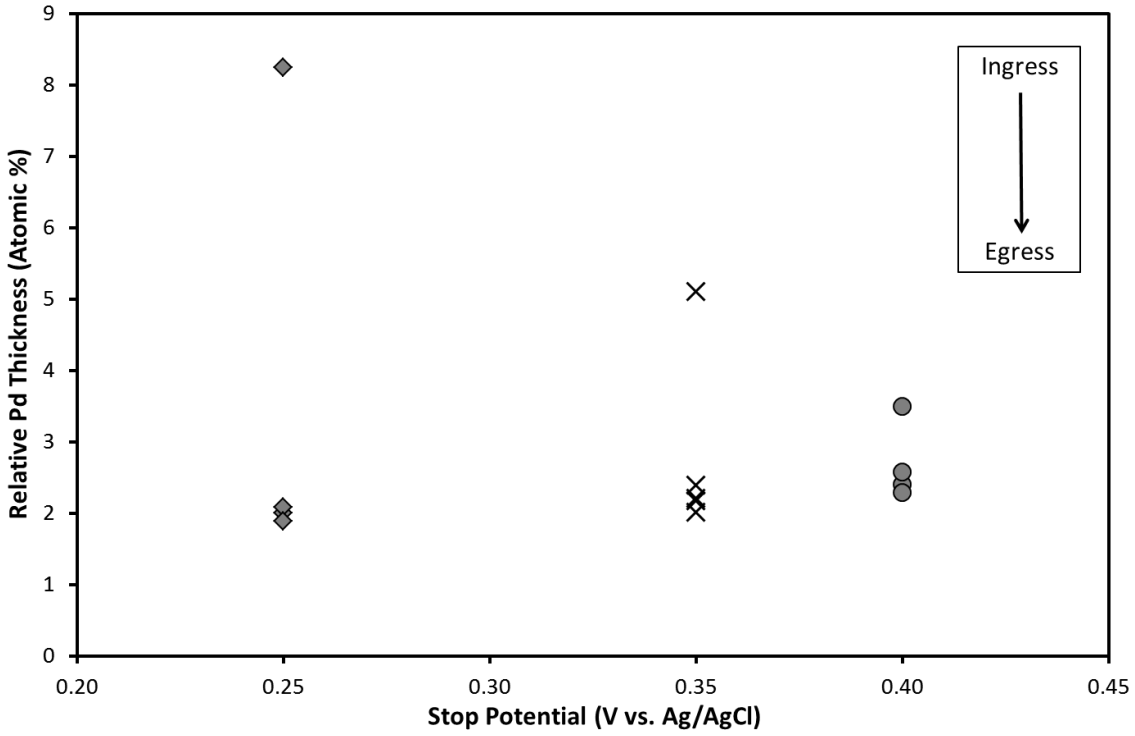

Figure 2.12 Relative Pd thickness, in atomic %, obtained from EPMA of 50 cycle deposits formed using different stop potentials and Cu deposited at 0.10 V. The Pd solution composition was $[Pd^{2+}]$ / [EDTA] = 1.

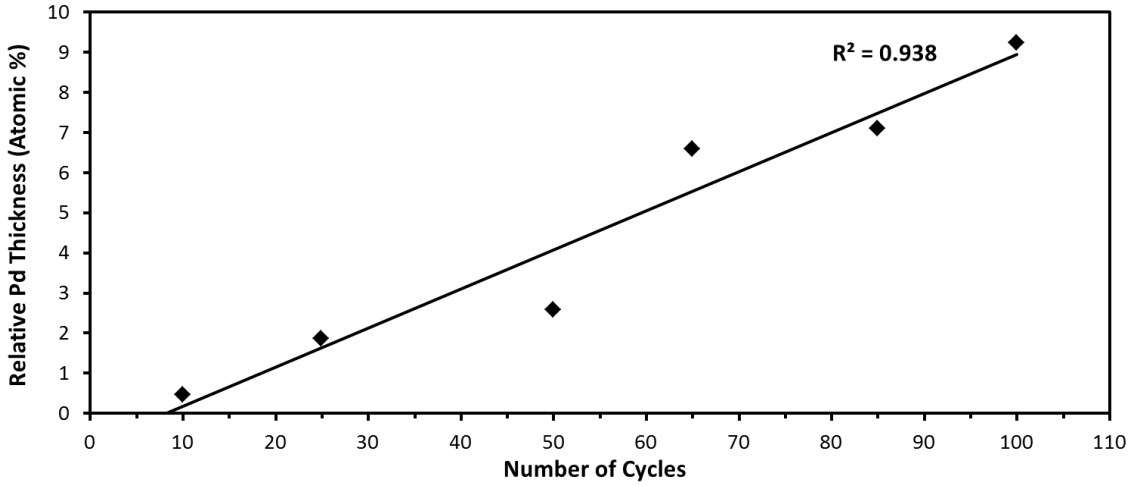

Figure 2.13 Plot illustrating the linear relationship between a film's thickness and the number of E-ALD cycles used to form that film. The Pd solution composition was $[Pd^{2+}]$ / [EDTA] = 1.

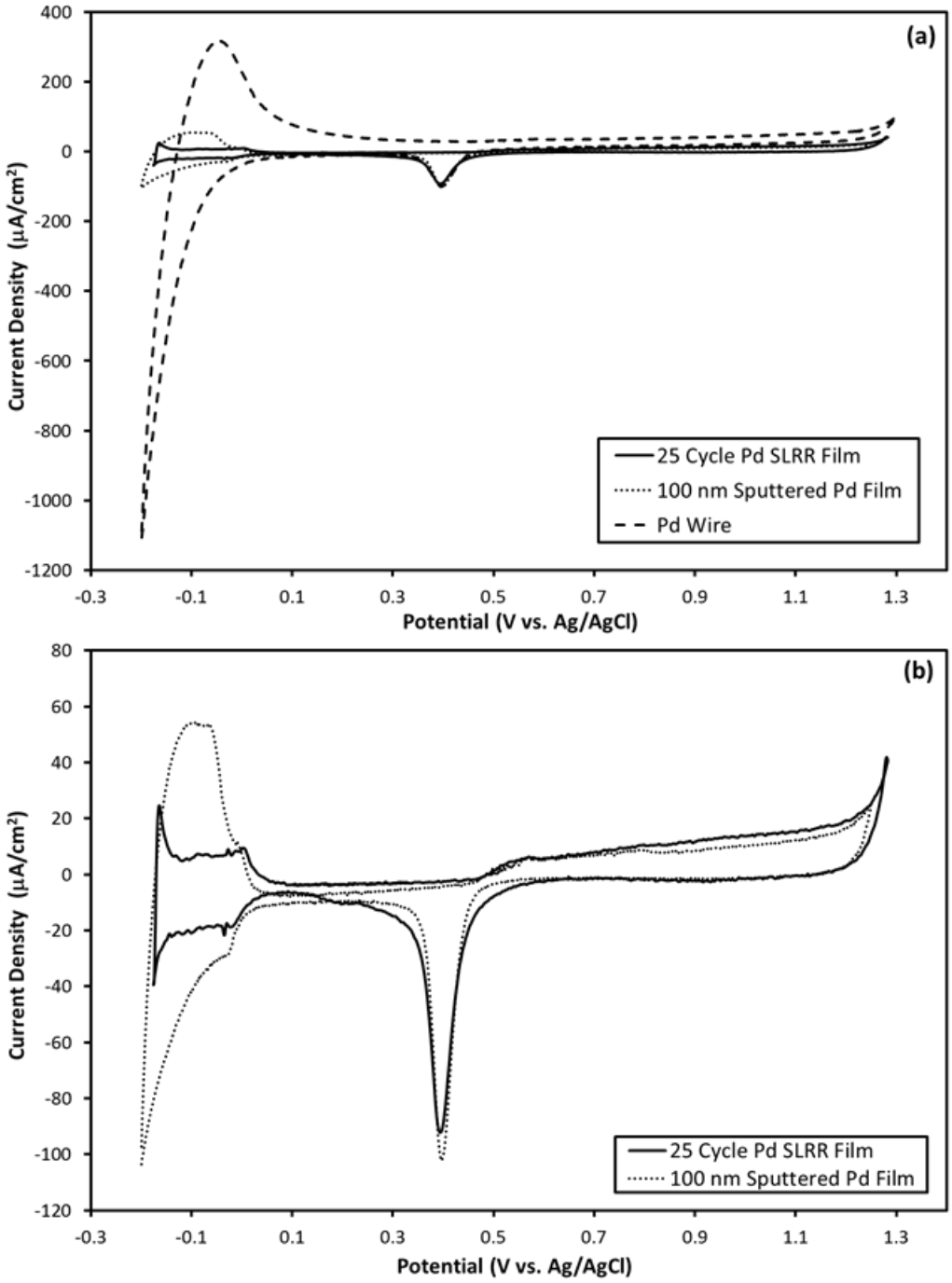

Figure 2.14 CVs of various Pd electrodes in 0.1 M H_2SO_4 at 10 mV/s. (a) Comparison of a 25 cycle E-ALD Pd film, a 100 nm sputtered Pd film and a Pd wire (d = 0.5 mm). (b) Same as in (b) without the Pd wire.

CHAPTER 3

FORMATION OF PALLADIUM NANOFILMS USING ELECTROCHEMICAL ATOMIC LAYER DEPOSITION (E-ALD) WITH CHLORIDE COMPLEXATION[2]

[2] L. B. Sheridan, D. K. Gebregziabiher, J. L. Stickney and D. B. Robinson, *Langmuir* [Online early access]. DOI: 10.1021/la303816z. Published Online: December 10, 2012.
Reprinted here with permission of the publisher.

Abstract

Pd thin films were formed by electrochemical atomic layer deposition (E-ALD) using surface limited redox replacement (SLRR) of Cu underpotential deposits (UPD) on polycrystalline Au substrates. An automated electrochemical flow deposition system was used to deposit Pd atomic layers using a sequence of steps referred to as a cycle. The initial step was Cu UPD, followed by its exchange for Pd ions at open circuit, and finishing with a blank rinse, to complete the cycle. Deposits were formed with up to 75 cycles, and displayed proportional deposit thicknesses. Previous reports by this group indicated excess Pd deposition at the flow cell ingress, from electron probe microanalysis (EPMA). Those results suggested the SLRR mechanism was not direct transfer between a Cu_{upd} atom and a Pd^{2+} ion which would take its position. Instead, it was proposed that electrons are transferred through the metallic surface to reduce Pd^{2+} ions near the surface where their activity is highest. It was proposed that if the cell was filled completely before a significant fraction of the Cu_{upd} atoms had been oxidized, the deposit would be homogeneous. Previous work with EDTA indicated the hypothesis had merit, but it proved to be highly sensitive to the EDTA concentration. In the present study chloride was used to complex Pd^{2+} ions, forming $PdCl_4^{2-}$, to slow the exchange rate. Both complexing agents led to a decrease in the rate of replacement, producing more homogeneous films. While use of EDTA improved homogeneity, it also decreased the deposit thickness by a factor of 3 compared with chloride.

Introduction

Thin films are an important part of today's technology, found in numerous applications from electronics and photonics to gas and biomedical sensors. Pd is well known for its ability to selectively and reversibly absorb large volumes of hydrogen at room temperature and atmospheric pressure, and as a suitable replacement for Pt as an electrocatalyst for many useful reactions[1]. As a result, Pd thin films have found applications in hydrogen sensors, storage devices[2-5] and as catalysts in fuel cells[6-8].

There are a wide range of methods for forming nanofilms, including various forms of physical vapor deposition (PVD), chemical vapor deposition (CVD) and molecular beam epitaxy (MBE).[9] The formation of conformal nanofilms with atomic level control can be achieved by the layer-by-layer deposition of a material in what is referred to as atomic layer deposition (ALD). [10, 11]

To discuss ALD, a few terms should be defined. ALD is a nanofilm formation methodology based on the use of surface limited reactions (SLRs). SLRs are where a reaction is limited to the top layer of a deposit, and stops when the surface has been covered. An SLR should result in deposition of an atomic layer. An atomic layer is a monolayer (ML) or less, though no more than one atom thick. A ML is a unit of coverage, atoms/cm^2, defined in surface chemistry as one adsorbate per substrate surface atom.

ALD is typically performed under vacuum at temperatures above 100 °C and involves the repeated application of SLRs to form nanometer thick films with atomic layer control of thickness[10, 11]. E-ALD is the electrochemical version of ALD, and uses electrochemical SLRs in solution to conformally deposit nanofilms.[12] Most

electrochemical SLRs involve underpotential deposition (UPD), which is an SLR driven by the free energy of formation of a surface compound or alloy. UPD involves the electrodeposition of one element on another, at a potential positive of, or "under," that needed to deposit the element on itself.[13-15] UPD results in the formation of atomic layers with coverages of a ML or less. On a Au(111) single-crystal surface, 1 ML is 1.38 x 10^{15} atoms/cm^2, or 224 $\mu C/cm^2$ for a one electron process.

E-ALD breaks atomic layer deposition into a sequence of steps. A step is the introduction of a solution, a potential change, rinse, etc. The steps needed to deposit the atomic layer compose a cycle. The number of cycles determines the deposit thickness. E-ALD is the use of UPD in a cycle to deposit nanofilms layer-by-layer.[12]

E-ALD was initially developed to form compound semiconductors. Metal nanofilms were only made possible later by the development of surface limited redox replacement (SLRR) by Brankovic et al.[16], Mrozek et al.[17], Vasilic and Dimitrov,[18] and Kim et al.[19] The SLRR cycle starts with UPD of a less noble "sacrificial" metal, which is then exchanged for a more noble metal by redox replacement at open circuit. The exchange involves oxidation of the less noble sacrificial metal, which supplies the electrons for reducing an ion of the more noble metal onto the surface. This cycle can then be repeated to grow nanofilms of the desired thickness.[20-22] At present, SLRR has been used to form nanofilms of Cu,[20, 21, 23, 24] Ag[25], Ru,[22] Pt[16, 17, 26-28], Pt/Ru[29], and Pd[30], using various experimental configurations ranging from one-cell to an automated flow-cell system.

A recent report by this group described development of an E-ALD cycle for Pd, based on SLRR, on polycrystalline Au substrates.[30]. That study highlighted the importance of the rate of exchange between the depositing metal and the sacrificial metal on the resulting film homogeneity and thickness. Initial Pd films formed in that study, using Cu_{upd} as the sacrificial metal, displayed a coverage gradient that decreased from flow cell ingress to egress. Excess growth at the ingress supported a SLRR mechanism where electrons were transferred from the sacrificial metal to depositing metal ions through the electrode, rather than directly from atom to ion. The majority of Pd^{2+} ion reduction occurred where its activity was the highest, at the flow cell ingress. The hypothesis here is that the differential deposition can be overcome by reducing the exchange rate relative to the timescale for introduction of the Pd^{2+} ion solution uniformly across the whole sample. Having homogeneous Pd^{2+} ion activity in the cell before the majority of the exchange takes place should promote a homongeneous deposit.

Similar inhomogeneity issues arose in the formation of E-ALD Cu films via SLRR on Ru/Ta[20]. Citrate was used as a complexing agent to reduce the free Cu^{2+} ion activity and thus the exchange rate relative to solution introduction, which improved deposit uniformity. The same principle was applied in the previous Pd study, [30] where Pd films were formed using Pd^{2+} ions complexed with ethylenediamine tetraacetic acid (EDTA). Those Pd films displayed improved uniformity, but at the expense of 2/3 of their thickness.[30]

The present report describes the use of Cl^- ions as an alternative Pd^{2+} complexing agent for the E-ALD formation of Pd nanofilms via SLRR. Cu_{upd} was used to form the sacrificial atomic layer on polycrystalline Au on glass electrodes. Film composition was

determined using electron probe microanalysis (EPMA) and structure with X-ray diffraction (XRD). Coulometry was used to calculate the exchange efficiency between Cu and Pd and to monitor the E-ALD process. Cyclic voltammetry (CV) was used to characterize Pd film surface chemistry.

There have been several excellent reports on the electrodeposition of Pd thin films on Au[31-34] and Pt[35, 36] single crystal surfaces. Studies by this group on the E-ALD formation of Pd nanofilms on Au single crystals are underway, and will be the topic of a subsequent report where a more direct comparison with previous atomic level work will be presented.

Experimental

Pd nanofilms were deposited on 100 nm thick polycrystalline Au on glass substrates, with a 5 nm Ti adhesion layer (EMF Corporation). Features in the CV for Au oxidation suggest a primarily Au(111) surface. An automated electrochemical flow cell deposition system[12, 37, 38] (Electrochemical ALD L.C.), based on a single variable speed pump, 5 valves, 5 solution reservoirs, a potentiostat and an electrochemical flow cell (volume ≈ 0.15 mL) were used to form all deposits. "Sequencer" E-ALD control software was used to program the deposit cycles (Electrochemical ALD L.C.). The electrochemical flow cell included an imbedded Au wire auxiliary electrode in the top face of the flow cell cavity, with the working electrode as the bottom face. The reference electrode was Ag/AgCl (3 M KCl) (Bioanalytical Systems, Inc.), housed downstream in an external compartment. Au substrates were cleaned before deposition by cycling between 1.40 V and -0.20 V in 0.1 M H_2SO_4 until a stable Au CV was obtained. The working electrode surface area was 3.5 or 2 cm^2.

A Nanopure water filtration system (Barnstead) provided 18 MΩ-cm water and was used to prepare all solutions. The initial Pd^{2+} solution composition used for E-ALD by this group was taken from a report by Sanabria-Chinchilla et al. for the electrodeposition of ultrathin Pd films on Au(332) and Au(111) single crystals[39]. It contained 0.1 mM $PdCl_2$ (Aldrich, 99.999%), 0.6 mM HCl and 0.1 M H_2SO_4 (J.T. Baker, Reagent Grade). In our group's previous studies using EDTA to complex the Pd^{2+} ions, $PdCl_2$ concentrations ranged from 0.1 to 0.2 mM and the EDTA concentration was either 0.1 or 1 mM. In the present studies, where chloride was used as the complexing agent, the solution was 0.1 mM $PdCl_2$ and 50 mM HCl. In this report solutions will be referred to by their concentration ratio, [complexing agent] / [Pd^{2+}]. For example: the solution containing 0.1 mM EDTA and 0.1 mM $PdCl_2$ will be written as [EDTA] / [Pd^{2+}] = 1 , while 0.6 mM HCl and 0.1 mM $PdCl_2$ will be [Cl^-] / [Pd^{2+}] = 8. All Pd solutions were adjusted to pH 1.5 with H_2SO_4. The sacrificial metal ion solution was 2 mM $CuSO_4$ (J.T. Baker, 99.8%) in 0.1 M H_2SO_4, pH 1.2, and the blank solution was 0.1 M H_2SO_4. All solutions were degassed using N_2 to minimize dissolved O_2, prior to electrochemical studies. All potentials are reported versus Ag/AgCl (3 M KCl). EPMA data was collected using a JEOL 8600 wavelength-dispersive scanning electron microprobe, which generated data in terms of atomic percent (atomic %) assuming the sample was a homogeneous alloy, rather than a nanofilm of Pd on Au. Experience has shown that the atomic percent (atomic %) for nanofilms scale linearly with coverage for deposits up to about 30 nm. The minimum detection limits (MDL), in atomic % for the EPMA studies were 0.3% for Pd and 1% for Cu. Glancing-angle XRD patterns were obtained using a

PANalytical X'Pert PRO MRD diffractometer, with Cu Kα radiation (λ= 1.5418 Å) and an incident angle of 1°.

Results and Discussion

A diagram of the automated electrochemical flow cell deposition system has been reported.[30] Figure 3.1 is a schematic of the Pd SLRR method. Figure 3.2 displays current and potential vs. time plots for two E-ALD cycles. The Cu^{2+} solution was rinsed into the cell at 17 mL/min and held at 0.15 V for 18 s to form the sacrificial UPD atomic layer. The charge was 1.3 mC, corresponding to $2x10^{-9}$ mol Cu/cm^2 or $1x10^{15}$ atoms/cm^2, corresponding to a coverage of 0.8 ML vs. Au(111). It is assumed that the charge for Cu deposition approaches zero by the end of the step. The behavior of Cu as a sacrificial metal is relatively well understood and has been used in the deposition of Ag[16], Pt[16, 17, 29, 40], and Pd[16, 17, 41] on Au. The Pd^{2+} ion solution was then introduced at open circuit and allowed to exchange with the Cu_{upd} to form a Pd atomic layer. The open circuit potential (OCP) was observed to drift positive until reaching the stop potential, 0.4 V. The stop potential was set in the software and triggered an OCP blank rinse to remove any remaining Pd^{2+} or Cu^{2+} ions. Note that although the stop potential was set to 0.4 V the potential continued to increase to 0.53 as the blank solution was flushed into the cell, corresponding to the onset of Pd oxidation, while the blank solution was flushed into the cell. In the present studies, the cycle was generally repeated 25 times. Current and potential vs. time data was collected for all 25 cycles to aid in optimization of cycle parameters.

Comparison of complexing agents

The E-ALD cycle described above was developed in an earlier study of Pd nanofilm formation.[30] This report concerns optimization of the complexing agent to improve E-ALD film uniformity. Previously[30], Pd E-ALD films were grown from a $PdCl_2$ solution containing 0.6 mM HCl and 0.1 M H_2SO_4.[39] EPMA results in Figure 3.3 (●), show that deposition was inhomogeneous across the deposit, with excess at the ingress, decreasing towards the egress. EDTA, a well understood complexing agent, was added to the $PdCl_2$ solution to decrease the rate of the exchange reaction, relative to the solution exchange time, and resulted in increased homogeneity. Various EDTA to Pd^{2+} concentration ratios were examined, with [EDTA] / [Pd^{2+}] = 1 resulting in the most homogeneous films, though the overall Pd coverage was suppressed (Figure 3.3, ■).[30] EPMA results showed an average Pd atomic % (relative thickness) of ~1.5 for a 25 cycle deposit. Previous studies suggest that a 25 cycle deposit should be closer to 4 atomic %.[27, 29] In the present study, it was hypothesized that a more labile complexing agent than EDTA would offer increased flexibility for optimizing the exchange kinetics relative to the rate of solution introduction.

Acidic chloride baths for electrodeposition of dense, crack-free Pd films have been used for decades.[42] Over the last two decades, Uosaki et al[43, 44] and Kolb et al[45, 46] have extensively studied the deposition of Pd on Au single crystals from solutions containing $PdCl_4^{2-}$. Both found that the $PdCl_4^{2-}$ complex promoted the formation of high quality deposits. Pd forms thermodynamically stable, yet kinetically labile, complexes with chloride of the general form $[PdCl_n(H_2O)_{4-n}]^{2-n}$ (n=0–4), for which the overall stability constant (β_4 or K_f) is $10^{11.5}$.[47-49] Several values of the formal

reduction potential ($E^{0'}$) for Pd from $PdCl_4^{2-}$ (1 M Cl^-) have been reported, and all are near 0.4 V vs. Ag/AgCl[42, 50], ~0.3 V negative of the standard reduction potential for the Pd^{2+}_{aq} (E^0), 0.7 V.[51] Formation of the palladium-chloride complex shifts the reduction potential negative by decreasing the concentration of free Pd^{2+} ions. The previous Pd E-ALD deposition studies [30] used a $[Cl^-]/[Pd^{2+}]$ ratio of 8 [39]. The results shown in Figure 3.3(●), display a significant gradient in deposit thickness, suggesting the exchange rate was too fast with this degree of complexation. It was anticipated that a further increase in the $[Cl^-]$ would decrease the free Pd^{2+} ions available, slowing the exchange process. Using a $[Cl^-] / [Pd^{2+}] = 500$ (Figure 3.3(▲)) resulted in a dramatic improvement in homogeneity.

Figure 3.3 shows that films formed using $[Cl^-] / [Pd^{2+}] = 8$ (●) are inhomogeneous, while those formed using $[Cl^-] / [Pd^{2+}] = 500$ (▲) and $[EDTA] / [Pd^{2+}] = 1$ (■) show good uniformity from ingress to egress. The Pd film formed in the presence of chloride had a relative Pd thickness of ~5 atomic %, while that formed in the presence of EDTA was ~1.5 atomic %. β_4 for $PdCl_4^{2-}$ is $10^{11.5}$ while at pH 2 the conditional complex formation constant (K_f') for $Pd(EDTA)^{2-}$ is 8×10^{12}, indicating the formation of complexes of similar stability. [52] However, the $[Cl^-] / [Pd^{2+}] = 500$ complex resulted in a significantly thicker film when compared to that formed using the $[EDTA] / [Pd^{2+}] = 1$ complex. It is proposed that the differences in deposit thicknesses result from differences in the lability of the complexes. Stable and unstable are thermodynamic terms, while the terms labile and inert refer to kinetics.[36] According to the literature, $PdCl_4^{2-}$ is considered labile while $Pd(EDTA)^{2-}$ is relatively inert [49, 53, 54], accounting for the dearth of Pd^{2+} ions deposited from the $Pd(EDTA)^{2-}$ complex.

Figure 3.4 demonstrates the effect of the solution composition on the exchange rate. At time zero the cell switches to open circuit and the Pd solution is introduced. The table inset in Figure 3.4 lists the times required for the OCP to change by 0.1V, denoted ΔE. When the chloride concentration is low (Solution 1:----) the OCP changes by 0.1 V in less than 7 s, while it takes ~5 s to fill the cell with the Pd ion solution for the exchange. This suggests that by the time the Pd ion solution has fully replaced the Cu ion solution, the majority of the Cu has oxidized, most likely reducing Pd ions to Pd^0. The result is that most of the deposition process occurs for solution 1 while the solution is exchanged and a gradient in Pd ion concentration is present in the cell. If electron transfer is from the electrode, not individual atoms, and the highest Pd ion concentration is initially at the ingress, then so will be the majority of the deposition, creating the gradient seen in Figure 3.3 (●). Figure 3.5 shows three possible schemes for the transfer of electrons between Cu_{UPD} and Pd^{2+} during SLRR. Scheme (A) illustrates homogeneous distribution of Pd from the flow-cell ingress to egress when electrons are transferred directly from a Cu_{UPD} atom to a Pd^{2+} ion. Schemes (B) and (C) present two different scenarios for indirect transfer of electrons from Cu_{UPD} to Pd^{2+} through the metal electrode. In (B), insufficient Pd^{2+} complexation leads to inhomogeneous distribution of Pd from the ingress to egress, while in (C) the complexation of Pd^{2+} is sufficient enough to slow down the exchange and generate a homogeneous deposit.

When the $[Cl^-]/[Pd^{2+}]$ is increased from 8 to 500 (Solution 3:·····), the ΔE increases from 7 to 40 s, suggesting that the exchange reaction is $1/6^{th}$ as fast, which allows exchange of the solutions while a majority of the sacrificial Cu atomic layer is still present on the surface, as depicted in Figure 3.5 (C). It is this situation which affords a

more homogeneous deposit from ingress to egress. Solutions 2 (—) and 3(·····) display similar behavior up to 0.25 V, though Solution 2 is clearly slower from 0.25V to 0.5V. This decrease in exchange rate for Solution 2 is probably related to the lower Pd coverages observed when it is used (Figure 3.3). This raises questions concerning why the deposits are thinner when EDTA is used, and where the electrons from the Cu sacrificial layer go. It appears that the EDTA complex with Pd^{2+} ions are so stable that an alternative oxidizing agent must be present to dissolve the rest of the Cu_{upd} sacrificial layer. The most likely species is residual traces of O_2 left after sparging or picked up through the tubing or flow cell.

All subsequent deposits in this report will focus on films grown using the $[Cl^-]$ / $[Pd^{2+}]$ = 500 solution, as it produces homogeneous deposits of a reasonable thickness. That is, the atomic % of Pd from EPMA for a 25 cycle deposit is similar to those recorded for E-ALD of other metals by this group.[55]

Optimization of Pd films formed using $PdCl_4^{2-}$

In E-ALD, coulometry is frequently used as an indicator of layer-by-layer growth. The current and potential vs. time data are used to calculate the sacrificial metal coverage for each cycle, and should result in a constant coverage from cycle to cycle, for a layer-by-layer process. Cu coulometric data for the formation of films with 10 and 60 s rinses is shown in Figure 3.6. Initially, the two curves follow the same trend, leveling out after about 4 cycles, where the changes in coverage during those 4 cycles probably result from differences in Cu affinity for Au vs. Pd, and thus the observed small systematic increases in UPD coverage. Beyond 18 cycles, both samples showed systematic Cu coverage increases from cycle to cycle, suggesting surface roughening. Possible reasons for

surface roughening during an SLRR include: deposition of more than a ML of sacrificial metal each cycle, 3D nucleation and growth or excessive adsorption and deposition of reactants. The Cu coverages where rinses were 60 s always resulted in less than a ML/cycle, as expected using a UPD potential. However, with a 10 s rinse, the incremental increases in coverage were three times that for 60 s. With 10 s rinses the Cu coverage/cycle exceeded a ML after 35 cycles. Considering the possible reasons above for increases in Cu coverage from cycle to cycle, bulk Cu deposition is not possible, due to the use of an underpotential. Based on the literature for Pd deposition on Au from Cl^- containing solutions, 3D nucleation and growth (Volmer-Weber or Stranski-Krastanov growth modes[56]) are highly unlikely.[34, 46, 57] However, much of the same literature suggests that adlayers of $PdCl_4^{2-}$ ions form on Au and Pd substrates[32, 44, 58], which could result in excess Pd electrodeposition if the adlayer is not removed during rinsing. After about 18 cycles the two curves begin to diverge, deposits formed with 10s rinses slowly increase in coverage each cycle, while deposits formed with 60 s rinses (nearly 24 cell volumes of blank) resulted in only 29% of the increase in Cu_{upd}, between the 18^{th} and 50^{th} cycle, than that experienced with 10s rinses. These results show that longer blank rinses lead to less roughening in the Pd films, suggesting that the $PdCl_4^{2-}$ ions were strongly adsorbed in these studies.

Similar results were observed for the formation of E-ALD Pt films via SLRR using Cu as a sacrificial metal.[55] Insufficient rinsing left Pt precursor ions adsorbed on the surface, which were subsequently electrodeposited when the potential was dropped for the Cu UPD step. The result was excess Pt deposition and surface roughening. The excess Pt was avoided by increasing the time for the blank rinse and by selection of a

lower stop potential (where the coulombic interaction of the surface with the anionic Pt precursor ions was reduced).

In an effort to quantify any contribution to the Pd coverage by adsorbed Pd ions present when the potential was dropped for the Cu UPD step, the experiments shown in Figure 3.7 were run. Prior to the Cu UPD step, the potential was held at 0.15V (the Cu UPD potential), with blank flowing for 10 seconds. After the additional 10 seconds of blank rinse at 0.15V, the Cu^{2+} solution was introduced, resulting in Cu_{upd} formation. Figure 3.7 displays current and potential vs. time data for films grown using 10s (**A**) and 60s (B) of blank rinse prior to the two part Cu UPD step. Integration of the charges after the potential was dropped to 0.15V in blank gave charges equivalent to 0.2 and 0.1 ML (or 75 and 44 $\mu C/cm^2$) for 10 and 60 s rinse times, respectively. Double layer charging could account for about ~10-20 $\mu C/cm^2$, and together with reduction of traces of O_2 the 44 $\mu C/cm^2$ could be accounted for. The higher value for the 10s rinse suggests the difference was deposition of adsorbed Pd precursor ions. It is thus suggested here that the increase in Cu_{upd} as a function of cycle number seen in Figure 3.6 is caused by the accumulation of this excess Pd. It might be asked why this excess Pd roughens the surface, while that deposited at open circuit during the exchange of Cu did not? The difference is that the Pd deposited during the exchange was deposited at equilibrium, where there was an exchange current, and atoms were more likely to obtain optimal sites. On the other hand, the excess Pd from adsorbed Pd ions was deposited at an overpotential, where the exchange current was too small, so atoms deposit where they hit, and there is very little mobility, thus the observed roughening. All deposits described subsequently in this report use 60s rinses.

The possibility that Cu can become incorporated into the Pd deposits was also considered, as it has been seen using SLRR by Fayette et al.[26] for Pt nanofilm deposition. Initially EPMA analysis was used to characterize film composition, though signals for Cu were typically below the MDL[30], however use of XPS to analyze 15 and 25 cycle deposits indicated the presence of trace amounts of Cu in the films: ~0.9 and 1.7% Cu respectively.

Figure 3.8 is a plot of the Pd coverage determined by Pd oxidation coulometry in ML (versus Au(111)) as a function of the number of E-ALD cycles performed. Deposits were immediately stripped in 0.1 M HCl by scanning at 5 mV/s from 0.15 to 0.78 V. The linear relationship expected for ALD was observed, suggesting a layer-by-layer growth mode for films formed with up to 75 cycles.

Determining how many Cu atoms are replaced by Pd atoms, the exchange efficiency, aids understanding of the SLRR mechanism. Assuming that Cu is oxidized to Cu^{2+} and that $PdCl_4^{2-}$ is Pd(II), an exchange efficiency of 100% means the charge for Cu deposition is equivalent to that for Pd stripping, and that no side reactions, such as O_2 reduction, are important. Figure 3.9 displays anodic stripping for films ranging from 5 to 50 cycles in thickness. The average exchange efficiency was 95 ± 6%, a value close to 100%, with variation likely resulting from background subtractions for the coulometry.

Note, dissolved oxygen should be removed from all solutions prior to deposition for accurate coulometry and to avoid side reactions. Control experiments indicated that lower Pd coverages resulted when N_2 degassing was incomplete. The authors believe this results from some Cu electrons reducing O_2, rather than Pd^{2+}, given that O_2 starts to

reduce at about 0.15 V, where Cu_{UPD} was formed. The net result is a lower calculated exchange efficiency and thinner Pd deposit.

Characterization of Pd SLRR Films formed using $PdCl_4^{2-}$

Figure 3.10 (A) shows a CV in 0.1 M H_2SO_4, for a 25 cycle Pd E-ALD film. Oxide formation begins at ~ 0.45 V with its corresponding reduction at ~ 0.46 V. These features agree with those for bulk Pd, as well as E-ALD Pd films formed using $Pd(EDTA)^{2-}$.[30] When comparing Pd CVs note that the position of the oxide reduction peak is dependent on the positive potential limit; the reduction shifts negatively as the positive limit increases.[59] Since the potential was scanned positively to 1.1 V, any exposed Au would have begun to oxidize. The lack of a reduction peak at ~ 0.9 V verifies that the Pd film covers the entire Au substrate. At more negative potentials hydrogen sorption and desorption take place. The features labeled 1 and 4 correspond to hydrogen adsorption and desorption, while those labeled 2 and 3 are due to hydrogen absorption/desorption. Figure 3.10 (B) compares the hydrogen sorption/desorption region of the same 25 cycle Pd E-ALD film shown in part (A) with a 100 nm sputtered Pd film. The most notable difference is the earlier onset of hydrogen absorption into the bulk of the 100 nm Pd film, which overlaps with surface adsorption, causing the peaks for hydrogen adsorption and desorption to appear as shoulders on the principal absorption/desorption peaks. The separation of the features for surface adsorption from bulk absorption is one of the advantages of studying Pd nanofilms rather than bulk Pd electrodes.[60, 61] The separation of adsorption and absorption is also characteristic of nanoporous Pd films[62] and nanoparticles[63].

Figure 3.11 shows the results of XRD analysis of a 75 cycle Pd E-ALD film on Au. XRD, which samples the Pd and Au bulk polycrystalline structures, indicates a predominance of Au(220) planes parallel to the substrate, demonstrated by the prominent (220) peak. The (220) peak is also the most intense Pd peak, suggesting the Pd(220) planes are parallel with the Au(220) planes, an indication that some epitaxial relationship exists. CV of the polycrystalline Au substrates implied primarily Au(111) oriented surface structure, as evidenced by the shape of Au oxidation features.[64] Work to be published later by our group involves the use of Au(111) single crystals, and the CVs of the oxide region are closely matched to the present polycrystalline Au CVs.

Conclusion

Improved ability to fabricate uniform Pd nanofilms via E-ALD using SLRR of Cu_{UPD} on polycrystalline Au electrodes was demonstrated. The deposition showed characteristics of true atomic layer growth, with greater efficiency than previously demonstrated. Chloride is an effective Pd^{2+} complexing agent, but it must be present at a significant excess. Films formed using low concentrations of Cl^- ($[Cl^-] / [Pd^{2+}] = 8$) resulted in excess deposition near the flow cell ingress. This implies a non-local SLRR mechanism where electron transfer is mediated by charge passage through the electrode, rather than directly from atom to ion. Use of higher concentrations of Cl^- ($[Cl^-] / [Pd^{2+}] = 500$) decreased the Pd-for-Cu exchange rate relative to the rate of Pd ion solution introduction into the cell. Slowing the exchange rate improved film uniformity across the deposit. That is, the more homogeneous the $[Pd^{2+}]$ in the cell, prior to the majority of the exchange, the more homogeneous the resulting deposit.

An earlier study using EDTA as a Pd^{2+} complexing agent showed similar improvements in homogeneity, though the resulting films were only a 1/3 as thick as those formed here using the Cl^- complex. The decreased thickness with EDTA is proposed to result from the low lability of the $Pd(EDTA)^{2-}$ complex, relative to $PdCl_4^{2-}$.

Comparing the coulometry for Cu_{UPD} with anodic stripping of the resulting Pd films indicated an exchange efficiency for the replacement of 95 ± 6%. A clear distinction between hydrogen adsorption and absorption was evident in CVs for a 25 cycle film, and there was no evidence of exposed Au. XRD of a 75 cycle Pd film showed it to be polycrystalline with a predominant (220) orientation. The Au substrate was also predominantly (220), implying an epitaxial deposit.

Acknowledgements

Acknowledgment is made of the support of the National Science Foundation, Division of Materials Research #1006747, as well as Sandia National Laboratories, a multi-program laboratory managed and operated by Sandia Corporation, a wholly owned subsidiary of Lockheed Martin Corporation, for the U.S. Department of Energy's National Nuclear Security Administration under contract DE-AC04-94AL85000.

References

1. Adams, B.D. and A.C. Chen, *The role of palladium in a hydrogen economy.* Materials Today, 2011. **14**(6): p. 282-289.
2. Randler, R.J., et al., *Electrochemical copper deposition on Au(100): a combined in situ STM and in situ surface X-ray diffraction study.* Surface Science, 2000. **447**(1-3): p. 187-200.
3. Noh, J.S., J.M. Lee, and W. Lee, *Low-Dimensional Palladium Nanostructures for Fast and Reliable Hydrogen Gas Detection.* Sensors, 2011. **11**(1): p. 825-851.
4. Niessen, R.A.H., P. Vermeulen, and P.H.L. Notten, *The electrochemistry of Pd-coated MgySc(1-y) thin film electrodes: A thermodynamic and kinetic study.* Electrochimica Acta, 2006. **51**(12): p. 2427-2436.
5. Tan, Z.P., et al., *Thermodynamics, kinetics and microstructural evolution during hydrogenation of iron-doped magnesium thin films.* International Journal of Hydrogen Energy, 2011. **36**(16): p. 9702-9713.
6. Lai, B.K., K. Kerman, and S. Ramanathan, *Methane-fueled thin film micro-solid oxide fuel cells with nanoporous palladium anodes.* Journal of Power Sources, 2011. **196**(15): p. 6299-6304.
7. Kang, S., et al., *Low intermediate temperature ceramic fuel cell with Y-doped BaZrO(3) electrolyte and thin film Pd anode on porous substrate.* Electrochemistry Communications, 2011. **13**(4): p. 374-377.
8. Zhang, J.T., et al., *Facile fabrication and unexpected electrocatalytic activity of palladium thin films with hierarchical architectures.* Journal of Physical Chemistry C, 2008. **112**(36): p. 13970-13975.

9. Barlow, F., Elshabini-Riad, Aicha, Brown, R., *Film Deposition Techniques and Processes*, in *Thin Film Technology Handbook*, F. Barlow, Elshabini-Riad, Aicha, Editor. 1997, McGraw-Hill: New York.

10. *Electrochemical Society Transactions*. Atomic Layer Deposition Applications 3, ed. A. Londergan, Elam, J.W., van der Straten, O., De Gendt, S. Bent, S.F., Kang, S.B. Vol. 11 no. 7. 2007, Pennington: The Electrochemical Society.

11. George, S.M., *Atomic Layer Deposition: An Overview.* Chemical Reviews, 2010. **110**(1): p. 111-131.

12. Stickney, J.L., *Electrochemical Atomic Layer Epitaxy (EC-ALE): Nanoscale Control in the Electrodeposition of Compound Semiconductors*, in *Advances in Electrochemical Science and Engineering*, R.C.A.a.D.M. Kolb, Editor. 2002, Wiley-VCH: Weinheim.

13. Adzic, R.R., *Electrocatalytic Properties of the Surfaces Modified by Foreign Metal Adatoms* Advances in Electrochemistry and Electrochemical Engineering, ed. H.G.a.C.W. Tobias. Vol. 13. 1984, New York: Wiley-Interscience. 159-260.

14. Herrero, E., L.J. Buller, and H.D. Abruna, *Underpotential deposition at single crystal surfaces of Au, Pt, Ag and other materials.* Chemical Reviews, 2001. **101**(7): p. 1897-1930.

15. Kolb, D.M., *Advances in Electrochemistry and Electrochemical Engineering*, ed. H.G.a.C.W. Tobias. Vol. 11. 1978, New York: John Wiley. 125.

16. Brankovic, S.R., J.X. Wang, and R.R. Adzic, *Metal monolayer deposition by replacement of metal adlayers on electrode surfaces.* Surface Science, 2001. **474**(1-3): p. L173-L179.

17. Mrozek, M.F., Y. Xie, and M.J. Weaver, *Surface-enhanced Raman scattering on uniform platinum-group overlayers: Preparation by redox replacement of underpotential-deposited metals on gold.* Analytical Chemistry, 2001. **73**(24): p. 5953-5960.

18. Vasilic, R. and N. Dimitrov, *Epitaxial growth by monolayer-restricted galvanic displacement.* Electrochemical and Solid State Letters, 2005. **8**(11): p. C173-C176.

19. Kim, Y.G., et al., *Platinum nanofilm formation by EC-ALE via redox replacement of UPD copper: Studies using in-situ scanning tunneling microscopy.* Journal of Physical Chemistry B, 2006. **110**(36): p. 17998-18006.

20. Thambidurai, C., et al., *E-ALD of Cu Nanofilms on Ru/Ta Wafers Using Surface Limited Redox Replacement.* Journal of the Electrochemical Society, 2010. **157**(8): p. D466-D471.

21. Thambidurai, C., et al., *Copper Nanofilm Formation by Electrochemical ALD.* Journal of the Electrochemical Society, 2009. **156**(8): p. D261-D268.

22. Thambidurai, C., Y.G. Kim, and J.L. Stickney, *Electrodeposition of Ru by atomic layer deposition (ALD).* Electrochimica Acta, 2008. **53**(21): p. 6157-6164.

23. Gebregziabiher, D.K., et al., *Electrochemical atomic layer deposition of copper nanofilms on ruthenium.* Journal of Crystal Growth, 2010. **312**(8): p. 1271-1276.

24. Viyannalage, L.T., R. Vasilic, and N. Dimitrov, *Epitaxial growth of Cu on Au(111) and Ag(111) by surface limited redox replacement - An electrochemical and STM study.* Journal of Physical Chemistry C, 2007. **111**(10): p. 4036-4041.

25. Vasilic, R., L.T. Viyannalage, and N. Dimitrov, *Epitaxial growth of Ag on Au(111) by galvanic displacement of Pb and Tl monolayers.* Journal of the Electrochemical Society, 2006. **153**(9): p. C648-C655.

26. Fayette, M., et al., *From Au to Pt via Surface Limited Redox Replacement of Pb UPD in One-Cell Configuration.* Langmuir, 2011. **27**(9): p. 5650-5658.

27. Jayaraju, N., et al., *Electrochemical Atomic Layer Deposition (E-ALD) of Pt Nanofilms Using SLRR Cycles.* Journal of the Electrochemical Society, 2012. **159**(10): p. D616-D622.

28. McCurry, D.A., et al., *All Electrochemical Fabrication of a Platinized Nanoporous Au Thin-Film Catalyst.* Acs Applied Materials & Interfaces, 2011. **3**(11): p. 4459-4468.

29. Jayaraju, N., *Electrochemical atomic layer deposition (E-ALD) of Pt and PtRu nanofilms*, in *Chemistry*. 2010, University of Georgia: Athens.

30. Sheridan, L.B., Czerwiniski, J.; Jayaraju, N.; Gebregziabiher, D. K.; Stickney, J. L.; Robinson, D. B. and Soriaga, M. P., *Electrochemical Atomic Layer Deposition (E-ALD) of Palladium Nanofilms by Surface Limited Redox Replacement (SLRR), with EDTA Complexation.* Electrocatalysis, 2012. **3**(2): p. 96-107.

31. Tang, J., et al., *Pd deposition onto Au(111) electrodes from sulphuric acid solution.* Electrochimica Acta, 2005. **51**(1): p. 125-132.

32. Kibler, L.A., et al., *Initial stages of Pd deposition on Au(hkl) - Part I: Pd on Au(111).* Surface Science, 1999. **443**(1-2): p. 19-30.

33. Quayum, M.E., S. Ye, and K. Uosaki, *Mechanism for nucleation and growth of electrochemical palladium deposition on an Au(111) electrode.* Journal of Electroanalytical Chemistry, 2002. **520**(1-2): p. 126-132.

34. Takahasi, M., et al., *Pseudomorphic growth of Pd monolayer on Au(111) electrode surface.* Surface Science, 2000. **461**(1-3): p. 213-218.

35. Lebouin, C., et al., *Electrochemically elaborated palladium nanofilms on Pt(111): Characterization and hydrogen insertion study.* Journal of Electroanalytical Chemistry, 2009. **626**(1-2): p. 59-65.

36. Baricuatro, J.H., et al., *UHV-EC Characterization of Ultrathin Films Electrodeposited on Well-Defined Noble Metals. I: Pd on Pt(111).* Electrocatalysis, 2010. **1**(1): p. 28-33.

37. Wade, T.L., T.A. Sorenson, and J.L. Stickney, *Interfacial Electrochemistry*, ed. A. Wieckowski. 1999, New York: Marcel Dekker.

38. Stickney, J.L., *Electrochemical atomic layer epitaxy*, in *Electroanalytical Chemistry, Vol 21*, A.J.B.a.I. Rubinstein, Editor. 1999, Marcel Dekker, Inc.: New York. p. 75-209.

39. Sanabria-Chinchilla, J., et al., *Electrocatalytic hydrogenation and oxidation of aromatic compounds studied by ITEMS: Benzene and p-dihydroxybenzene at ultrathin Pd films electrodeposited on Au(hkl) surfaces.* Journal of Colloid and Interface Science, 2007. **314**(1): p. 152-159.

40. Gokcen, D., S.E. Bae, and S.R. Brankovic, *Stoichiometry of Pt Submonolayer Deposition via Surface-Limited Redox Replacement Reaction.* Journal of the Electrochemical Society, 2010. **157**(11): p. D582-D587.

41. Ghodbane, O., L. Roue, and D. Belanger, *Study of the electroless deposition of Pd on Cu-modified graphite electrodes by metal exchange reaction.* Chemistry of Materials, 2008. **20**(10): p. 3495-3504.

42. Dullaghan, J.A.A.a.C.A., *Electrodeposition of Palladium and Palladium Alloys*, in *Modern Electroplating*, M.S.a.M. Paunovic, Editor. 2000, John Wiley & Sons, Inc.: New York. p. 483-554.

43. Takahasi, M., et al., *Orientation dependence of Pd growth on Au electrode surfaces.* Journal of Physics-Condensed Matter, 2010. **22**(47).

44. Naohara, H., S. Ye, and K. Uosaki, *Electrochemical layer-by-layer growth of palladium on an Au(111) electrode surface: Evidence for important role of adsorbed Pd complex.* Journal of Physical Chemistry B, 1998. **102**(22): p. 4366-4373.

45. Kibler, L.A., A.M. El-Aziz, and D.M. Kolb, *Electrochemical behaviour of pseudomorphic overlayers: Pd on Au(111).* Journal of Molecular Catalysis a-Chemical, 2003. **199**(1-2): p. 57-63.

46. Baldauf, M. and D.M. Kolb, *A Hydrogen Adsorpiton and Absorption Study with Ultrathin Pd Overlayers on Au(111) and Au(100)* Electrochimica Acta, 1993. **38**(15): p. 2145-2153.

47. Cruywagen, J.J. and R.J. Kriek, *Complexation of palladium(II) with chloride and hydroxide.* Journal of Coordination Chemistry, 2007. **60**(4): p. 439-447.

48. Elding, L.I., *Palladium(II) halide complexes. I. Stabilities and spectra of palladium(II) chloro and bromo aqua complexes.* Inorganica Chimica Acta, 1972. **6**(0): p. 647-651.

49. Basolo, F., *Mechanisms of inorganic reactions; a study of metal complexes in solution*. 2d ed. ed, ed. R.G. Pearson. 1967, Wiley: New York.

50. Templeton, D.H., G.W. Watt, and C.S. Garner, *The Formal Electrode Potentials of Palladium in Aqueous Hydrochloric and Perchloric Acid Solutions. Stability of Chloropalladite Ion1*. Journal of the American Chemical Society, 1943. **65**(8): p. 1608-1612.

51. Izatt, R.M., D. Eatough, and Christen.Jj, *A Study of Pd2+(Aq) Hydrolysis. Hydrolysis Constants and Standard Potential for Pd Pd2+ Couple.* Journal of the Chemical Society a -Inorganic Physical Theoretical, 1967(8): p. 1301-&.

52. Kragten, J., *The stability constant of Pd-EDTA.* Talanta, 1978. **25**(4): p. 239-240.

53. Aochi, Y.O. and D.T. Sawyer, *Proton Nuclear Magnetic Resonance Studies of Ethylenediaminetetraacetic Acid Complexes of Zirconium(4), Hafnium(4) and Palladium(2) S.* Inorganic Chemistry, 1966. **5**(12): p. 2085-2092.

54. Ware, M.J., *An Investigation of Platinum and Palladium Printing* Journal of Photographic Science, 1986. **34**(5-6): p. 13-25.

55. Nagarajan Jayaraju, D.V., Youn Guen Kim, Dhego Banga, and John L Stickney, *Electrochemical Atomic Layer Deposition (ALD) of Pt Nanofilms.* Journal of the Electrochemical Society, Under Review. **XX**.

56. Venables, J., *Introduction to surface and thin film processes*. 2000, Cambridge University Press: Cambridge ;.

57. Kibler, L.A., et al., *Initial stages of palladium deposition on Au(h k l) Part III: Pd on Au(110).* Surface Science, 2002. **498**(1-2): p. 175-185.

58. Naohara, H., S. Ye, and K. Uosaki, *Epitaxial growth of a palladium layer on an Au(100) electrode.* Journal of Electroanalytical Chemistry, 1999. **473**(1-2): p. 2-9.

59. Grden, M., et al., *Electrochemical behaviour of palladium electrode: Oxidation, electrodissolution and ionic adsorption.* Electrochimica Acta, 2008. **53**(26): p. 7583-7598.

60. Lukaszewski, M., K. Hubkowska, and A. Czerwinski, *Electrochemical absorption and oxidation of hydrogen on palladium alloys with platinum, gold and rhodium.* Physical Chemistry Chemical Physics, 2010. **12**(43): p. 14567-14572.

61. Czerwinski, A., et al., *The study of hydrogen sorption in palladium limited volume electrodes (Pd-LVE) I. Acidic solutions.* Journal of Electroanalytical Chemistry, 1999. **471**(2): p. 190-195.

62. Bartlett, P.N., et al., *The preparation and characterisation of H-1-e palladium films with a regular hexagonal nanostructure formed by electrochemical deposition from lyotropic liquid crystalline phases.* Physical Chemistry Chemical Physics, 2002. **4**(15): p. 3835-3842.

63. Tateishi, N., et al., *Electrochemical properties of ultra-fine palladium particles for adsorption and absorption of hydrogen in an aqueous HClO4 solution.* Electrochimica Acta, 1991. **36**(7): p. 1235-1240.

64. Hamelin, A., *Cyclic voltammetry at gold single-crystal surfaces .1. Behaviour at low-index faces.* Journal of Electroanalytical Chemistry, 1996. **407**(1-2): p. 1-11.

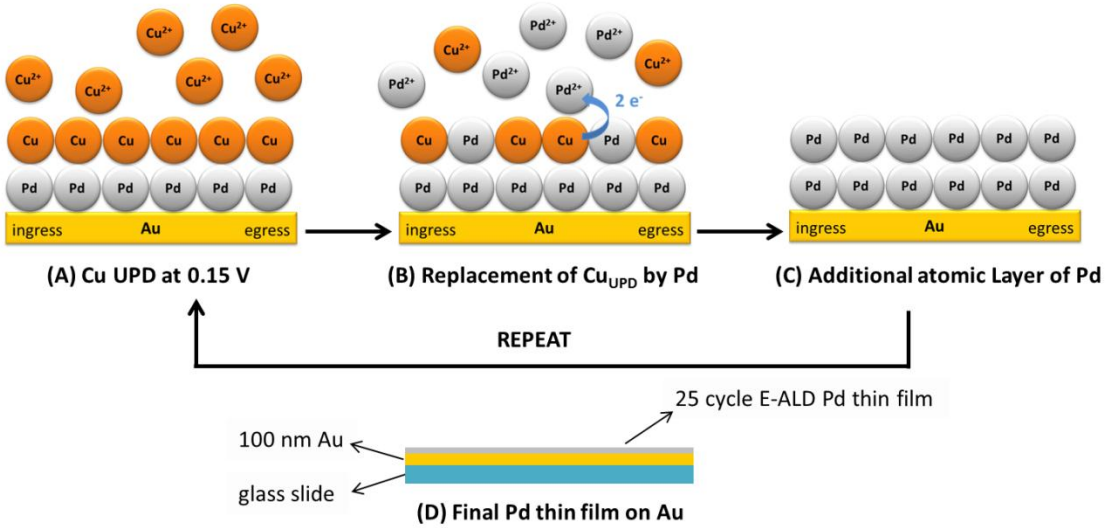

Figure 3.1 Schematic for the formation of an E-ALD Pd film on gold using SLRR. Note that the first atomic layer of Pd is formed by replacement of Cu_{UPD} deposited directly on Au.

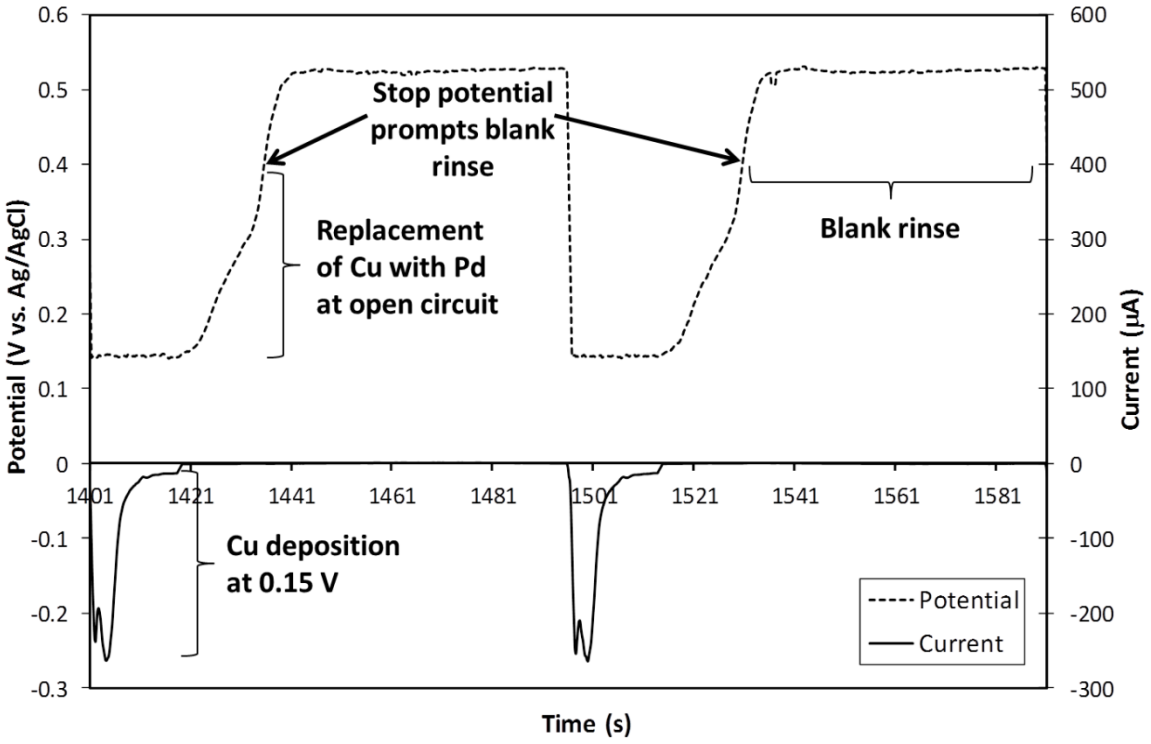

Figure 3.2 Time-Potential-Current plot showing two cycles of Pd SLRR. Cu UPD was deposited at 0.15 V and replaced by Pd^{+2} until reaching an OCP of 0.4 V. The cell remained at open circuit for a 60 s blank rinse.

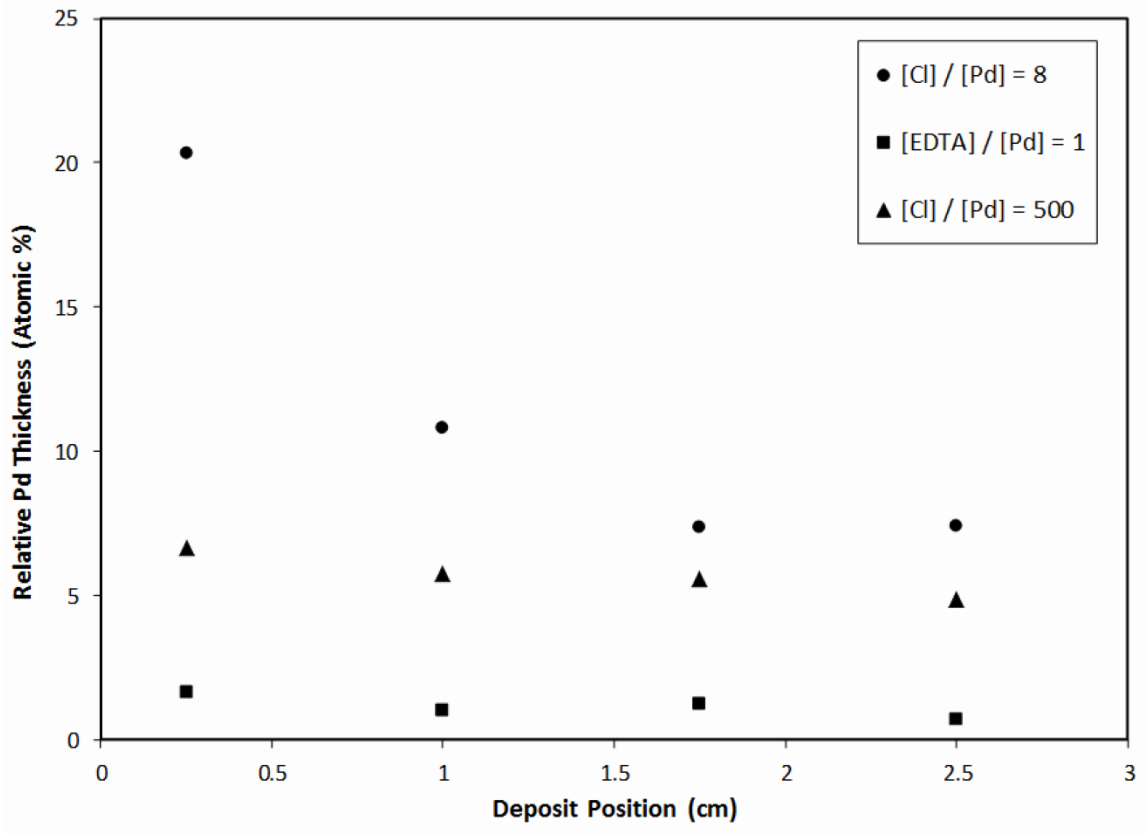

Figure 3.3 Relative Pd thickness, reported as atomic %, obtained from EPMA of 25 cycle deposits formed using 3 different Pd solutions with variations in complexing agent. Cu was deposited at 0.15 V and a 0.4 V stop potential was used. Points were taken from the ingress end (0.25 cm) towards the egress (2.5 cm).

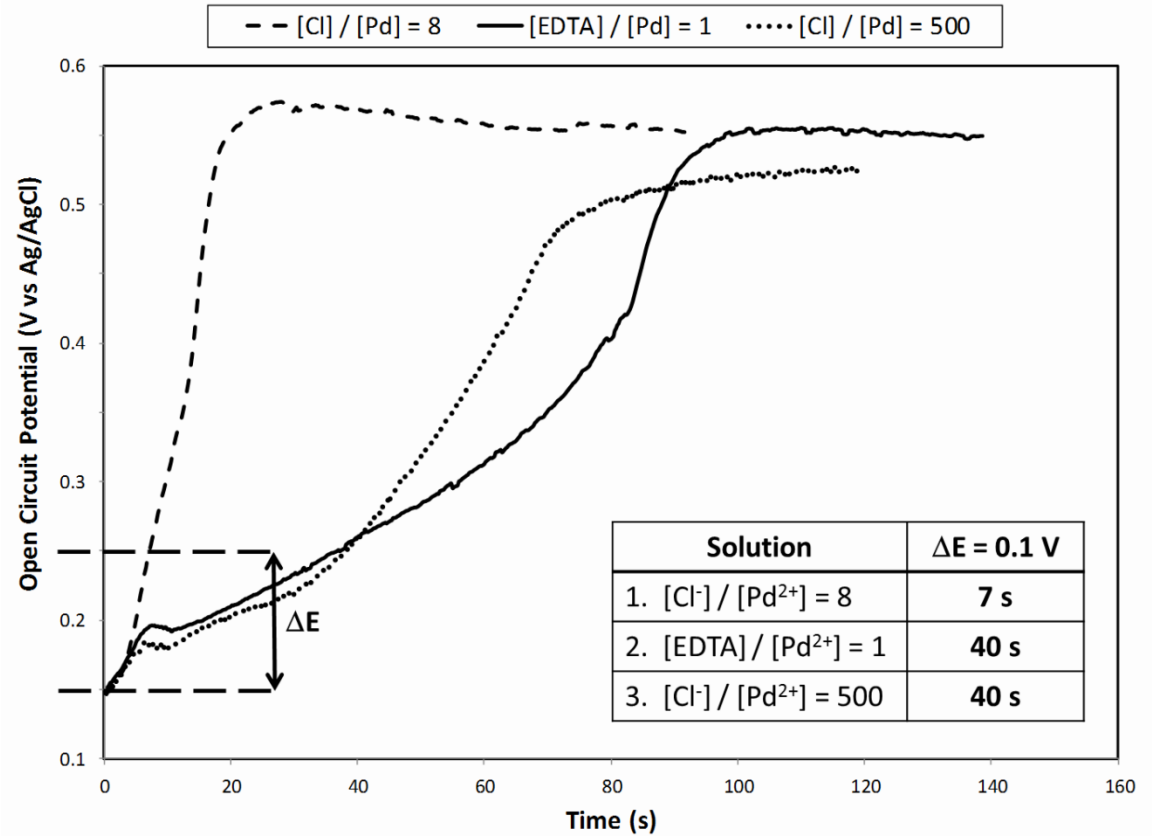

Figure 3.4 The OCP of the 2nd of 25 cycles is plotted as a function of time where time 0 s marks the start of the replacement reaction and the flowing of Pd solution. The table inset includes the average time needed for the OCP to shift from 0.15 to 0.25 V (ΔE = 0.1 V) for different Pd solutions. All films were grown using Cu deposited at 0.15 V and a 0.4 V stop potential.

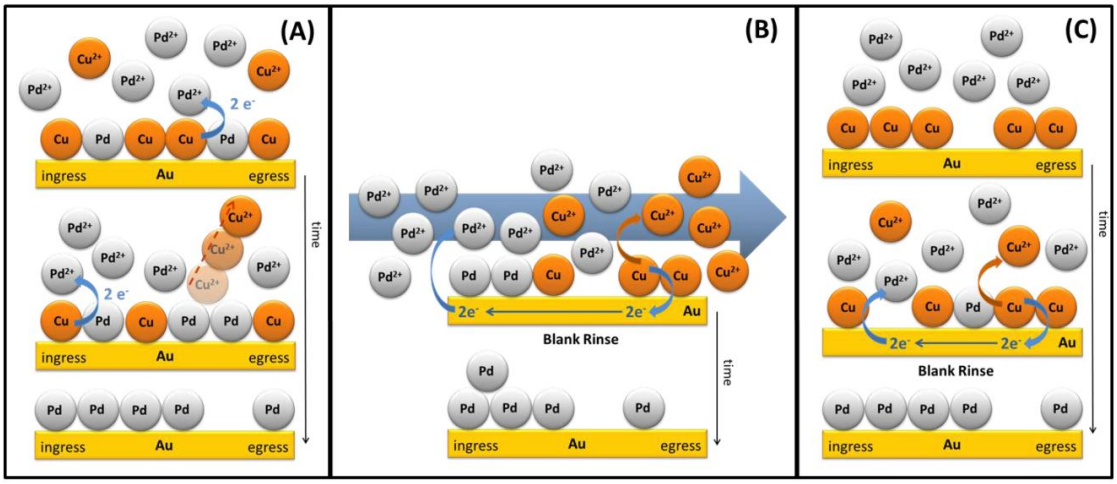

Figure 3.5 Three possible electron transfer schemes for SLRR of Cu_{UPD} for Pd^{2+}. (A) Direct transfer of electrons from a Cu_{UPD} atom to a Pd^{2+} ion, suggesting replacement of the Cu atom by the reduced Pd ion; (B) indirect transfer of electrons from Cu_{UPD} to Pd^{2+} through the electrode, with insufficient Pd^{2+} complexation, resulting in an inhomogeneous distribution of Pd from ingress to egress; (C) indirect transfer of electrons from Cu_{UPD} to Pd^{2+} ions through the electrode, where the Pd^{2+} was complexed, slowing the exchange, and producing a homogeneous deposit.

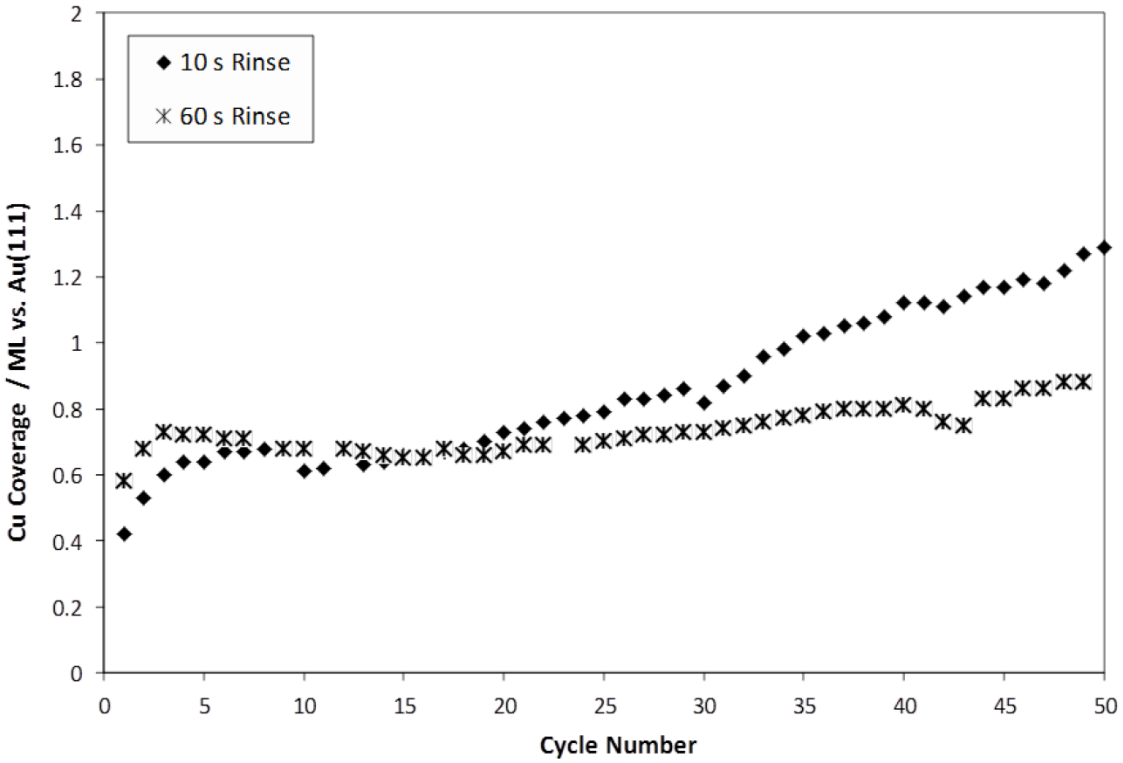

Figure 3.6 Cu coverage calculated from deposition current for each cycle of two 50 cycle E-ALD Pd deposits. The blank rinse time was either 10 or 60 s. The films were formed using $[Cl^-] / [Pd^{2+}] = 500$, a Cu deposition potential of 0.15 V and a stop potential of 0.4 V.

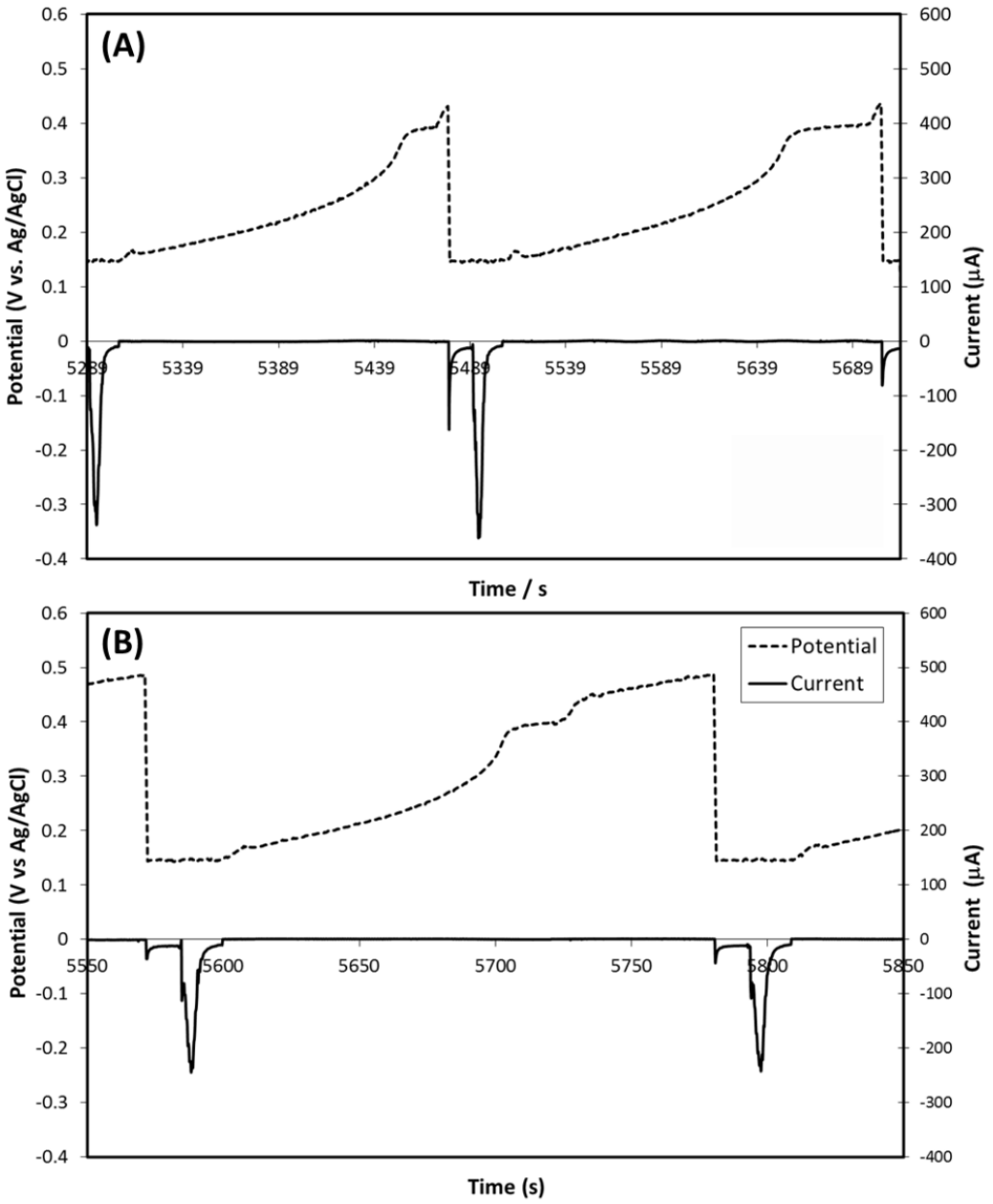

Figure 3.7 Time-Potential-Current graphs of two cycles of Pd SLRR with the addition of a step in which 0.15 V is applied to the cell for 10 s immediately following either a (A) 10 s blank rinse or a (B) 60 s blank rinse. H_2SO_4 (blank) continued flowing during this step. Both films were formed using $[Cl^-] / [Pd^{2+}] = 500$, a Cu deposition potential of 0.15 V and a stop potential of 0.4 V.

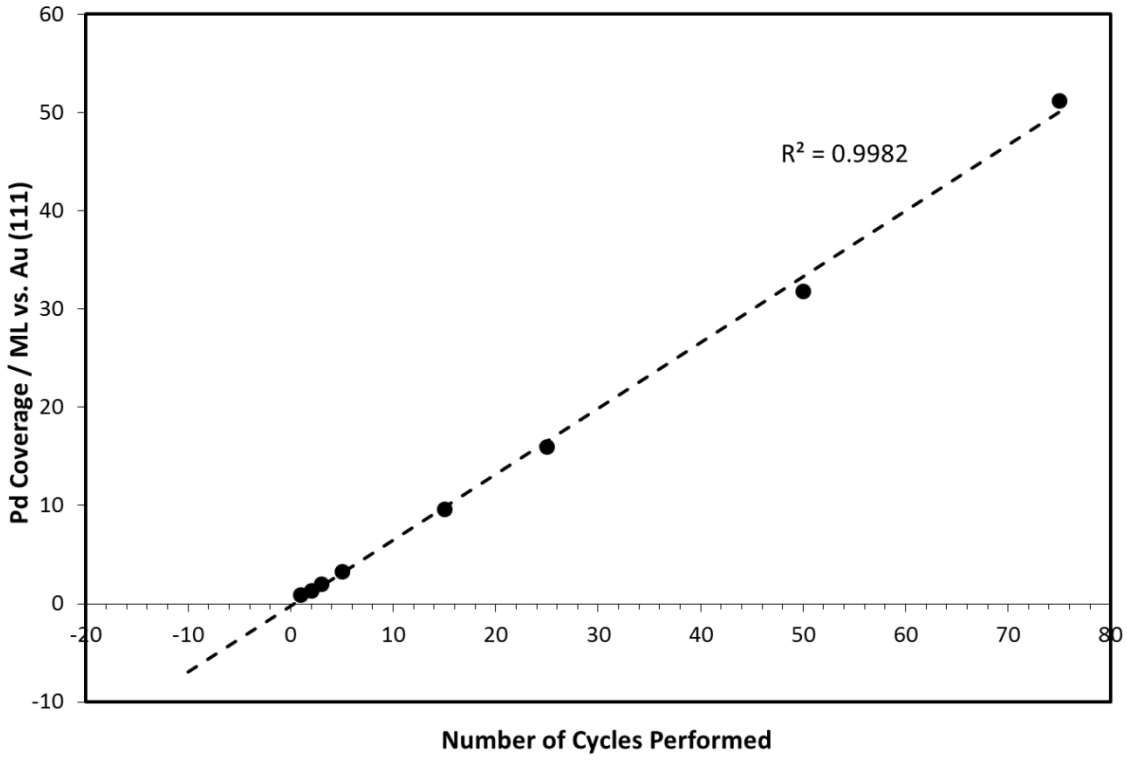

Figure 3.8 Plot illustrating the linear relationship between Pd coverage (i.e. film thickness) and the number of E-ALD cycles performed. The Pd solution composition was $[Cl^-] / [Pd^{2+}] = 500$.

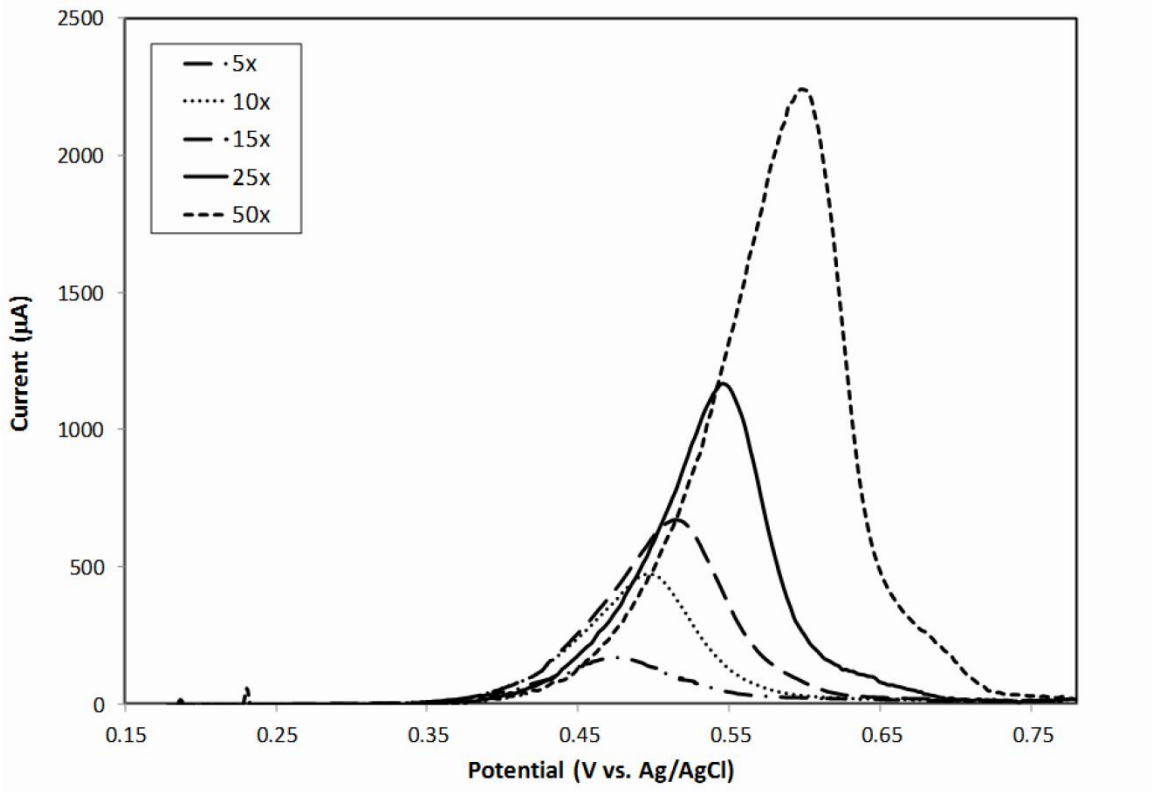

Figure 3.9 Anodic stripping curves of various E-ALD Pd films formed using between 5 and 50 cycles. The potential was scanned at 5 mV/s from 0.15 to 0.78 V in while flowing 0.1 M HCl.

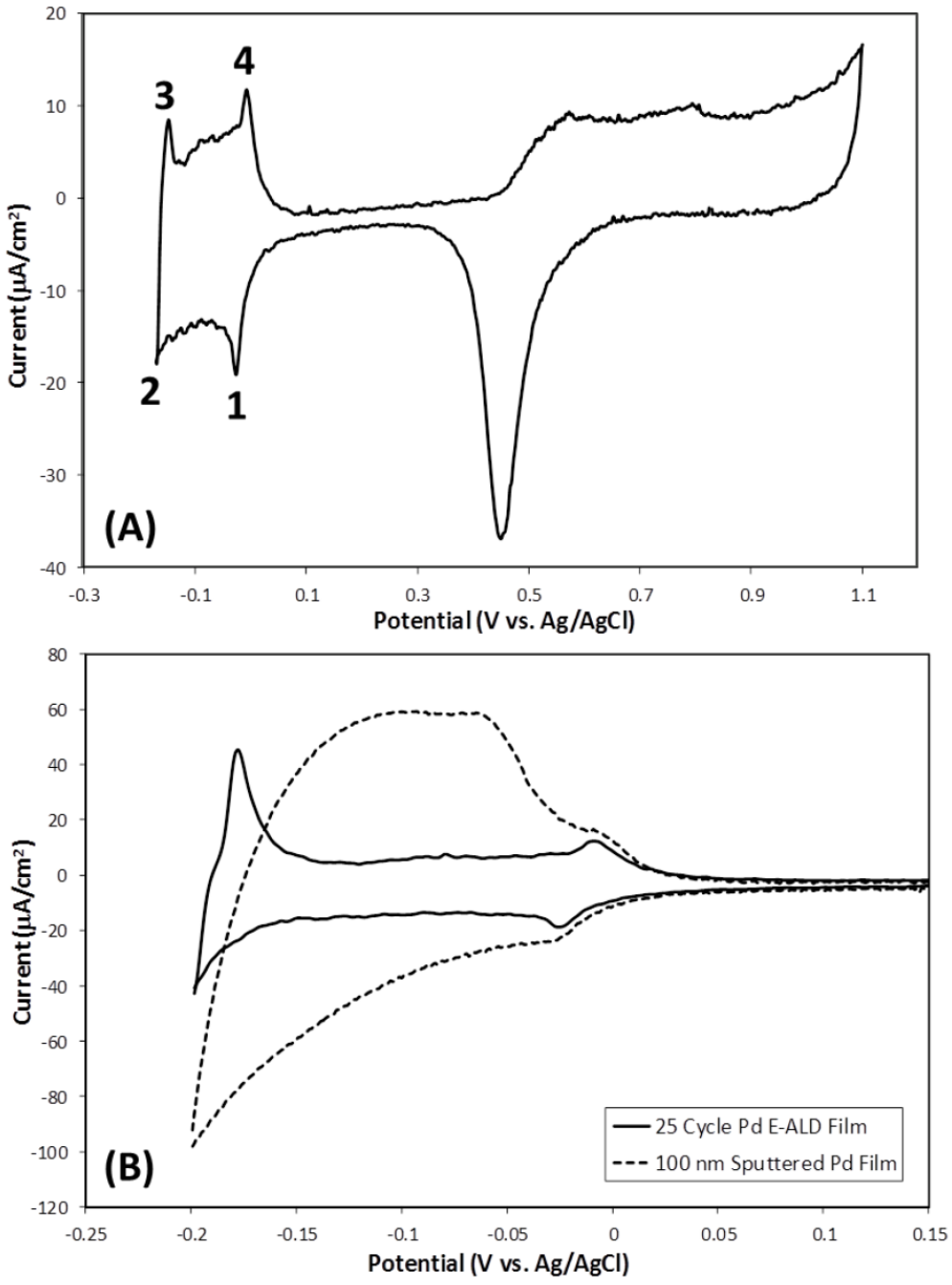

Figure 3.10 CVs of (A) 25 cycle E-ALD Pd film (B) compared with a 100 nm sputtered Pd film in 0.1 M H_2SO_4 at 10 mV/s.

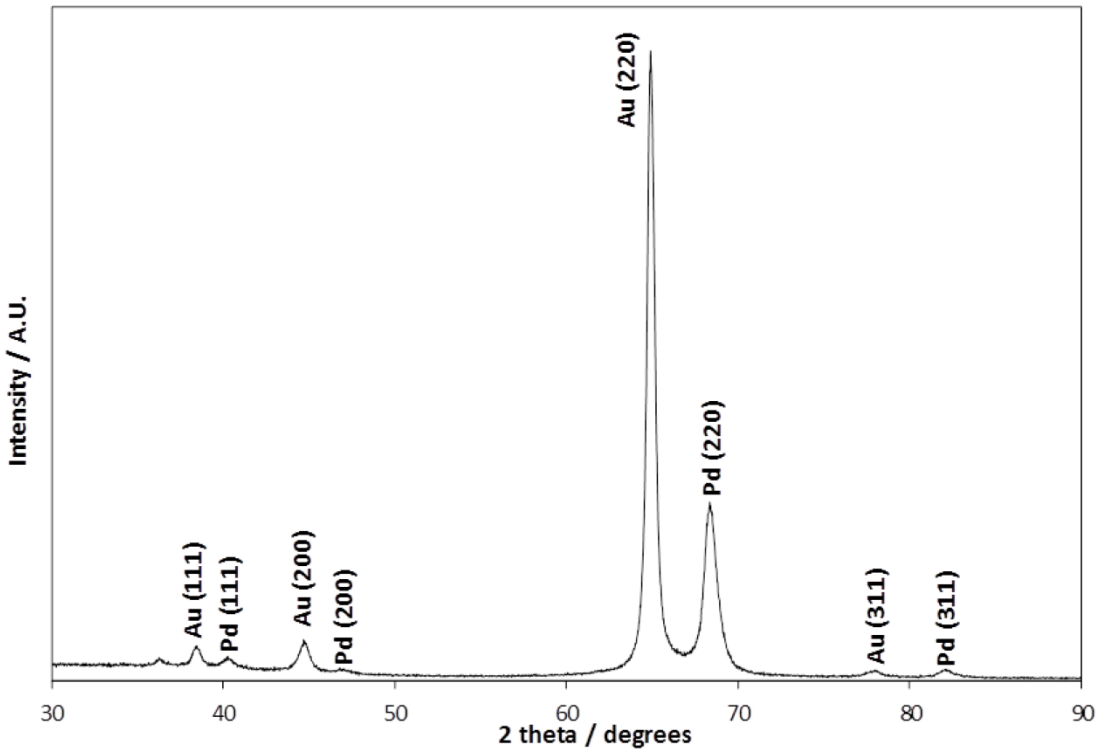

Figure 3.11 XRD of a 75 cycle deposit formed using $[Cl^-] / [Pd^{2+}] = 500$, a Cu deposition potential of 0.15 V and a stop potential of 0.40 V. Angle of incidence is 1º, Cu Kα source.

CHAPTER 4

PALLADIUM NANOFILMS ON AU(111) FORMED USING ELECTROCHEMICAL ATOMIC LAYER DEPOSITION (E-ALD) WITH CHLORIDE COMPLEXATION: STUDIES USING VOLTAMMETRY AND IN-SITU SCANNING TUNNELING MICROSCOPY[3]

[3] L. B. Sheridan, Y. G. Kim, K. Jagganathan, J. L. Stickney and D. B. Robinson, To be submitted to *Journal of Physical Chemistry C* (2013)

Abstract

Pd nanofilms were grown on Au(111) using the electrochemical form of atomic layer deposition (E-ALD). Deposits were formed by the repeated application of surface limited redox replacement (SLRR) in a cycle. Each cycle produced an atomic layer of Pd, allowing the reproducible formation of nanofilms of Pd, the thickness being proportional to the number of cycles performed, up to 30 in the present study. The resulting deposits were used as a platform for studying hydrogen sorption and desorption properties of Pd as a function of thickness. The SLRR involved initial formation of an atomic layer of Cu by underpotential deposition, followed by galvanic exchange of the Cu with $PdCl_4^{2-}$ ions at open circuit. The first 3 cycles were studied using in-situ electrochemical scanning tunneling microscopy (EC-STM), which showed a consistent morphology from cycle to cycle and the monoatomic steps indicative of layer by layer growth.

The hydrogen sorption and desorption properties were studied as a function of film thickness using cyclic voltammetry (CV) in 0.1 M H_2SO_4. The results indicate that the underlying Au structure greatly affects the hydrogen adsorption, as does film thickness for deposits below 5 cycles, for which an average hydrogen to Pd molar ratio (H/Pd) of 0.6 was calculated. No hydrogen absorption occurs for the thinnest films, while it increases for thicker films. Simple electrochemical annealing procedures were also developed. CVs of a post annealed Pd nanofilm showed improved surface order, closely resembling CVs of bulk Pd(111).

Introduction

The interactions of Pd nanofilms and nanostructures with hydrogen continue to be of significant interest due to their potential use in hydrogen storage, sensing and catalysis. Pd nanofilms or nanostructures must be used in order to readily differentiate the electrochemical formation of the Pd surface hydride and bulk hydride in cyclic voltammetry (CV). There are a multitude of techniques for forming nanofilms, including various forms of physical vapor deposition (PVD), chemical vapor deposition (CVD), molecular beam epitaxy (MBE) and electrodeposition.[1]

Atomic layer deposition (ALD) is a more recent technique for depositing nanofilms. ALD is typically performed under vacuum at temperatures above 100 $^{\circ}$C, resulting in the layer by layer deposition of conformal nanofilms of a material, with atomic level control.[2, 3] The electrochemical analog of ALD, E-ALD, uses solution based electrochemical surface limited reactions to deposit conformal nanofilms.[4] The advantages of electrochemical deposition are well known, such as its low cost, low temperature, flexibility and simplicity.

Surface limited reactions (SLR) are those where the amount deposited is limited by the surface area of the deposit, the reaction stopping once the surface is covered. Most SLR result in the deposition of an atomic layer. An atomic layer is defined as no more than one atom thick, with a coverage of a monolayer (ML) or less. A ML, in surface science, is a unit of coverage equal to the number substrate surface atoms (atoms/cm^2). Electrochemical SLR typically involve underpotential deposition (UPD). UPD is the electrodeposition of one element on another at a potential prior to, or "under,"

that needed to deposit the element on itself. It is the result of the ΔG_f° of a surface compound or alloy.[5-7] In E-ALD, the formation of an atomic layer takes place in a cycle, where the more cycles performed, the thicker the deposit. The cycle is divided into a sequence of steps, such as introduction of a solution, a potential change, rinse, etc.

Semiconductor and superlattice nanofilms[4, 8], nanoclusters[4, 8] and nanowires have all been formed using E-ALD. The development of surface limited redox replacement (SLRR) by Brankovic et al.[9], Mrozek et al.[10], Vasilic and Dimitrov,[11] and Kim [12] made it possible to extend E-ALD to the formation of metal nanofilms. The cycle for an SLRR begins with the formation of an atomic layer of a "sacrificial" metal via UPD. That atomic layer is subsequently exchanged for a more noble metal by redox replacement (i.e. galvanically) at open circuit. That is, the UPD solution is exchanged for one containing a precursor ion for the desired, more noble metal, and electrons are transferred from the sacrificial atomic layer to the precursor ions, which then deposit on the surface while atoms of the sacrificial metal are oxidized from the surface. The extent of the reaction is limited by the number of atoms in the sacrificial atomic layer, and the stoichiometry of the exchange reaction. A nanofilm is formed by repeating this cycle the desired number of times, with the thickness being proportional to the number of cycles.[13-15] To date, SLRR has been used to form nanofilms of Cu,[13, 14, 16, 17] Ag[18], Ru,[15] Pt[9, 10, 19, 20], Pt/Ru[21] and Pd[22, 23].

The first report of Pd deposition using a SLRR was by Brankovic et al.[9], who observed that a single replacement of Cu_{UPD} produced a nearly uniform Pd ML on Au(111). Soon after, Weaver and coworkers[10] reported the formation of Pd SERS-active substrates by depositing MLs of Pd on roughened Au by replacing either Pb_{UPD} or

Cu_{UPD}. More recently this technique has been used to form bimetallic CuPd particles on graphite[24], Pd ML coated nanoporous Au film electrodes[25] and Pd ML coated IrCo alloy nanoparticles[26]. An E-ALD cycle has been developed and optimized by this group for the formation of Pd nanofilms on polycrystalline Au via SLRR of Cu_{UPD} and is described in detail elsewhere. [22, 23] To briefly summarize, these reports suggest an SLRR mechanism where some of the electrons are indirectly transferred from the sacrificial metal to the depositing metal precursor ion, by way of the electrode. This is in contrast to speculation that electrons were transferred directly between the sacrificial metal and depositing metal ion. This indirect mechanism suggests that inhomogeneous deposition across the electrode surface can occur, depending on the rate of exchange between the depositing and sacrificial metals, relative to the rate of solution introduction. Addition of an adequate concentration of Cl^- to complex the Pd^{2+} ions has been shown to effectively reduce the exchange rate relative to the timescale for solution introduction, promoting homogeneity of the deposit. Those results also showed 96% exchange efficiency for electrons from the sacrificial Cu atomic layer to the deposited Pd.

The use of single crystal substrates is of interest for fundamental studies of Pd nanofilms, since a well-defined surface structure produces distinct features in cyclic voltammetry, and they allow atomic scale characterization by in-situ electrochemical scanning tunneling microscopy (EC-STM). Over the last few decades the electrodeposition of Pd on a variety of single crystal noble metal substrates has been reported.[27-31] Specifically, Pd electrodeposition on Au(111) from Cl^- containing solutions has been extensively studied, which provides a good comparison for E-ALD Pd films. Kolb et al. [32, 33] reported the formation of epitaxial Pd overlayers on Au(111)

with a well-ordered structure. However, this epitaxial nature only persists for the first 2 MLs, beyond which roughness and defects increased. Both Uosaki et al. [34, 35] and Kolb et al.[33] imaged Pd overlayers on Au(111) with EC-STM and found no signs of significant surface alloying. They also described the role of a distorted hexagonal adlayer of $PdCl_4^{2-}$ in promoting layer by layer growth.

In the present study, E-ALD of Pd nanofilms on Au(111) was investigated using EC-STM and CV. EC-STM analysis was conducted for the first 3 cycles of deposition in order to probe the growth mode of Pd via SLRR using Cu_{UPD} sacrificial layers. CVs were used to examine thicker deposits of up to 30 cycles, as well as the first few deposition cycles. The effects of deposit thickness on the sorption reactions of Pd with hydrogen, both surface and bulk hydride formation, are discussed. Additionally, an "electrochemical annealing" procedure was developed and found to improve the surface order of the resulting films. When possible, results are compared with those available in the literature for Pd deposited on Au(111) at constant potential.

Experimental

EC-STM experiments employed a Au bead with single-crystal surfaces prepared using a variation of the Clavilier method.[36, 37] The flame-annealed bead electrode was quenched in hydrogen saturated 18 MΩ-cm water, and then quickly transferred, with a protective water film, through air into the EC-STM cell. The flow cell used for EC-STM studies allowed flow and exchange of solutions over the Au bead working electrode and included a downstream reference/auxiliary to avoid contamination. A single peristaltic pump (0.9 mL/min) was used to maintain equivalent flow rates in and out of the cell ensuring a constant solution level, as described previously.[12, 38] The supporting

electrolyte contained 0.05 M H_2SO_4 (Aldrich Chemicals, Milwaukee, WI), doubly distilled and made using 18 MΩ-cm water. The Pd solution consisted of ultrapure-grade 0.1 mM $PdCl_2$ (Aldrich Chemicals, Milwaukee, WI) in 50 mM HCl and the Cu solution was 1 mM ultrapure-grade $CuSO_4$ (Aldrich Chemicals, Milwaukee, WI) in 0.05 M H_2SO_4. The electrochemical cell included a Au-wire auxiliary electrode and a Ag/AgCl reference electrode (3 M KCl) (Bioanalytical Systems, Inc.). All potentials are reported versus this reference electrode. A Nano-scope III (Digital Instruments, Santa Barbara, CA) equipped with W tips, electrochemically etched (15 VAC in 1 M KOH) from a 0.25 mm wire, were used in all EC-STM measurements. Transparent nail polish was used to coat the tip and minimize Faradaic currents. Wide-angle and atom-resolved EC-STM in pure electrolyte was used prior to each experiment to confirm the presence of a well-ordered Au(111)-(1 x 1) structure.

For voltammetric studies, Pd films were deposited on a Au(111) single-crystal disk. All deposits were formed using an automated electrochemical flow cell deposition system[4, 39, 40] (Electrochemical ALD L.C.) consisting of a variable speed pump, 5 valves, 5 solution reservoirs, a potentiostat and an electrochemical flow cell (volume ≈ 0.15 mL). The system was controlled with custom "Sequencer" software designed for E-ALD (Electrochemical ALD L.C.). The electrochemical cell included an imbedded Au wire auxiliary electrode, parallel with the working electrode but on the opposite side of the flow cell. The cell also contained a Ag/AgCl (3 M KCl) reference electrode (Bioanalytical Systems, Inc.). The Au(111) disk had an exposed area of 0.283 cm^2, defined by the hardware used to hold the disk in the flow cell. Prior to loading the disk into the flow cell, it was sonicated in acetone, then rinsed 3 times with 18 MΩ-cm water

(Milli-Q Advantage A10 water filtration system), then sonicated in concentrated HNO_3, also followed with 3 rinses in 18 MΩ-cm water. The final step was flame-annealing in a H_2 flame with subsequent cooling in a N_2 gas stream. CV's were taken over a potential range from -0.2 to 0.9 V in 0.1 M H_2SO_4 and -0.2 to 0.7 V in 50 mM HCl to ensure the quality of the crystal surface.

All solutions were prepared using 18 MΩ-cm water. The Pd^{2+} solution contained 0.1 mM $PdCl_2$ (Aldrich, 99.999%) and 50 mM HCl (J.T. Baker, Reagent Grade). The sacrificial metal ion solution was 2 mM $CuSO_4$ (J.T. Baker, 99.8%) in 0.1 M H_2SO_4, and the blank solution was 0.1 M H_2SO_4. All solutions were degassed using N_2 to minimize dissolved O_2 prior to electrochemical studies. All potentials are reported versus Ag/AgCl (3 M KCl).

Results and Discussion

The SLRR mechanism is depicted in the schematic in Figure 4.1 and a time-potential-current plot of the 4th E-ALD cycles of a 5 cycle Pd nanofilm is shown in Figure 4.2. The cycle begins by rinsing the Cu^{2+} solution into the cell at 17 mL/min under an applied potential of 0.15 V for 18 s, to deposit Cu_{UPD}. The charge passed during formation of the sacrificial atomic layer of Cu was 463 μC/cm^2, a charge equivalent to 0.95 ML vs. Pd(111). Okada et al.[41] reported the formation of a complete (1X1) ML of Cu_{UPD} on bulk Pd(111), while Cuesta et al.[42] reported a slightly lower coverage of 0.82 ML, but concluded that error due to double layer corrections and possible anion coadsorption could account for the lower value. The auxiliary electrode was then disconnected, allowing the cell to adopt its open circuit potential, and the Pd^{2+} ion solution was introduced to exchange with the Cu_{UPD} atoms, forming a Pd atomic layer. The open

circuit potential (OCP) shifted positively until it reached 0.4 V, the stop potential. The stop potential was programmed into the cycle to trigger the start of the blank rinse, assuring removal of excess Pd^{2+} ions and any Cu^{2+} ions formed from the cell. OCP was maintained during the blank rinse and the potential continued to drift up to ~0.5 V, near the onset of Pd oxidation. In these studies this cycle was repeated between 1 and 30 times.

EC-STM Measurements

A CV of Cu UPD on Au(111) in 1 mM $CuSO_4$ solution is shown in Figure 4.3 (A) and displays two well-known UPD features.[12, 43-45] The first feature, at 0.23 V, represents the formation of the 2/3 ML ($\sqrt{3}X\sqrt{3}$)R30° structure. The second feature, at 0.03 V, accounts for deposition of the remaining 1/3 ML of Cu, completing a pseudomorphic Cu ML, forming a (1X1) structure. Figure 4.3 (B) displays an STM image of the "honeycomb" structure[12, 46-48], composed of sulfate anions (0.33 ML) residing in the center of Cu hexagons, formed at 0.25 V. A similar UPD layer of Cu, formed at 0.15 V, was replaced by Pd at open circuit followed by a blank rinse of the cell.

Wide-area EC-STM images (300 x 300 nm) taken at 0.45 V after 1, 2 and 3 replacement cycles (Figure 4.4) shows evenly dispersed mono-atomically high islands, as determined by section analysis. Qualitatively, these images illustrate consistent morphology from cycle to cycle. High resolution images were also obtained (Figure 4.5) however, atomic resolution was not possible. After the 2^{nd} replacement cycle, the height profile shows an average step height of 0.21 ± 0.01 nm (Figure 4.5), a value indicative of Pd monoatomic steps. Monoatomic steps provide strong evidence for layer by layer growth (Frank–van der Merwe)[49].

Metal surface ordering due to the adsorption of various electrolyte anions is well-known.[50, 51] Iodine adsorption on single-crystal Au, Cu, Pd and Pt and its promotion of surface mobility has been extensively studied using UHV-EC methods and EC-STM.[52-57] Room temperature iodine adsorption on disordered Pd(111) and (100) surfaces has been shown to promote spontaneous reordering via surface reconstruction.[12, 52, 58] Extensive studies of halide adsorption on metal surfaces indicate that close-packed hexagonal adlayers, having high surface mobility, are frequently formed. Halide atoms typically need to share a single electron with the underlying metal atoms, with the adsorbed atoms adopting something near their van der Waals diameter. This halide atom layer then acts as a blanket, covering the surface conformally. Figure 4.6 compares EC-STM images of 3 cycle Pd thin films before and after iodine adsorption at 0.45 V. Note that the iodine atomic layer is imaged, not the underlying Pd atoms, though since the iodine atomic layer is conformal and a monolayer thick it is a representation of the underlying Pd atoms. The increased surface mobility of the Pd atoms appears to be induced by adsorbed iodine and the use of potentials close to that needed to oxidize the Pd atoms, and is referred to here as a type of electrochemical annealing.[59, 60] Increases in terrace sizes and surface order are evident in Figure 4.6(E-F). The height profile of a high-resolution image (Figure 4.7) shows an average step height of 0.22 ± 0.01 nm, indicating preservation of the original monoatomic terraces.

Voltammetric Measurements: Hydrogen Adsorption

Varying thicknesses of Pd films were formed on Au(111) using between 1 and 30 E-ALD cycles. The total amount of Pd deposited was subsequently determined by anodic stripping in 50 mM HCl, by scanning at 5 mV/s from 0.15 to 0.70 V. The Pd coverages

were calculated with respect to the Au(111) surface where 1 ML is equivalent to 448 $\mu C/cm^2$. Figure 4.8 is a plot of the Pd coverage as a function of the number of E-ALD cycles performed and closely resembles that previously reported for E-ALD Pd films on polycrystalline Au substrates.[23] The relationship is linear and passes through the origin, an important indicator of an ALD process. These results along with the EC-STM images support a layer-by-layer growth mechanism.

Figure 4.9 compares CVs of 1 (solid line) and 2 (dot-dash line) cycle Pd films in 0.1 M H_2SO_4 with that for a clean Au(111) (dotted line). As the potential was scanned negatively, two peaks were evident at −0.03 V and −0.08 V, for both the 1 and 2 cycle deposits. These are due to hydrogen adsorption/sulfate desorption on the Pd surface and are completely absent from the CV of bare Au(111).[61] At potentials more negative than -0.17V, hydrogen absorption becomes more important, which will be discussed later. Reversal of the scan at -0.25 V results in three oxidative features. The broad peak at −0.074 V and a sharper peak (dot-dashed line) at 0.015 V represent desorption of the Pd surface hydride. Figure 4.10 shows CVs for the 2 cycle film along with films made with 3, 5, and 10 cycles. The potential of the main peak for reductive hydrogen adsorption shifts negative by 5 mV for films of 3 cycles or more, while the potential for the primary hydrogen desorption peak shifts negative by 15 mV. The CV of the 3 cycle film (Figure 4.10, dashed line) clearly suggests a transition between the 2 cycle and 5 cycle films, as the primary hydrogen desorption peak is a doublet. For more than 5 cycles, the hydrogen adsorption and desorption peaks show more reversibility, and essentially overlap.

Nearly identical results have been reported by Baldauf and Kolb[32] and Kibler et al.[62] for Pd deposited at constant potential on Au(111) from Cl^- containing solutions. In those studies, it was suggested that the more positive peak represents hydrogen adsorbed/desorbed from Pd island edge sites. As the Pd islands coalesce, forming more uniform terraces, the more negative hydrogen adsorption/desorption peak emerges. Pd deposited at constant potential on Au(111) has been shown, using surface X-ray scattering (SXS), to undergo a transition from a strained pseudomorphic ML to a thicker deposit with properties closely resembling bulk Pd[63]. In the present study (Figure 4.10) the observed shifts in the hydrogen adsorption/desorption peaks and the increase in their reversibility with film thickness are consistent with a deposit more closely resembling bulk Pd(111) CVs.[61, 64]

Adsorption energies (E_{ads}) were recently calculated in density functional theory (DFT) studies for Pd on Au(111), and given that the position of the adsorption/desorption peaks are a direct measure of the stability of the surface hydride, may help explain the present results. It was suggested that the strain typically found in thin deposits causes the d-band center to shift to higher energies, leading to stronger adsorbate interactions with the surface, possibly resulting from geometric or electronic effects due to the underlying Au.[65] Kibler et al.[66] suggest that a pseudomorphic Pd ML on Au(111) experiences an up-shift in the d-band center compared to Pd(111), corresponding with a positive shift in the adsorption potential (more negative E_{ads}). A second report by Kibler[67] and earlier reports by Roudgar et al.[68, 69] indicate that the largest E_{ads} occurs for 2 pseudomorphic MLs and decreases with increasing thickness until becoming equivalent

to bulk Pd(111). These calculated values for E_{ads} directly correlate with the observed peak shifts seen in Figures 4.9 and 4.10, for deposits formed using E-ALD.

Figure 4.11 is a plot of the hydrogen adsorption charges calculated using the data in Figures 4.9 and 4.10 by integrating the desorption peaks between −0.12 and 0.08 V. Reports indicate that desorption (adsorption) of hydrogen on Pd in sulfuric acid occurs simultaneously with HSO_4^-/SO_4^{2-} adsorption (desorption).[61, 70, 71] This notation (HSO_4^-/SO_4^{2-}) is used here due to conflicting reports as to which species is adsorbed. Wan et al.[61] studied Pd(111) using STM and suggested that sulfate adsorption was accompanied by adsorption of water molecules, while Alvarez et al. [70] suggested the coadsorbed species was HSO_4^- based on IR spectra of Pd overlayers on Pt(111). The CO displacement method, introduced by Clavier et al.,[72] has been used to correct the charge for the coadsorbed species.[70, 71] In contrast to all of the above mentioned studies, Duncan and Lasia[73] studied Pd on Au(111) in $HClO_4$ and H_2SO_4 and reported very little difference in charge for the hydrogen adsorption/desorption peaks as a function of anion. Given the limited anionic dependence suggested by Duncan and Lasia, for the studies reported below the expedient assumption was made that the charges were simply due to hydrogen.

Figure 4.11 indicates a maximum hydrogen adsorption charge for the 3 cycle film (2.5 ML, Figure 4.8), then diminishes slightly over the next 7 cycles. The same trend was first reported by Baldauf and Kolb[32] for Pd films deposited at constant potential on Au(111). They suggested that the decrease in charge was likely due to coalescence of islands and smoothening of the film as thicker deposits were formed. The coverages

plateau (Figure 4.11) at 254 μC/cm^2, slightly higher than the 240 μC/cm^2 expected for a ML of hydrogen adsorbed on an ideal Pd(111).

The Pd coverage resulting from the first cycle was 0.6 ML (see Figure 4.8), while the corresponding hydrogen desorption was 0.68 ML of hydrogen, for a ratio of 1.1. After 2 E-ALD cycles the Pd coverage was 1.5 ML and the hydrogen desorption coverage was 1.1 ML, more than needed to cover an ideal Pd(111). These coverages are consistent with the STM images in Figures 4.4 and 4.5, and suggest some hydrogen is adsorbing at step and island edges. A recent computational study predicted a Pd(211) surface would be expected to have more than 1 ML (up to ~1.3 MLs) of adsorbed hydrogen.[74]

Voltammetric Measurements: Hydrogen Absorption

Hydrogen absorption, which becomes significant below −0.1 V, is clearly evident in Figure 4.10. Upon potential reversal, the corresponding desorption is rapid. The charges for this absorption and desorption both increase with increasing numbers of Pd E-ALD cycles, as expected.

From Figure 4.9 hydrogen absorption and desorption appears to be present after only 1 and 2 cycles (Pd coverage of 0.6 and 1.4 ML), though previous reports indicate hydrogen absorption only occurs for Pd films greater than 2 MLs.[32, 75, 76] It is possible that there were some Pd islands 3 atomic layers thick on the surface, though there was no indication of them from EC-STM (Figures 4.4 and 4.5). Alternatively, the features below -0.175 V (Figure 4.9) are probably due to the hydrogen evolution reaction (HER) and oxidation of some of the resulting H_2 or some other adsorption phenomenon, such as weakly adsorbed hydrogen. Pd overlayers on Au(111) have been studied as

catalysts for the HER and a significant increase in activity for Pd submonolayers was reported, apparently due to the presence of mixed Pd/Au step sites.[77-79] A review by Jerkiewicz[80] indicates that two surface hydride species are formed on Pt group metals at different surface sites and potentials, due to their distinct Gibbs energies of adsorption. Based on the results presented here, it is not possible to definitively conclude which of these processes is responsible for the charge observed below -0.175 V (Figure 4.9).

The hydrogen to Pd molar ratios (H/Pd) were obtained in 0.1 M H_2SO_4 by pulsing to −0.25 V for an amount of time sufficient to saturate the Pd film with hydrogen, as determined by coulometry, followed by oxidation of the absorbed hydrogen by scanning to 0.15 V. Since the HER is ongoing at -0.25 V, the oxidation charge, rather than reduction charge, was used to quantify the moles of absorbed hydrogen. The films were subsequently stripped, to calculate the moles of Pd, by scanning from 0.15 V to 0.7 V in 50 mM HCl. The average H/Pd was 0.6 for 3, 5, 10 and 30 cycle films. This value agrees well with those reported in the literature, which range from 0.59 to 0.73.[81-84]

Voltammetric Measurements: EC Annealing

Figures 4.9 and 4.10 suggested that the hydrogen adsorption and desorption peak morphologies are sensitive to Pd coverages. In addition, cycling the potentials in the hydrogen region for a given Pd coverage resulted in changes to the shapes and positions of the peaks, even though Pd surface oxidation was avoided. For example, CVs of a 23 cycle Pd film in the hydrogen sorption region are plotted in Figure 4.12. The arrows in Figure 4.12 indicate the increases and decreases in peak height with increasing numbers of CVs. These shifts were most evident for hydrogen adsorption, where the peak begins to diminish as a shoulder forms at a more positive potential, eventually forming a new

peak. This behavior was not a function of film thickness, as similar results were observed for 3 and 10 cycle films. The trend was to more reversibility in the voltammetry, suggesting a more ordered film. Analogously, Duncan and Lasia[73] reported similar behavior for a 0.8 ML Pd film on Au(111) and attributed the shift to a decrease in steps due to coalescence of islands.

Additional investigation into the effect of potential cycling on the Pd E-ALD films was conducted to determine if the surface order could be further improved. The application of potentials that are near the start of surface reactions such as oxidation or hydrogen evolution reaction (HER) are known to increase the surface mobility of atoms, similar to the increase in surface diffusion rates with increasing temperature. Use of a potential program and surface active electrolyte to improve an electrode's surface structure has been referred to as electrochemical (EC) annealing.[85, 86] A wide range of studies have shown that EC annealing can result in significant surface and electronic changes.[87-90] The potential program employed here involved a 15 cycle film subjected to 20 CVs in 0.1 M H_2SO_4 at 10 mV/s between 0.1 and 0.5 V, where there are no significant voltammetric features besides charging. CVs into the hydrogen sorption region (0.15 to -0.2 V) were performed before and after this EC annealing program (Figure 4.13). The hydrogen adsorption/desorption peaks for the as-deposited film were broad, and shifted from each other by 0.06 V (short-dashed line). In scan 1(long-dashed line), immediately following EC annealing, the adsorption peak is shifted positive by 0.02 V and the desorption peak shifts positive by 0.005 V, but is sharper and more symmetric. However in scan 2, after only one cycle into the hydrogen absorption region the adsorption/desorption peak splitting is reduced to 0.01 V and both adsorption and

desorption are sharper. The position and shapes of the peaks stabilize after scan 5 into the hydrogen absorption region. The appearance and position of the stabilized peaks agree well with reported CVs of flame-annealed Pd(111) electrodes, indicating excellent surface order.[61, 71, 91]

This type of EC annealing is similar to using adsorbed iodine to promote surface ordering, as was described in the EC-STM results (Figure 4.6 and 4.7). The use of iodine in the CV studies was problematic, however, as the iodine had to be removed before CVs in the hydrogen adsorption/desorption region could be performed on the Pd surface. Schimpf et al.[92] reported a procedure for regenerating clean and ordered Pd(100) using iodine adsorption and desorption. Similar studies are planned to investigate the effect of iodine on E-ALD Pd nanofilms.

Returning to Figure 4.12, note that the final peak positions appear somewhere between the as-deposited and post-EC annealed (scan 5) CVs shown in Figure 4.13. It is plausible that the peaks would have continued improving if cycling had been prolonged. However, repeated cycling into the hydrogen absorption region induces stress and can cause plastic deformation of the film due to Pd lattice expansion and contraction upon insertion and removal of hydrogen[93]. For this reason EC annealing was investigated by performing 20 CVs between 0.1 to 0.5 V, and finishing with only 5 scans to -0.2 V.

Conclusion

E-ALD Pd nanofilms were formed on Au(111) by SLRR. The SLRR involved redox replacement of underpotentially deposited Cu for Pd. EC-STM images after 1, 2 and 3 cycles demonstrate monoatomic steps and consistent morphology from cycle to cycle, indicating layer-by-layer growth. Adsorbed iodine on a 3 cycle Pd nanofilm

increased Pd atom surface mobility, promoting the formation of larger and more ordered terraces and monoatomic steps.

The hydrogen adsorption and absorption features of Pd nanofilms formed with 1 to 30 E-ALD cycles were examined using CV in 0.1 M H_2SO_4. The results indicated a significant influence of the underlying Au on the position of the hydrogen adsorption/desorption features of deposits formed with less than 5 cycles. Hydrogen absorption occurred for films formed with more than 2 cycles, and had an average H/Pd of 0.6, in good agreement with the literature. Films formed with 1 and 2 cycles also appeared to absorb hydrogen, however, it is more likely that some H_2 gas was being evolved, with some being oxidized during the subsequent anodic scan, or a less strongly bound surface hydride was present. The literature indicates that 2 MLs of Pd are required for absorption to occur[32, 75, 77], and the STM studies presented here showed no evidence of a third layer of Pd for the 1 and 2 cycle films.

CVs taken after EC annealing indicated improved surface ordering, as evidenced by sharper peaks and increased reversibility for the adsorption/desorption peaks. The peak positions also resembled those of bulk Pd(111) for films formed with 15 cycles, another sign of improved surface order. However, analysis such as low-energy electron diffraction (LEED) would provide more valuable information about the surface structure modification.

Acknowledgements

Acknowledgment is made of the support of the National Science Foundation, Division of Materials Research #1006747, as well as Sandia National Laboratories, a multi-program laboratory managed and operated by Sandia Corporation, a wholly owned

subsidiary of Lockheed Martin Corporation, for the U.S. Department of Energy's National Nuclear Security Administration under contract DE-AC04-94AL85000.

References

1. Barlow, F., Elshabini-Riad, Aicha, Brown, R., *Film Deposition Techniques and Processes*, in *Thin Film Technology Handbook*, F. Barlow, Elshabini-Riad, Aicha, Editor. 1997, McGraw-Hill: New York.
2. *Electrochemical Society Transactions*. Atomic Layer Deposition Applications 3, ed. A. Londergan, Elam, J.W., van der Straten, O., De Gendt, S. Bent, S.F., Kang, S.B. Vol. 11 no. 7. 2007, Pennington: The Electrochemical Society.
3. George, S.M., *Atomic Layer Deposition: An Overview.* Chemical Reviews, 2010. **110**(1): p. 111-131.
4. Stickney, J.L., *Electrochemical Atomic Layer Epitaxy (EC-ALE): Nanoscale Control in the Electrodeposition of Compound Semiconductors*, in *Advances in Electrochemical Science and Engineering*, R.C.A.a.D.M. Kolb, Editor. 2002, Wiley-VCH: Weinheim.
5. Adzic, R.R., *Electrocatalytic Properties of the Surfaces Modified by Foreign Metal Adatoms* Advances in Electrochemistry and Electrochemical Engineering, ed. H.G.a.C.W. Tobias. Vol. 13. 1984, New York: Wiley-Interscience. 159-260.
6. Herrero, E., L.J. Buller, and H.D. Abruna, *Underpotential deposition at single crystal surfaces of Au, Pt, Ag and other materials.* Chemical Reviews, 2001. **101**(7): p. 1897-1930.
7. Kolb, D.M., *Advances in Electrochemistry and Electrochemical Engineering*, ed. H.G.a.C.W. Tobias. Vol. 11. 1978, New York: John Wiley. 125.

8. Cavallini, M., et al., *Two-dimensional self-organization of CdS ultra thin films by confined electrochemical atomic layer epitaxy growth.* Journal of Physical Chemistry C, 2007. **111**(3): p. 1061-1064.

9. Brankovic, S.R., J.X. Wang, and R.R. Adzic, *Metal monolayer deposition by replacement of metal adlayers on electrode surfaces.* Surface Science, 2001. **474**(1-3): p. L173-L179.

10. Mrozek, M.F., Y. Xie, and M.J. Weaver, *Surface-enhanced Raman scattering on uniform platinum-group overlayers: Preparation by redox replacement of underpotential-deposited metals on gold.* Analytical Chemistry, 2001. **73**(24): p. 5953-5960.

11. Vasilic, R. and N. Dimitrov, *Epitaxial growth by monolayer-restricted galvanic displacement.* Electrochemical and Solid State Letters, 2005. **8**(11): p. C173-C176.

12. Kim, Y.G., et al., *Platinum nanofilm formation by EC-ALE via redox replacement of UPD copper: Studies using in-situ scanning tunneling microscopy.* Journal of Physical Chemistry B, 2006. **110**(36): p. 17998-18006.

13. Thambidurai, C., et al., *E-ALD of Cu Nanofilms on Ru/Ta Wafers Using Surface Limited Redox Replacement.* Journal of the Electrochemical Society, 2010. **157**(8): p. D466-D471.

14. Thambidurai, C., et al., *Copper Nanofilm Formation by Electrochemical ALD.* Journal of the Electrochemical Society, 2009. **156**(8): p. D261-D268.

15. Thambidurai, C., Y.G. Kim, and J.L. Stickney, *Electrodeposition of Ru by atomic layer deposition (ALD).* Electrochimica Acta, 2008. **53**(21): p. 6157-6164.

16. Gebregziabiher, D.K., et al., *Electrochemical atomic layer deposition of copper nanofilms on ruthenium.* Journal of Crystal Growth, 2010. **312**(8): p. 1271-1276.

17. Viyannalage, L.T., R. Vasilic, and N. Dimitrov, *Epitaxial growth of Cu on Au(111) and Ag(111) by surface limited redox replacement - An electrochemical and STM study.* Journal of Physical Chemistry C, 2007. **111**(10): p. 4036-4041.

18. Vasilic, R., L.T. Viyannalage, and N. Dimitrov, *Epitaxial growth of Ag on Au(111) by galvanic displacement of Pb and Tl monolayers.* Journal of the Electrochemical Society, 2006. **153**(9): p. C648-C655.

19. Fayette, M., et al., *From Au to Pt via Surface Limited Redox Replacement of Pb UPD in One-Cell Configuration.* Langmuir, 2011. **27**(9): p. 5650-5658.

20. Nagarajan Jayaraju, D.V., Youn Guen Kim, Dhego Banga, and John L Stickney, *Electrochemical Atomic Layer Deposition (ALD) of Pt Nanofilms.* Journal of the Electrochemical Society, Under Review. **XX**.

21. Jayaraju, N., *Electrochemical atomic layer deposition (E-ALD) of Pt and PtRu nanofilms*, in *Chemistry*. 2010, University of Georgia: Athens.

22. Sheridan, L.B., Czerwiniski, J.; Jayaraju, N.; Gebregziabiher, D. K.; Stickney, J. L.; Robinson, D. B. and Soriaga, M. P., *Electrochemical Atomic Layer Deposition (E-ALD) of Palladium Nanofilms by Surface Limited Redox Replacement (SLRR), with EDTA Complexation.* Electrocatalysis, 2012. **3**(2): p. 96-107.

23. Sheridan, L.B.G., D. K.; Stickney, J. L. and Robinson, D. B. , *Formation of Palladium Nanofilms using Electrochemical Atomic Layer Deposition (E-ALD) with Chloride Complexation.* Langmuir, 2013. **Accepted**.

24. Ghodbane, O., L. Roue, and D. Belanger, *Study of the electroless deposition of Pd on Cu-modified graphite electrodes by metal exchange reaction.* Chemistry of Materials, 2008. **20**(10): p. 3495-3504.

25. Kiani, A. and E.N. Fard, *Fabrication of palladium coated nanoporous gold film electrode via underpotential deposition and spontaneous metal replacement: A low palladium loading electrode with electrocatalytic activity.* Electrochimica Acta, 2009. **54**(28): p. 7254-7259.

26. Gong, K.P., et al., *Platinum-monolayer electrocatalysts Palladium interlayer on IrCo alloy core improves activity in oxygen-reduction reaction.* Journal of Electroanalytical Chemistry, 2010. **649**(1-2): p. 232-237.

27. Baricuatro, J.H., et al., *UHV-EC Characterization of Ultrathin Films Electrodeposited on Well-Defined Noble Metals. I: Pd on Pt(111).* Electrocatalysis, 2010. **1**(1): p. 28-33.

28. Kibler, L.A., M. Kleinert, and D.M. Kolb, *Initial stages of Pd deposition on Au(hkl) part II: Pd on Au(100).* Surface Science, 2000. **461**(1-3): p. 155-167.

29. Hoyer, R., L.A. Kibler, and D.M. Kolb, *Electrochemical Pd deposition onto Rh(111): from cluster to monolayer growth.* Surface Science, 2004. **562**(1-3): p. 275-283.

30. Santos, B., et al., *Structure of ultrathin Pd films determined by low-energy electron microscopy and diffraction.* New Journal of Physics, 2010. **12**.

31. Attard, G.A. and A. Bannister, *The Electrochemical Behavior of Irreversibly Adsorbed Palladium on Pt(111) in Acidic-media* Journal of Electroanalytical Chemistry, 1991. **300**(1-2): p. 467-485.

32. Baldauf, M. and D.M. Kolb, *A Hydrogen Adsorpiton and Absorption Study with Ultrathin Pd Overlayers on Au(111) and Au(100)* Electrochimica Acta, 1993. **38**(15): p. 2145-2153.

33. Kibler, L.A., et al., *Initial stages of Pd deposition on Au(hkl) - Part I: Pd on Au(111).* Surface Science, 1999. **443**(1-2): p. 19-30.

34. Naohara, H., S. Ye, and K. Uosaki, *Electrochemical layer-by-layer growth of palladium on an Au(111) electrode surface: Evidence for important role of adsorbed Pd complex.* Journal of Physical Chemistry B, 1998. **102**(22): p. 4366-4373.

35. Quayum, M.E., S. Ye, and K. Uosaki, *Mechanism for nucleation and growth of electrochemical palladium deposition on an Au(111) electrode.* Journal of Electroanalytical Chemistry, 2002. **520**(1-2): p. 126-132.

36. Clavilier, J., et al., *Preparation of Mono-crystalline Pt Microelectrodes and Electrochemical Study of the Plane Surfaces Cut in the Direction of the (111) and (110) Planes.* . Journal of Electroanalytical Chemistry, 1980. **107**(1): p. 205-209.

37. Soriaga, M.P.K., Y.G.; Soto, J.E., *Interfacial electrochemistry theory, experiment, and applications*, ed. A. Więckowski. 1999, New York Marcel Dekker.

38. Lay, M.D., T.A. Sorenson, and J.L. Stickney, *High-resolution electrochemical scanning tunneling microscopy (EC-STM) flow-cell studies.* Journal of Physical Chemistry B, 2003. **107**(38): p. 10598-10602.

39. Wade, T.L., T.A. Sorenson, and J.L. Stickney, *Interfacial Electrochemistry*, ed. A. Wieckowski. 1999, New York: Marcel Dekker.

40. Stickney, J.L., *Electrochemical atomic layer epitaxy*, in *Electroanalytical Chemistry, Vol 21*, A.J.B.a.I. Rubinstein, Editor. 1999, Marcel Dekker, Inc.: New York. p. 75-209.

41. Okada, J., J. Inukai, and K. Itaya, *Underpotential and bulk deposition of copper on Pd(111) in sulfuric acid solution studied by in situ scanning tunneling microscopy.* Physical Chemistry Chemical Physics, 2001. **3**(16): p. 3297-3302.

42. Cuesta, A., L.A. Kibler, and D.M. Kolb, *A method to prepare single crystal electrodes of reactive metals: application to Pd(hkl).* Journal of Electroanalytical Chemistry, 1999. **466**(2): p. 165-168.

43. Manne, S., et al., *Atomic-resolution Electrochemistry with the Atomic Force Microscope - Copper Deposition on Gold* Science, 1991. **251**(4990): p. 183-186.

44. Hachiya, T., H. Honbo, and K. Itaya, *Detailed Underpotential Deposition of Copper on Gold(111) in Aqueous Solutions* Journal of Electroanalytical Chemistry, 1991. **315**(1-2): p. 275-291.

45. Zhang, J., et al., *Underpotential deposition of Cu on Au(111) in sulfate-containing electrolytes: A theoretical and experimental study.* Journal of Chemical Physics, 1996. **104**(14): p. 5699-5712.

46. Zei, M.S., et al., *The Influence of Anions on the Structure of Underpotentially Deposited Cu on Au(111) - A LEED, RHEED and AES Study.* Berichte Der Bunsen-Gesellschaft-Physical Chemistry Chemical Physics, 1987. **91**(4): p. 349-353.

47. Vasiljevic, N., et al., *High resolution electrochemical STM: New structural results for underpotentially deposited Cu on Au(111) in acid sulfate solution.* Journal of Electroanalytical Chemistry, 2008. **613**(2): p. 118-124.

48. Shi, Z., et al., *Investigations of SO4(2-) Adsorption at the Au(111) Electrode by Chronocoulometry and Radiochemistry* Journal of Electroanalytical Chemistry, 1994. **366**(1-2): p. 317-326.

49. Bauer, E., *Phänomenologische Theorie der Kristallabscheidung an Oberflächen. I.* Zeitschrift für Kristallographie - Crystalline Materials, 1958. **110**(1-6): p. 372-394.

50. Stickney, J.L., I. Villegas, and C.B. Ehlers, *Insitu Restoration of Atomically Well-Ordered Copper Single-Crystal Electrode Surfaces.* Journal of the American Chemical Society, 1989. **111**(16): p. 6473-6474.

51. Soriaga, M.P. and J.L. Stickney, *Vacuum surface techniques in electroanalytical chemistry* in *Modern techniques in electroanalysis*, P. Vanýsek, Editor. 1996, John Wiley & Sons New York.

52. Kim, Y.G., et al., *Adsorbate-induced disorder-to-order surface reconstruction: iodine on Pd(111) revisited by EC-STM.* Journal of Electroanalytical Chemistry, 2001. **509**(2): p. 170-174.

53. Bothwell, M.E., et al., *Insitu Regeneration of Clean and Ordered Pd(111) Electrode Surfaces by Oxidative Chemisorption and Reductive Desorption of Iodine* Surface Science, 1991. **249**(1-3): p. L322-L326.

54. Huemann, S., et al., *X-ray diffraction and STM study of reactive surfaces under electrochemical control: Cl and I on Cu(100).* Journal of Physical Chemistry B, 2006. **110**(49): p. 24955-24963.

55. Goetting, L.B., et al., *Preparation of Au Single-Crystals for Studies of the ECALE Deposition of CdTe.* Electrochimica Acta, 1995. **40**(1): p. 143-158.

56. Wieckowski, A., et al., *Preparation of Well-Defined Surfaces at Atmospheric Pressure - Studies by Electrochemistry and LEED of Pt(100) Pretreated with Iodine* Inorganic Chemistry, 1984. **23**(5): p. 565-569.

57. Soriaga, M.P. and A.T. Hubbard, *Determination of the Orientation of Aromatic-Molecules Adsorbed on Platinum-Electrodes - The Influence of Iodide, A - Surface-Active Anion.* Journal of the American Chemical Society, 1982. **104**(10): p. 2742-2747.

58. Schimpf, J.A., J.B. Abreu, and M.P. Soriaga, *In-situ Reordering by Iodine Adsorption-Desorption of Extensively Disordered (Ion-bombarded) Pd(100) Electrode Surfaces* Electrochimica Acta, 1994. **39**(16): p. 2445-2448.

59. Kolb, D.M., *Electrochemistry - From Thermodynamics to Atomic Structures.* Berichte Der Bunsen-Gesellschaft-Physical Chemistry Chemical Physics, 1994. **98**(11): p. 1421-1432.

60. Villegas, I., C.B. Ehlers, and J.L. Stickney, *Ordering of Copper Single-crystal Surfaces in Solution - Confirmation by Low-energy-electron-diffraction* Journal of the Electrochemical Society, 1990. **137**(10): p. 3143-3148.

61. Wan, L.J., et al., *In situ scanning tunneling microscopy of adsorbed sulfate on well-defined Pd(111) in sulfuric acid solution.* Journal of Electroanalytical Chemistry, 2000. **484**(2): p. 189-193.

62. Kibler, L.A., A.M. El-Aziz, and D.M. Kolb, *Electrochemical behaviour of pseudomorphic overlayers: Pd on Au(111).* Journal of Molecular Catalysis a-Chemical, 2003. **199**(1-2): p. 57-63.

63. Takahasi, M., et al., *Pseudomorphic growth of Pd monolayer on Au(111) electrode surface.* Surface Science, 2000. **461**(1-3): p. 213-218.

64. Pluntke, Y. and L.A. Kibler, *Hydrogen Evolution Electrocatalysis on AgPd(111) Alloys.* Electrocatalysis, 2011. **2**(3): p. 192-199.

65. Kitchin, J.R., et al., *Role of strain and ligand effects in the modification of the electronic and chemical properties of bimetallic surfaces.* Physical Review Letters, 2004. **93**(15).

66. Kibler, L.A., et al., *Tuning reaction rates by lateral strain in a palladium monolayer.* Angewandte Chemie-International Edition, 2005. **44**(14): p. 2080-2084.

67. Kibler, L.A., *Dependence of electrocatalytic activity on film thickness for the hydrogen evolution reaction of Pd overlayers on Au(111).* Electrochimica Acta, 2008. **53**(23): p. 6824-6828.

68. Roudgar, A. and A. Gross, *Local reactivity of thin Pd overlayers on Au single crystals.* Journal of Electroanalytical Chemistry, 2003. **548**: p. 121-130.

69. Roudgar, A. and A. Gross, *Local reactivity of metal overlayers: Density functional theory calculations of Pd on Au.* Physical Review B, 2003. **67**(3).

70. Alvarez, B., et al., *Anion adsorption on Pd-Pt(111) electrodes in sulphuric acid solution.* Journal of Electroanalytical Chemistry, 2001. **497**(1-2): p. 125-138.

71. El-Aziz, A.M. and L.A. Kibler, *Influence of steps on the electrochemical oxidation of CO adlayers on Pd(111) and on Pd films electrodeposited onto Au(111).* Journal of Electroanalytical Chemistry, 2002. **534**(2): p. 107-114.

72. Clavilier, J., et al., *Study of the Charge Displacement at Constant Potential During CO Adsorption on Pt(110) and Pt(111) Electrodes in Contact witha Perchloric-acid Solution* Journal of Electroanalytical Chemistry, 1992. **330**(1-2): p. 489-497.

73. Duncan, H. and A. Lasia, *Mechanism of hydrogen adsorption/ab sorption at thin Pd layers on Au(111).* Electrochimica Acta, 2007. **52**(21): p. 6195-6205.

74. Johansson, M., et al., *Hydrogen adsorption on palladium and palladium hydride at 1 bar.* Surface Science, 2010. **604**(7-8): p. 718-729.

75. Alvarez, B., et al., *Electrochemical properties of palladium adlayers on Pt(100) substrates.* Surface Science, 2004. **573**(1): p. 32-46.

76. Tang, J., et al., *Pd deposition onto Au(111) electrodes from sulphuric acid solution.* Electrochimica Acta, 2005. **51**(1): p. 125-132.

77. Kibler, L.A., *Hydrogen electrocatalysis.* Chemphyschem, 2006. **7**(5): p. 985-991.

78. Pandelov, S. and U. Stimming, *Reactivity of monolayers and nano-islands of palladium on Au(111) with respect to proton reduction.* Electrochimica Acta, 2007. **52**(18): p. 5548-5555.

79. Bjorketun, M.E., et al., *Hydrogen evolution on Au(111) covered with submonolayers of Pd.* Physical Review B, 2011. **84**(4).

80. Jerkiewicz, G., *Hydrogen sorption at/in electrodes.* Progress in Surface Science, 1998. **57**(2): p. 137-186.

81. Bartlett, P.N., et al., *The preparation and characterisation of H-1-e palladium films with a regular hexagonal nanostructure formed by electrochemical deposition from lyotropic liquid crystalline phases.* Physical Chemistry Chemical Physics, 2002. **4**(15): p. 3835-3842.

82. Czerwinski, A., S. Zamponi, and R. Marassi, *The Influence of Carbon-monoxide on Hydrogen Absorption by Thin-films of Palladium* Journal of Electroanalytical Chemistry, 1991. **304**(1-2): p. 233-239.

83. Rafizadeh, H.A., *Lattice-Dynamics of Metal-Hydrides* Physical Review B, 1981. **23**(4): p. 1628-1632.

84. Gabrielli, C., et al., *Investigation of hydrogen adsorption and absorption in palladium thin films - II. Cyclic voltammetry.* Journal of the Electrochemical Society, 2004. **151**(11): p. A1937-A1942.

85. Park, Y.S., et al., *Highly-Ordered Ultrathin Pd Films on Pt(111): Electrodeposition and Structural Characterization.* ECS Transactions, 2007. **3**(34): p. 65-103.

86. Pichardo-Pedrero, E., G.L. Beltramo, and M. Giesen, *Electrochemical annealing and its relevance in metal electroplating: an atomistic view.* Applied Physics a-Materials Science & Processing, 2007. **87**(3): p. 461-467.

87. Ciapina, E.G. and E.A. Ticianelli, *The effect of electrochemical CO annealing on platinum-cobalt nanoparticles in acid medium and their correlation to the oxygen reduction reaction.* Electrochimica Acta, 2011. **58**: p. 172-178.

88. Stickney, J.L., et al., *Scanning Probe Techniques in Studies of the Digital Processing of Compound Semiconductors.* Abstracts of Papers of the American Chemical Society, 1994. **207**: p. 175-COLL.

89. Giesen, M., et al., *Step fluctuations on metals in contact with an electrolyte: a new access to dynamical processes at the solid/liquid interface.* Surface Science, 1997. **384**(1-3): p. 168-178.

90. Hirai, N., K. Watanabe, and S. Hara, *Potential dependence of decay rate of multi-layered on Au(100) single crystals in sulfuric acid solution.* Surface Science, 2001. **493**(1-3): p. 568-574.

91. Hoshi, N., K. Kagaya, and Y. Hori, *Voltammograms of the single-crystal electrodes of palladium in aqueous sulfuric acid electrolyte: Pd(S)- n(111) x (111) and Pd(S)- n(100) x (111).* Journal of Electroanalytical Chemistry, 2000. **485**(1): p. 55-60.

92. Schimpf, J.A., J.B. Abreu, and M.P. Soriaga, *Electrochemical Regeneration of Clean and Ordered Pd(100) Surfaces by Iodine Adsorption-Desorption - Evidence from Low-Energy-Electron Diffraction.* Journal of Electroanalytical Chemistry, 1994. **364**(1-2): p. 247-249.

93. Shin, J.W., U. Bertocci, and G.R. Stafford, *In Situ Stress Measurement During Hydrogen Sorption on Ultrathin (111)-Textured Pd Films in Alkaline Electrolyte.* Journal of the Electrochemical Society, 2011. **158**(7): p. F127-F134.

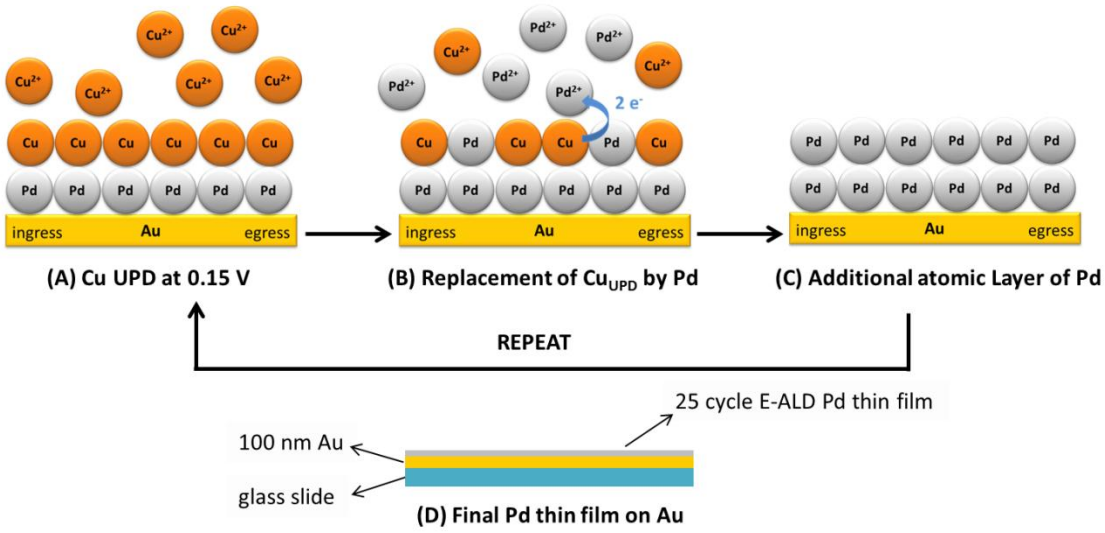

Figure 4.1 Schematic of an E-ALD cycle using SLRR to form a Pd nanofilm on Au(111). Note that Cu_{UPD} deposited directly on Au(111) is replaced by Pd ions to form the 1st Pd atomic layer.

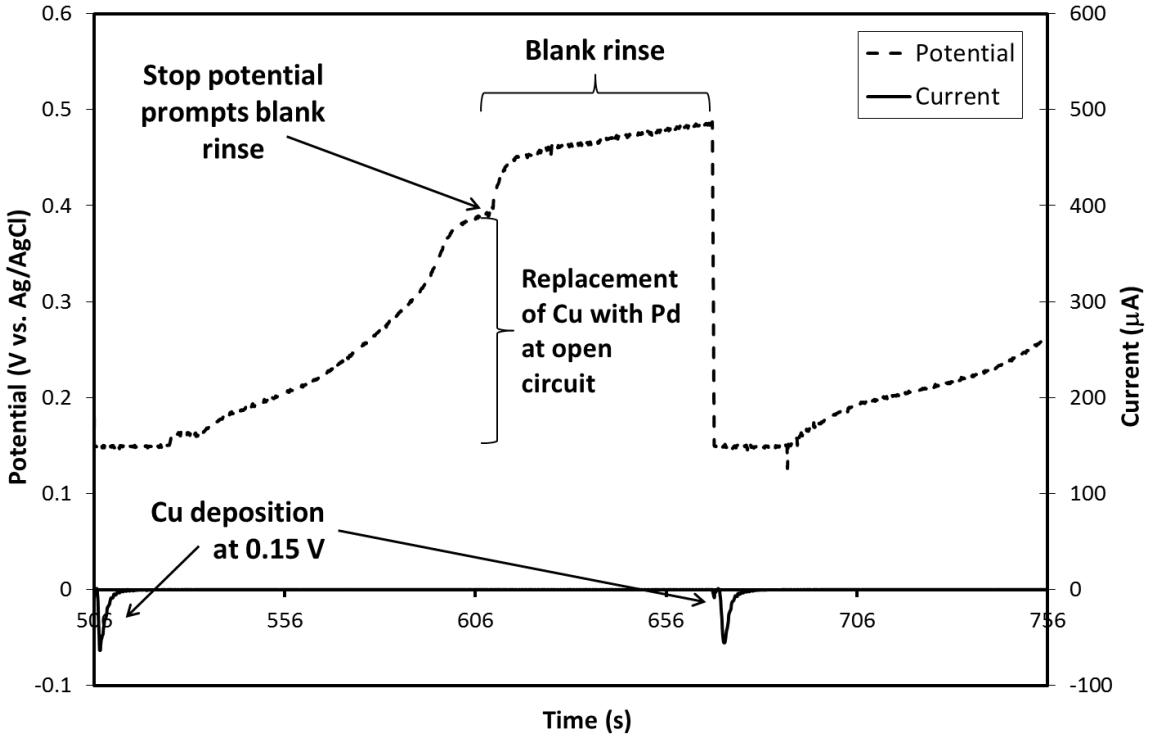

Figure 4.2 Time-Potential-Current plot of 1 complete Pd E-ALD cycle. Cu_{UPD} was formed at 0.15 V, Pd solution was flowed in and allowed to replace Cu until the OCP reached 0.4 V. A 60 s blank rinse, while still at OCP, completed the cycle.

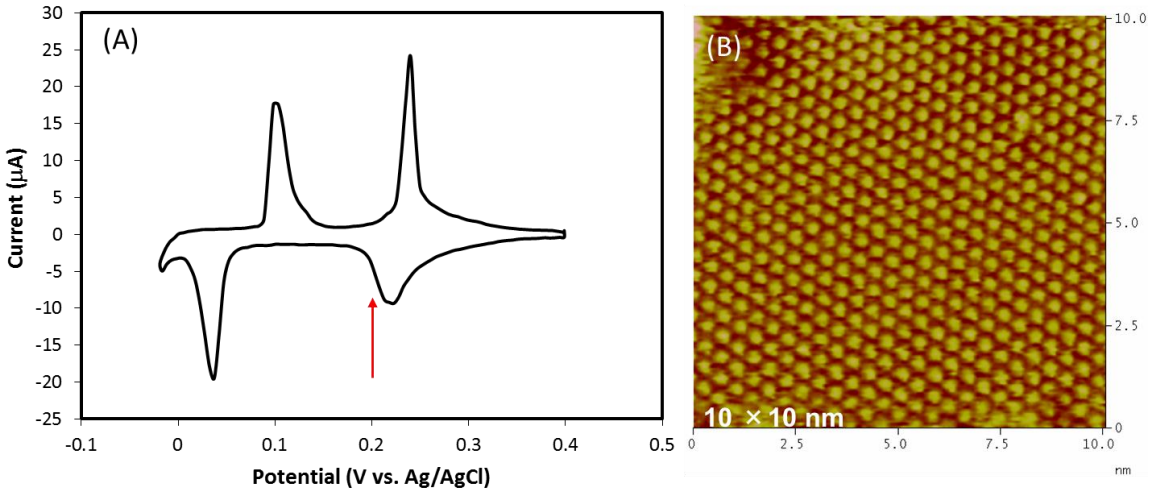

Figure 4.3 (A) CVs of the Au(111) disk in 2 mM $CuSO_4$, 0.05 M H_2SO_4 at 10 mV/s (B) EC-STM image of the honeycomb (√3 x √3)R30° structure (θ_{Cu} = *0.67 and* θ_{anion} = *0.33*) in 1 mM $CuSO_4$, 0.05 M H_2SO_4: Obtained at +0.2 V. Bias voltage: -200 mV, tunneling current: 20 nA.

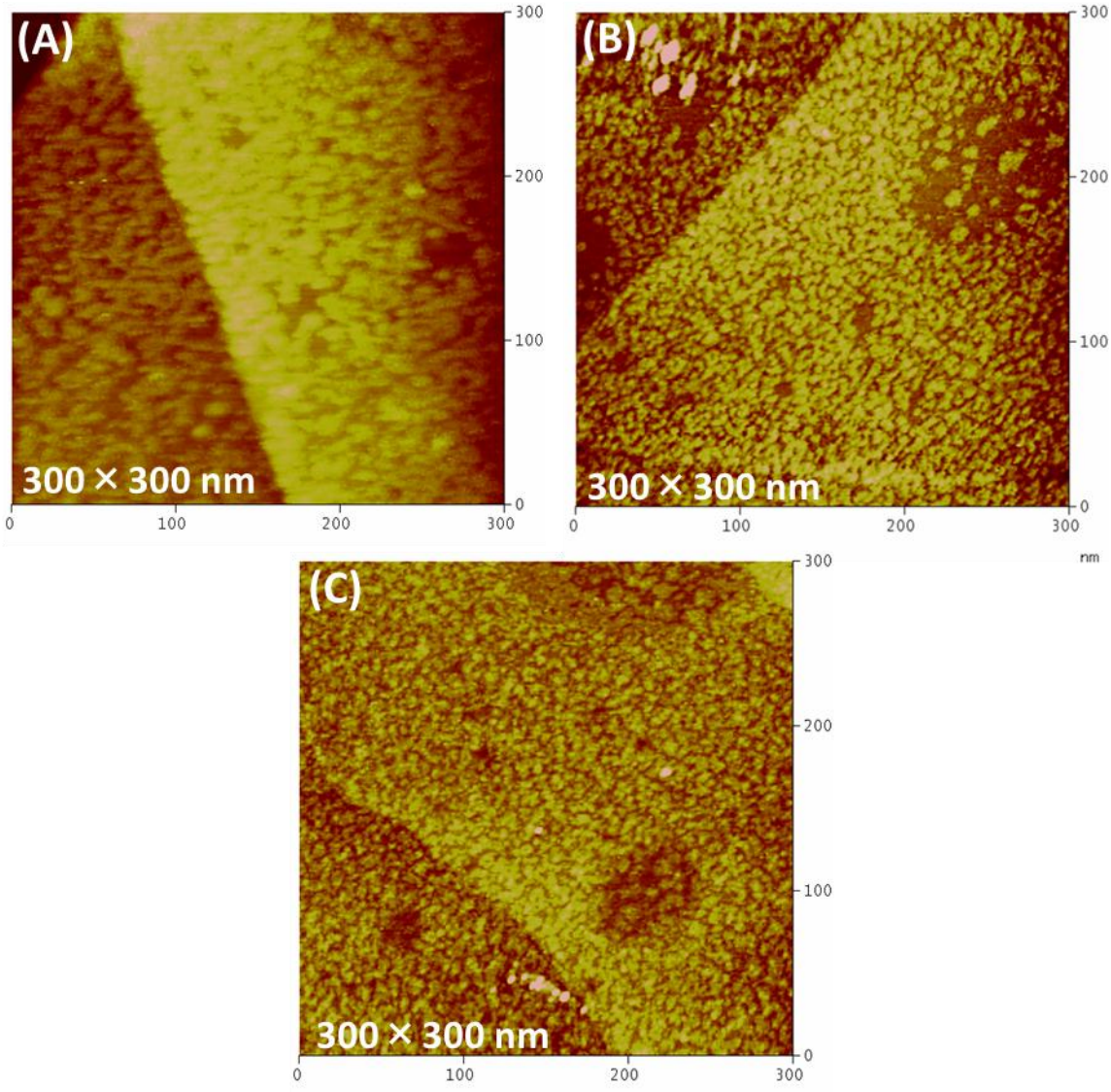

Figure 4.4 Wide-area (300 x 300 nm) EC-STM images of Pd deposited on Au(111) after 1 (A), 2 (B) and 3 (C) replacement cycles. Images were obtained at + 0.45 V. Bias voltage: -390 mV, tunneling current: 5 nA.

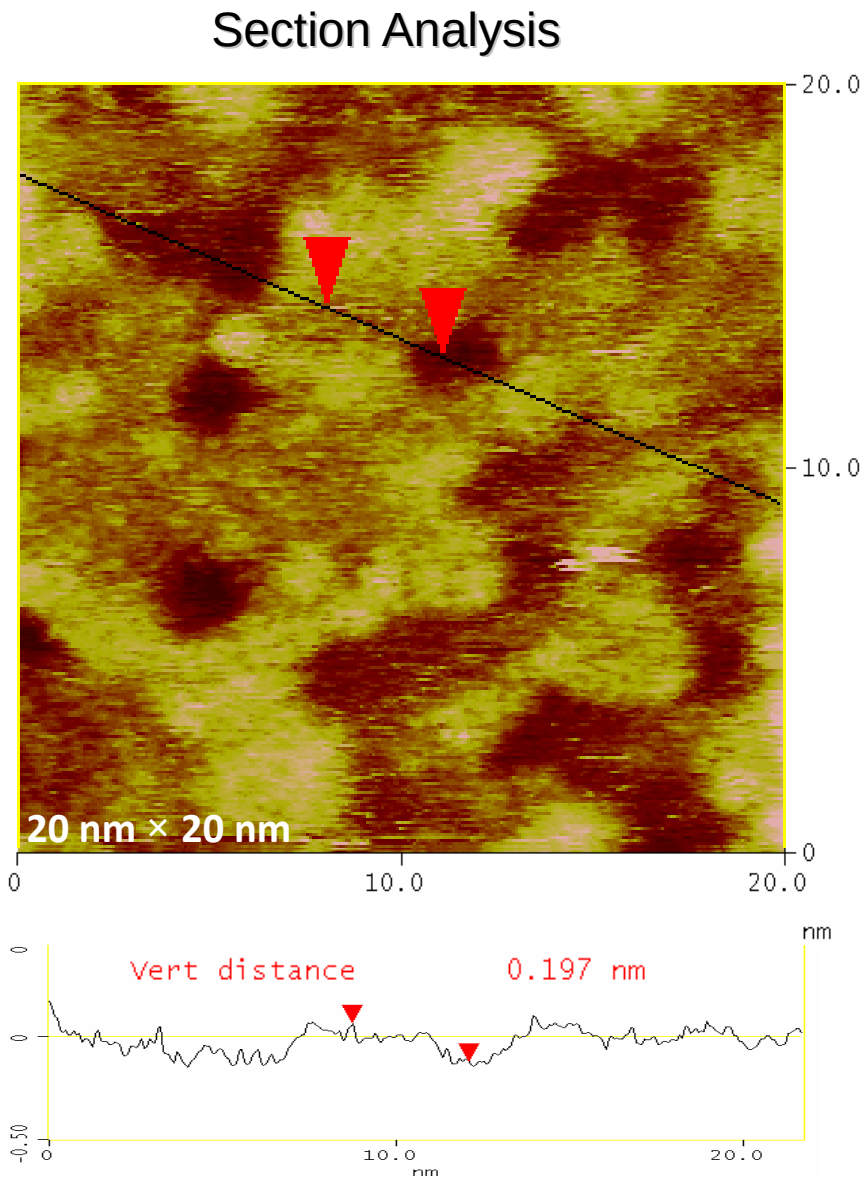

Figure 4.5 High-resolution EC-STM image and section analysis of Pd deposited on Au(111) after 2 replacement cycles. Height profile extracted along the black line is presented; average step height is 0.21 ± 0.01 nm. Image was obtained at + 0.45 V. Bias voltage: -390 mV, tunneling current: 10 nA.

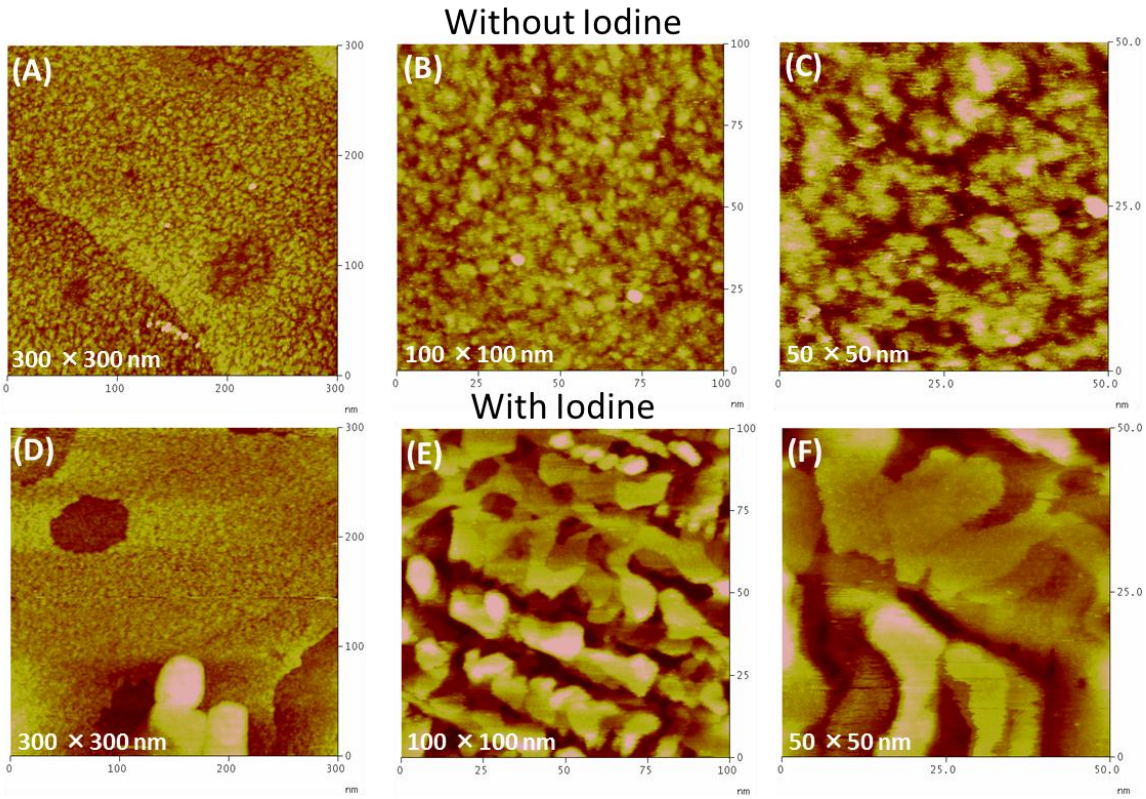

Figure 4.6 EC-STM images of 3 cycles of Pd SLRR on Au(111). (A), (B) and (C) show as deposited Pd, while (D), (E) and (F) were acquired after iodine adsorption. Images were obtained at + 0.45 V. Bias voltage: -390 mV, tunneling current: 5 nA.

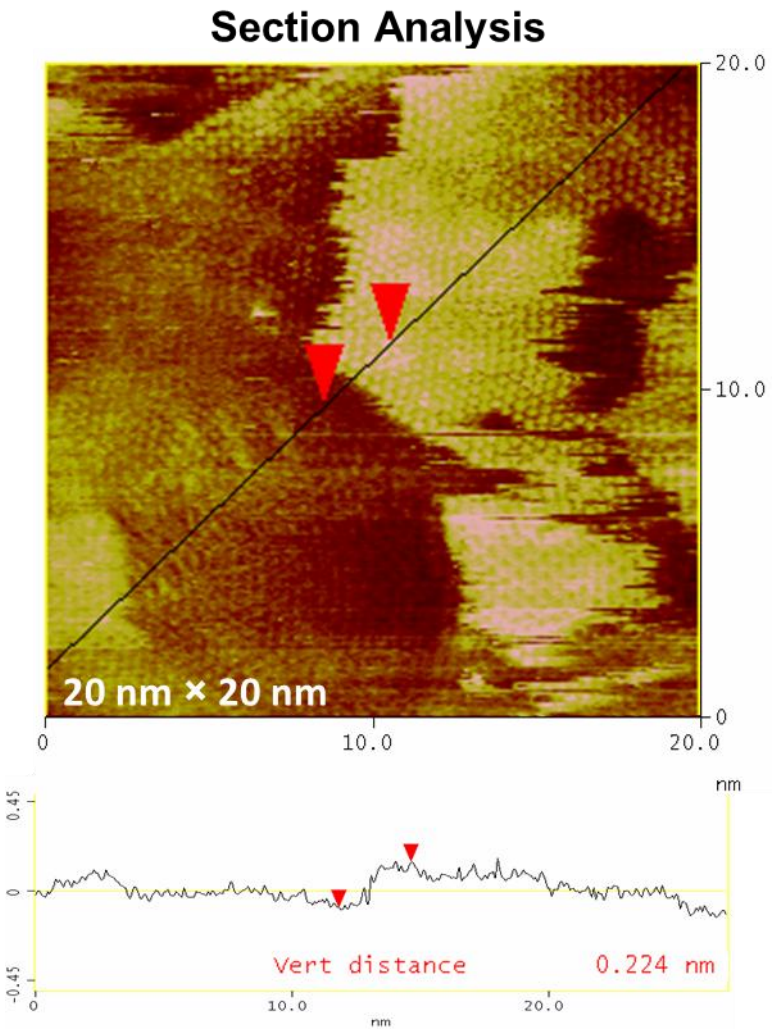

Figure 4.7 High resolution EC-STM image of 3 cycles of Pd SLRR on Au(111) after iodine adsorption and the corresponding height profile shows an average step height of 0.22 ± 0.01 nm. Images were obtained at + 0.45 V. Bias voltage: -390 mV, tunneling current: 10 nA.

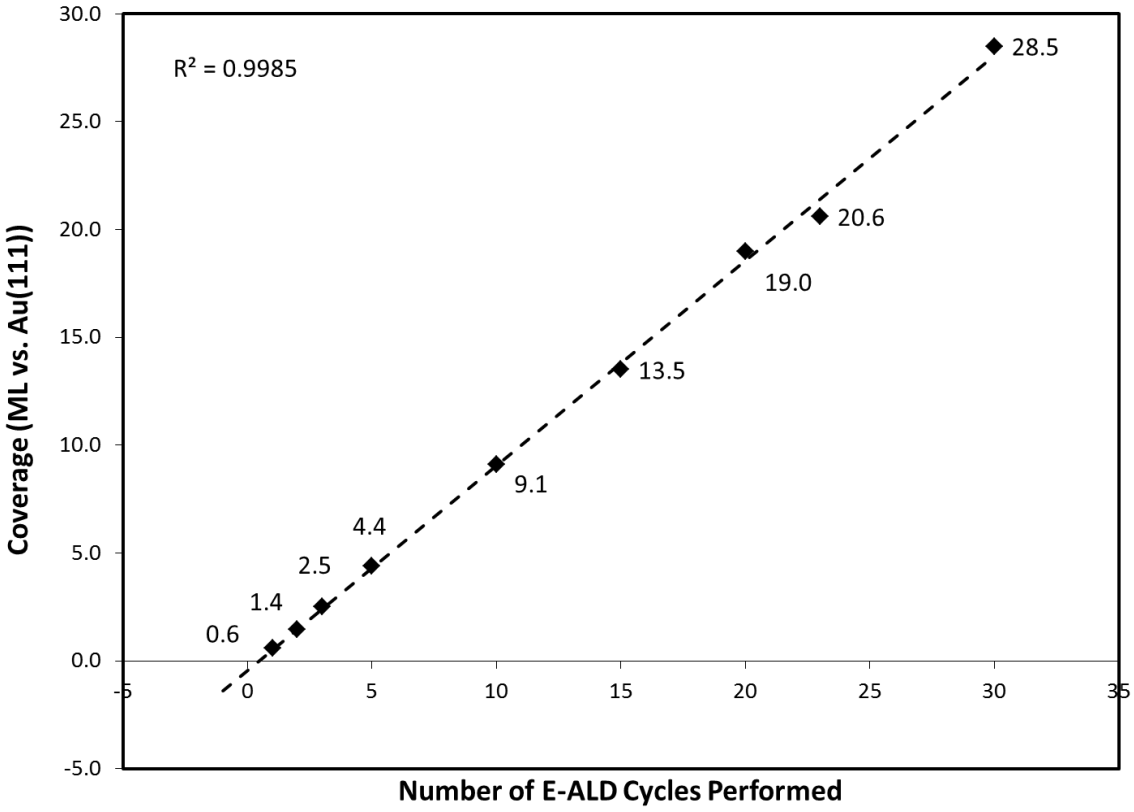

Figure 4.8 Plot of Pd coverage (i.e. film thickness) versus the number of E-ALD cycles performed, indicating a linear relationship.

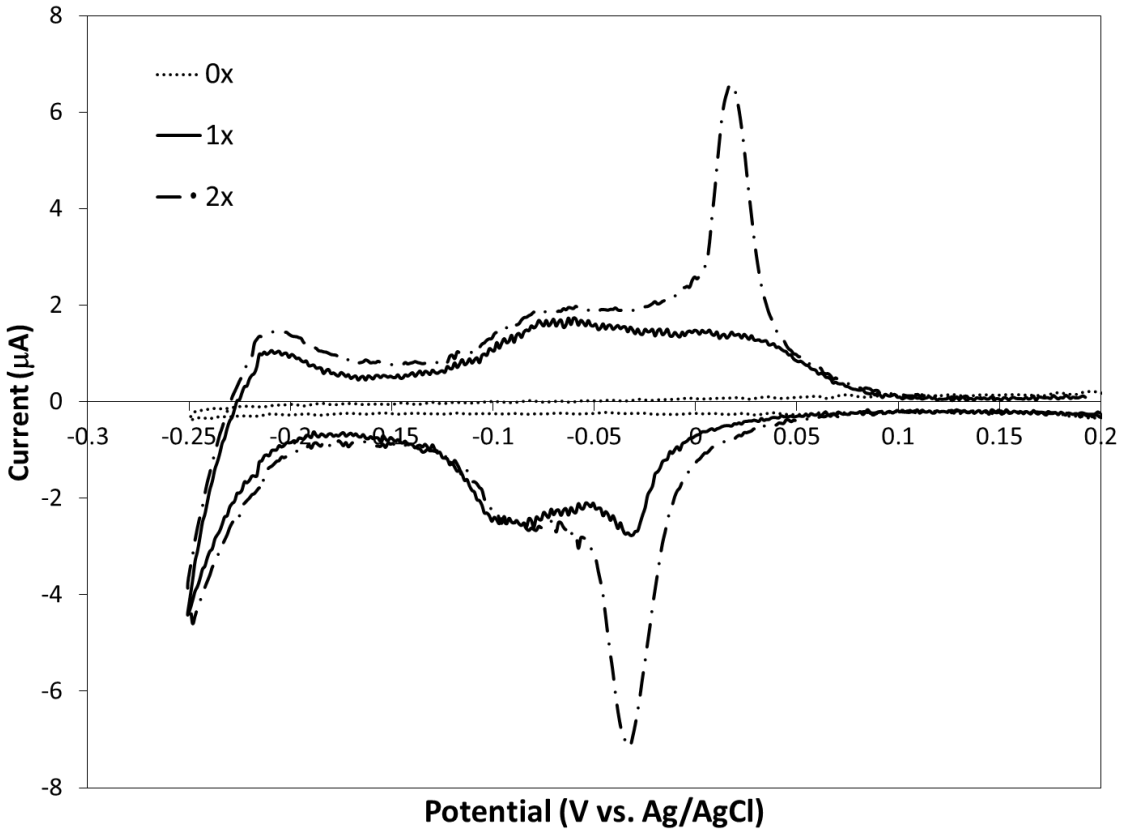

Figure 4.9 CVs of Au(111) without Pd (0x) compared with 1 and 2 E-ALD cycles of Pd on Au(111) in 0.1 M H_2SO_4 at 5 mV/s.

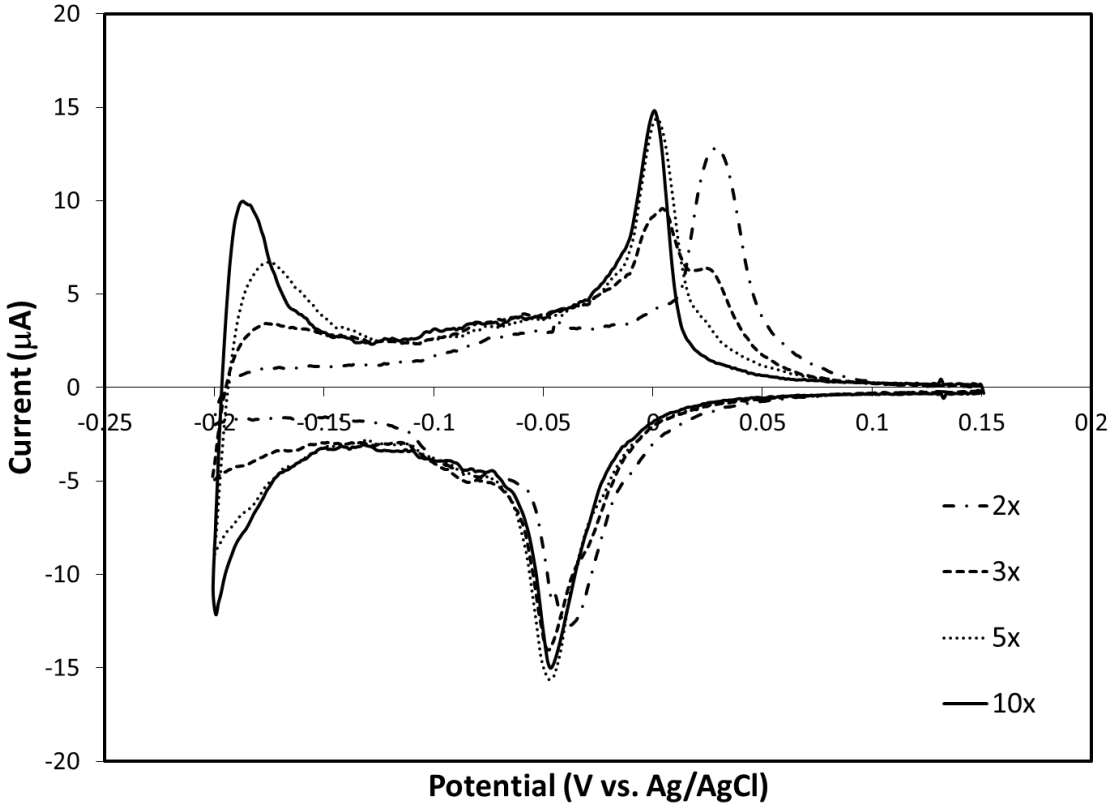

Figure 4.10 CVs of Pd nanofilms on Au(111), ranging from 2 to 10 E-ALD cycles in thickness, in 0.1 M H_2SO_4 at 10 mV/s.

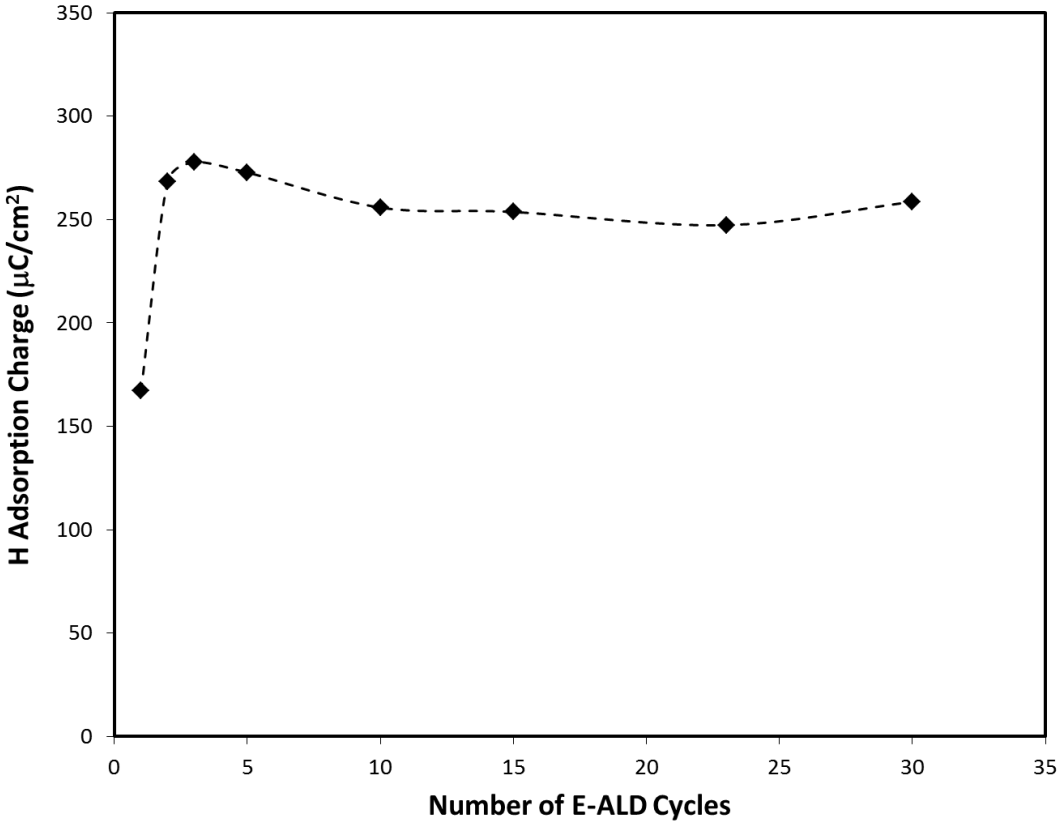

Figure 4.11 Plot of the H adsorption charge and the ratio of moles of H absorbed to moles of Pd versus the number of E-ALD cycles performed (i.e. thickness). H adsorption charges were obtained from CVs of Pd nanofilms taken in 0.1 M H_2SO_4. The moles of H was calculated from oxidation of H from fully saturated Pd films, while moles of Pd was calculated from anodic dissolution of the films in 50 mM HCl.

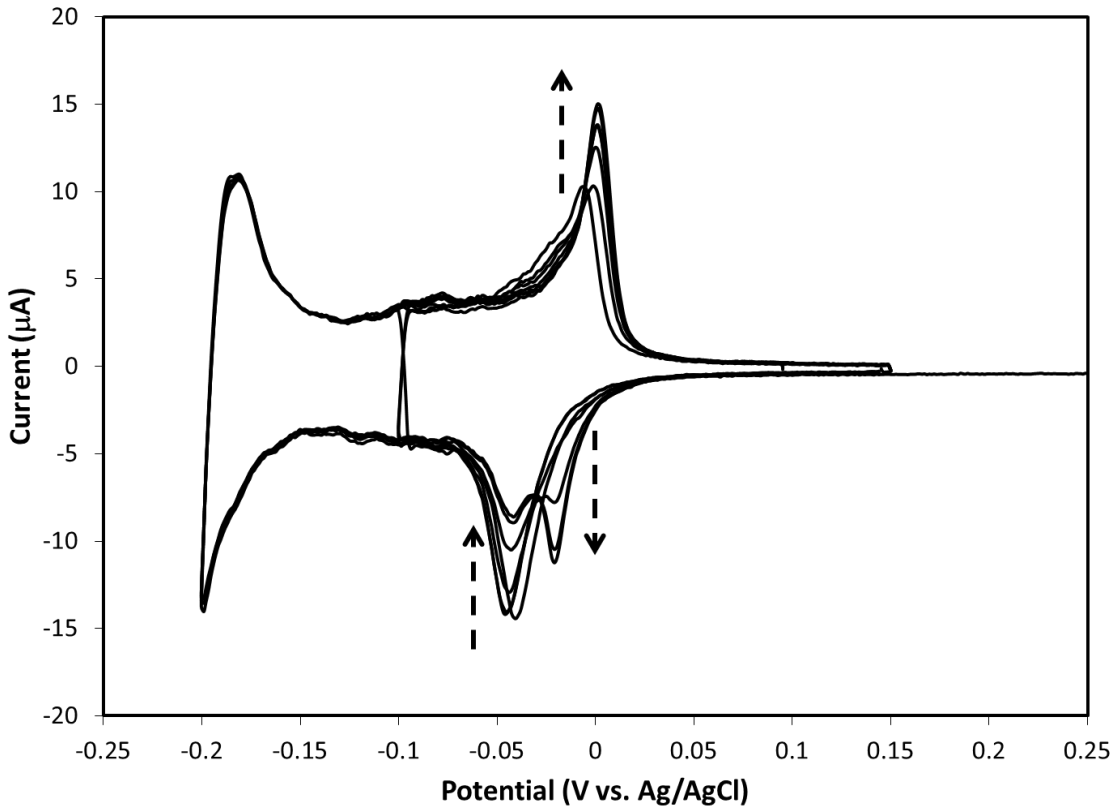

Figure 4.12 CVs of repeated cycling of a 23 cycle E-ALD Pd film in 0.1 M H_2SO_4 at 10 mV/s.

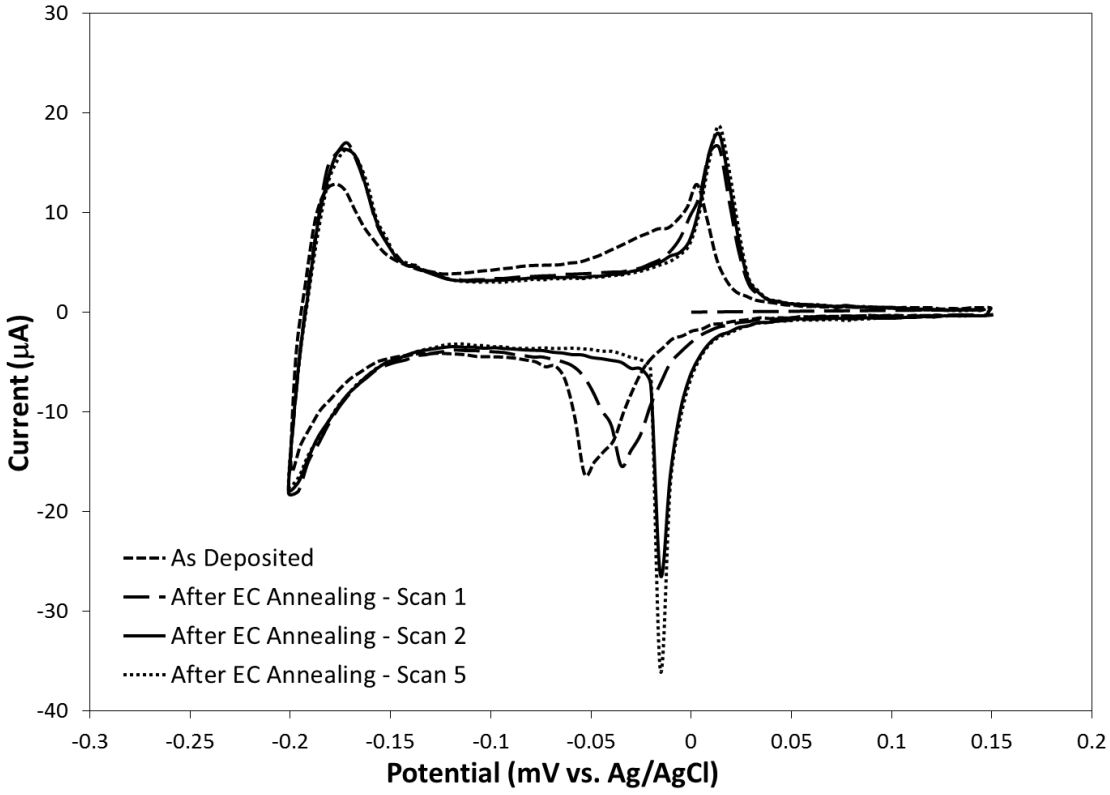

Figure 4.13 CVs of an as deposited 15 cycle E-ALD Pd film before and after EC annealing in 0.1 M H_2SO_4 at 10 mV/s. Scans 1, 2 and 5 were recorded after EC annealing

CHAPTER 5

HYDROGEN SORPTION PROPERTIES OF BARE AND RH-MODIFIED PD NANOFILMS GROWN VIA SURFACE LIMITED REDOX REPLACEMENT (SLRR) REACTIONS[4]

[4] L. B. Sheridan, J. L. Stickney, D. Benson and D. B. Robinson, To be submitted to *Journal of The Electrochemical Society* (2013)

Abstract

Pd nanofilms were grown using electrochemical atomic layer deposition (E-ALD) and used as a platform for investigations into changes in hydrogen absorption/desorption kinetics as a function of the coverage of Rh. Surface limited redox replacement (SLRR) reactions were used to form Pd atomic layers. That is Pd atomic layers were grown on polycrystalline Au by forming Cu UPD and then exchanging this Cu sacrificial monolayer for $PdCl_4^{2-}$ ions at open circuit. That cycle was then repeated 15 times to form the Pd nanofilms used in this study. Rh was deposited on the 15 cycle Pd films from a $RhCl_6^{3-}$ solution at constant potential or using an E-ALD procedure, similar to that employed to form the Pd nanofilms. Cyclic voltammetry (CV) of the Pd films with Rh over-layers formed at 0 V for 60, 300 and 1800 s, were compared with Pd films where Rh was deposited using 1, 5 and 10 E-ALD cycles. The resulting CVs all indicated enhanced rates of hydrogen absorption and desorption into and out of the underlying Pd nanofilm. Rh overlayers formed at 0 V for 60 s produced the greatest kinetic enhancement. Two possible explanations for the observed behavior are proposed and discussed.

Introduction

Pd is a classical hydrogen storage material with the ability to reversibly absorb up to 900 times its volume in hydrogen.[1] As a result, the reactions between Pd and hydrogen have been the subject of numerous studies. Pd undergoes surface limited hydrogen adsorption to form a surface hydride, while the bulk hydride is formed by diffusion and interstitial absorption of hydrogen atoms. The rates of absorption and desorption are critical in the development of materials for hydrogen storage and sensing. Ward and Dao[2] studied hydrogen permeation of thin Pd membranes and concluded that at low temperatures the surface hydride is rate-limiting in terms of desorption, while adsorption becomes rate-limiting in the presence of surface contaminants or at low H_2 partial pressures. On the other hand, Peden et al.[3] found that absorption was the rate-limiting step for clean Pd(110) and Delmelle et al.[4] described three kinetic regimes, two being rate-limited by absorption and one being rate-limited by adsorption. These conflicting reports indicate the complexity of the Pd-H system.

The mechanism of absorption also remains a topic of debate. There are two possible pathways for hydrogen electrosorption, one which proceeds through the surface hydride ($H^+ + e^- \leftrightarrow H_{ads} \leftrightarrow H_{abs}$) [5-8] and one in which hydrogen is absorbed simultaneously with proton reduction at the interface ($H^+ + e^- \leftrightarrow H_{abs}$) [9-12]. Lasia et al. have suggested that the mechanism for Pd absorption is a combination of fast, direct absorption and slower, indirect absorption that proceeds through the adsorbed hydrogen.[13, 14] In order to electrochemically differentiate the surface and bulk reactions requires the use of very thin Pd films. Otherwise, the features for absorption/desorption overwhelm those for adsorption/desorption.[15]

This group has recently developed an electrochemical atomic layer deposition (E-ALD) cycle for the formation of Pd nanofilms via surface limited redox replacement (SLRR).[16, 17] These nanofilms have been characterized using cyclic voltammetry (CV) and found to exhibit distinguishable features for hydrogen adsorption and absorption, making them an ideal platform for electrochemical investigations of the hydrogen sorption/desorption reactions.[18]

E-ALD is the condensed phase version of traditional, gas-phase atomic layer deposition (ALD).[19] In contrast to ALD, E-ALD is a room temperature technique that uses electrochemical rather than gas-phase surface limited reactions (SLRs) to form deposits one atomic layer at a time. E-ALD produces conformal deposits with atomic level control and provides excellent thickness tunability.[20] Underpotential deposition (UPD) is the most commonly used electrochemical SLR. UPD occurs when a material is electrodeposited at a potential positive of the potential required for the element to deposit on itself, resulting from the free energy of formation of an alloy or surface compound.[21-23] UPD results in an atomic layer: a layer of atoms no more than one atom thick with a coverage of a monolayer (ML) or less. The surface science definition of a ML is defined as one adsorbate per substrate surface atom.

E-ALD was initially developed for the formation of II-VI compound semiconductor thin films.[24] Over the years it has been extended to III-V[25] and IV-VI[26] semiconductors, superlattices[27, 28] and more complex structures like $CuInSe_2$.[29] A significant advance in E-ALD was prompted by the development of surface limited redox replacement (SLRR) around a decade ago.[30-33] This made the formation of metallic E-ALD thin films possible for the first time. The initial step in an

SLRR cycle is UPD of a "sacrificial" metal, one that is less noble than the metal desired for the nanofilm. The sacrificial metal is displaced using ionic precursors of the more noble metal at open circuit by redox replacement. In redox replacement the less noble metal becomes oxidized, supplying electrons to reduce the ionic precursors and deposit the more noble metal on the surface. Since UPD limits the sacrificial metal to an atomic layer, the depositing metal will be limited as well. The number of depositing atoms will be a function of the coverage of the sacrificial element, the oxidations states of reactants and products, and the exchange efficiency. The nanofilm thickness will be proportional to the number of cycles performed.[16, 34, 35] In addition to Pd nanofilms, SLRR has also been applied in the formation of Cu,[36-39] Ag[40], Ru,[34] Pt[30, 31, 35, 41] and Pt/Ru[42].

Recent theoretical modeling predicts that certain near-surface Pd alloys, defined as "submonolayers of alloy elements at or just below the Pd surface," lower the energetics of the adsorbed hydrogen state so that it more closely resembles those of bulk absorption, improving transport of hydrogen between them.[43] That work, along with experimental reports on Pd-rich bulk Pd-Rh alloys, indicate that Rh-modified Pd surfaces may enhance the kinetics for hydrogen absorption and desorption.[44, 45]

Electrodeposited Rh films have long been used in commercial applications.[46] However, detailed studies of the early stages of Rh electrodeposition, which are relevant to formation of nanofilms and submonolayers, are limited. Several studies of Rh electrodeposition on Pt[47-49] and Au[50-52] have been reported, but there do not appear to be any reports for Rh electrodeposition on Pd substrates. Electrochemical scanning tunneling microscopy (EC-STM) studies by Kibler et al.[51] revealed an adlayer of

$[RhCl_6]^{3-}$ on Au(111) that resulted in deposition of an epitaxial layer. Further deposition was kinetically slow and resulted in 3D growth. Furthermore, Rh deposition on Au(100)[52] and polycrystalline Au[50] were also found to be kinetically slow and to follow Stranski-Krastanov growth: 2D growth initially, followed by 3D growth. In the case of Pt(111) Rh was found to deposit in a pseudo layer-by-layer mode[48]; however, Rh deposited on Pt(100) was very disordered for coverages approaching a ML or more[49].

In the present work, we describe preliminary results of the hydrogen sorption/desorption properties of Rh modified E-ALD Pd nanofilms on polycrystalline Au. Rh was deposited by several different electrodeposition methods that will be described and compared. In all cases, the addition of Rh appears to enhance the kinetics for hydrogen absorption into and desorption out of the underlying Pd nanofilm.

Experimental

Polycrystalline Au on glass (100 nm on a 5 nm Ti adhesion layer) substrates (EMF Corporation) were used to form the E-ALD Pd nanofilms. Prior to deposition, the Au on glass substrates were cleaned in 0.1 M H_2SO_4 by scanning between 1.4 and -0.2 V, until a steady state CV was obtained. Based on CVs, the substrates appeared to have a predominantly Au(111) surface structure. E-ALD was performed using an automated electrochemical flow cell deposition system[20, 53, 54] (Electrochemical ALD L.C.), with a single variable speed pump, 5 valves, 5 solution reservoirs, a potentiostat and an electrochemical flow cell (volume $\approx$ 0.15 mL). All E-ALD cycles were programmed using "Sequencer" E-ALD control software (Electrochemical ALD L.C.). The standard three-electrode set-up, incorporated into a flow cell, consisted of a Au wire counter

electrode inserted in the flow cell wall opposite the Au on glass working electrode. A Ag/AgCl (3 M KCl) reference electrode (Bioanalytical Systems, Inc.) was inserted downstream in a separate compartment to avoid contamination; all potentials are reported vs. this Ag/AgCl reference. The working electrode surface area was 2.1 cm^2.

A water filtration system (Milli-Q Advantage A10) delivered 18 MΩ-cm water that was used in preparing all solutions. The Pd^{2+} solution contained 0.1 mM $PdCl_2$ (Aldrich, 99.999%) and 50 mM HCl. The $CuSO_4$ sacrificial metal ion solution was 2 mM (J.T. Baker, 99.8%) in 0.1 M H_2SO_4 (J.T. Baker, Reagent Grade), and the blank solution was 0.1 M H_2SO_4. Rh was deposited from a solution containing 0.1 mM $RhCl_3$ in 10 mM HCl and 0.1 M H_2SO_4. Dissolved O_2 was minimized by purging all solutions with N_2 before and during all electrochemical studies.

Results and Discussion

Formation of E-ALD Pd Nanofilms

E-ALD Pd nanofilms were formed on polycrystalline Au via SLRR as depicted in Figure 5.1. The first step of the SLRR cycle was deposition of an atomic layer of the sacrificial metal. Cu has been shown to work well as a sacrificial metal for Pd SLRR[18] and was deposited at an underpotential using 0.15 V for 18 s. The Pd^{2+} ion solution was then pumped into the cell at open circuit and the potential was allowed to drift until it reached 0.4 V, the predetermined "stop" potential. The stop potential is set in the software to a potential positive enough to ensure the exchange was complete. Upon reaching the stop potential, the solution containing Pd^{2+} and Cu^{2+} (resulting from stripping of the sacrificial layer) is rinsed from the cell for 60 s with 0.1 M H_2SO_4. That

cycle is then repeated to grow the Pd nanofilms. This procedure has been optimized and described previously.[17, 18]

Figures 5.2 and 5.3 show CVs for different types of Pd electrodes. The CV in Figure 5.2 is for a 15 cycle E-ALD Pd nanofilm on Au(111).[19] This CV is very similar to that for a Pd(111) single crystal[56], displaying all the expected features. A sharp peak appears at 0.8 V for Pd surface oxidation, with the corresponding reduction, during the negative scan, at 0.4 V. The sharp reversible peaks labeled 1 and 4 are for hydrogen adsorption/sulfate desorption (1) and hydrogen desorption/sulfate adsorption (4) at the Pd surface. Bulk hydrogen absorption begins as the potential is shifted further negative (2) and its subsequent desorption occurs upon reversal of the scan direction (3). The main difference between this CV and that of bulk Pd(111)[55] is the clear separation between formation of the surface and bulk hydrides, which is characteristic of Pd nanofilms[14, 57] and nanoporous films[9, 58]. Figure 5.3 displays a CV of a 25 cycle E-ALD Pd nanofilm on polycrystalline Au (solid line) and a 100 nm sputtered Pd film (dashed line). Note that the hydrogen waves in the 25 cycle film on polycrystalline Au are essentially the same as those in Figure 5.2 for the deposit on the Au(111) single crystal, only differing in that peaks for the hydrogen waves are not as sharp or reversible, consistent with the Pd nanofilm on Au(111) being more ordered. The 100 nm film, on the other hand, shows little of the hydrogen adsorption features, as they are overwhelmed by those for hydrogen absorption/desorption.

Rh on Pd Nanofilms: Constant Potential Deposition

Initially, Rh was deposited at constant potential for varying amounts of time. It is assumed that Rh^{3+} exists as $RhCl_6^{3-}$ ions, due to the excess Cl^- present in the solution, and

has a standard reduction potential of 0.44 V vs. SHE or 0.24 V vs. Ag/AgCl.[59] Au CVs in the Rh solution are displayed in Figure 5.4 and show the initial onset of Rh deposition at 0.2 V, in good agreement with the literature.[51, 59] Rh deposition on Au is known to be kinetically slow and to proceed initially through nucleation [50-52]. Deposition was performed at 0 V, an overpotential of 0.23 V, in order to drive Rh reduction while avoiding formation of the Pd surface hydride.

Immediately after forming a 15 cycle Pd nanofilm, window opening CVs were performed in 0.1 M H_2SO_4, scanning from the open circuit potential (OCP) to −0.2, −0.225 and −0.25 V, with an upper limit of 0.15 V. This same window opening was then performed after Rh deposition to allow a comparison of the hydrogen sorption/desorption properties of bare Pd vs. Rh modified Pd. The upper limit of 0.15 V was selected to prevent surface oxidation of Pd and Rh, thereby minimizing disruption of the surface structure.

Figure 5.5 compares CVs in 0.1 M H_2SO_4 for Rh deposited for 60 s on polycrystalline Au (black), on a freshly prepared 15 cycle Pd nanofilm without Rh (red) and after Rh deposition at 0 V for 60 s (blue), 300 s (green) and 1800 s (purple). The most striking difference in the various samples is seen in hydrogen absorption/desorption region. For Pd films with Rh these features, on the left, are sharper, have higher peak currents and are more reversible. The hydrogen absorption current, into the Pd lattice, was faster when Rh was present. The majority of the subsequent hydrogen desorption occurs within just 50 mV, after reversing the scan back in the positive direction. These changes indicate enhanced kinetics for both hydrogen sorption and desorption. The

greatest enhancement was observed for the shortest deposition time (60 s), decreasing as the Rh deposition time increased (as the Rh coverage increased).

The black scan in Figure 5.5, included for comparison, is a CV of Rh deposited on polycrystalline Au at 0 V for 60. The pair of peaks around -0.18 V represent hydrogen adsorption/desorption on Rh, and occur at potentials similar to those for a Rh(111) electrode[51]. In sulfuric acid, hydrogen desorption/adsorption on Rh occurs simultaneously with HSO_4^-/SO_4^{2-} adsorption/desorption[56], similarly to hydrogen adsorption/desorption on Pd.[57] While these features are clearly seen for the CV of Rh deposited on Au, they are obscured by the onset of hydrogen absorption into Pd for CVs of Rh deposited on Pd.

At first glance, the hydrogen adsorption features for bare Pd are no longer visible after Rh deposition (Figure 5.5), suggesting that Rh is completely covering the underlying Pd and preventing hydrogen adsorption. However, a more detailed view of this region, as depicted in the inset, indicates a reaction is occuring between 0 V and – 0.15 V. When Rh is deposited for 60 s (blue) there are identifiable peaks, shifted negatively by ~ 50 mV. Those peaks suggests that Pd is still accessible to solution, though the negative shift indicates less strongly bound hydrogen in the presence of Rh. These results agree with the theory proposed by Conway and Jerkiewicz[58] in which the presence of a poison, such as thiourea, H_2S, and As compounds, on the Pd surface is thought to decrease the hydrogen adsorption coverage, while increasing the chemical potential of the remaining adsorbed hydrogen. Their theory was developed to explain why certain poisons promote hydrogen absorption and desorption for Pd. An increase in the chemical potential of adsorbed hydrogen correlates with a negative potential shift, as

seen for the blue scan in Figure 5.5. No clearly defined peaks are evident in the CVS with higher Rh coverages (green and purple), though current, greater than background charging, is passing between 0.0 and – 0.15 V. This suggests that a faradaic reaction, probably hydrogen adsorption, is occurring. The charge decreases with increasing Rh deposition time, consistent with covering more of the Pd surface. The lack of clear hydrogen adsorption features for Pd may result from the presence of only limited areas of exposed Pd in close proximity to Rh.

Rh is not capable of absorbing hydrogen[59], therefore, if absorption is observed, some of the underlying Pd must be exposed to solution, regardless of whether or not peaks for formation of Pd surface hydride are evident. Absorption should be shut-off once the Rh coverage reaches a critical value that blocks protons from accessing the Pd. Figure 5.6 shows CVs comparing a Pd nanofilm without Rh and with Rh deposited at −0.125 V for 300 s. These results show that, in the presence of presumably large Rh coverages, the Pd is still able to absorb significant amounts of hydrogen. The maximum peak currents are actually similar to those for Rh deposited at 0 V for 300 s (Figure 5.5, green) and larger than those for Rh deposited at 0 V for 1800 s (Figure 5.5, purple). In all of these examples in which substantial amounts of Rh have been deposited the absorption current still increases more rapidly and the reversibility remains improved compared to bare Pd. This suggests one of the following possibilities: (1) the deposition of Rh proceeds by initial nucleation followed by kinetically slow 3-D growth, leaving some fraction of underlying Pd exposed, (2) hydrogen is able to interact with Pd exposed at cracks and grain boundaries in the Rh overlayer or (3) Rh forms an alloy with Pd that is capable of absorbing hydrogen. Electrodeposited Rh has been reported to grow three-

dimensionally in the case of Au[51, 52] and on Pt(100)[49, 60]. Therefore, 3D growth is a reasonable explanation, but it is unclear if this mechanism would result in uncovered Pd for extended Rh deposition times at moderate to high overpotentials. If hydrogen only has access to Pd at cracks and grain boundaries, this would indicate that a minimal amount of bare Pd is required to drive hydrogen absorption. Finally, there is the possibility of alloying. It has been demonstrated that, under certain conditions, Pd-Rh alloys are able to store larger quantities of hydrogen than pure Pd[45, 61-63] and Łukaszewski et al. [44] has reported evidence of improved kinetics for bulk Pd-Rh alloys. Unfortunately, a determination has not yet been made as to which scenario accurately describes these results. However, XPS analysis is planned for establishing whether or not alloy formation is occurring and EC-STM may offer insight into the growth mechanism. These studies are beyond the scope of this article and will be the subject of future publications.

Rh on Pd Nanofilms: E-ALD

Based on the results presented thus far, the greatest enhancement for Pd absorption/desorption of hydrogen results from a lower Rh coverage (Figure 5.5, red), and so the effects of even lesser Rh coverages were investigated. These overlayers were formed by depositing Rh using E-ALD since this technique affords excellent control over deposit coverage and thickness. Just as in the formation of E-ALD Pd nanofilms, Rh was deposited by SLRR using Cu_{UPD}, following the exact procedure used for Pd (i.e. same stop potential, Cu_{UPD} potential and rinse time). Although the procedure was the same, the maximum coverage per cycle for replacement of 1 ML of Cu is 2/3 ML of Rh vs. 1 ML of Pd, due to their different oxidation states (Cu(II), Rh(III), and Pd(II)). Studies of E-

ALD of Pd have indicated that the Cu coverage averages ~0.7 ML per cycle vs. Au(111),[16] which means that the maximum Rh coverage per cycle is ~0.5 ML vs. Au(111).

CVs in 0.1 M H_2SO_4 of a freshly prepared 15 cycle Pd nanofilm without Rh and with 1, 5 and 10 E-ALD cycles of Rh are presented in Figure 5.7. These results, like those shown in Figure 5.5 and 5.6, indicate that the addition of a Rh overlayer enhances the rate of hydrogen absorption and desorption by Pd. One notable difference between the two sets of samples is that features for hydrogen adsorption/desorption on Pd are still plainly visible for 1-10 cycles of Rh E-ALD, while they are substantially reduced when Rh is deposited at 0 V or -0.125 V. These peaks represent the amount of exposed Pd and all three samples exhibit Pd surface hydride peaks that are sharper and shifted slightly positive. We believe this shift results from unintentional electrochemical annealing of the Pd nanofilm caused by the series of potentials applied during the experiment[18] (CVs of bare Pd, followed by deposition of Cu_{UPD} and OCP replacement by Rh), rather than the addition of Rh. It is possible that a less stable hydride, caused by the presence of Rh, is also formed at more negative potentials, as was suggested for the thicker Rh overlayers in Figure 5.5, and that the peaks around 0 V are due to hydrogen adsorption on large areas of exposed Pd. These peaks are greatest for 1 cycle of Rh and decrease for 5 and 10 cyles, which corresponds with a decrease in available Pd surface sites. The trend in Figure 5.7 is an increase in kinetics for formation of bulk Pd hydride with an increase in Rh coverage with the most substantial enhancement observed for 10 E-ALD cycles of Rh.

Figure 5.8 compares CVs of bare Pd, Pd with 10 E-ALD cycles of Rh, and Pd with Rh deposited at 0 V for 60 s. Both samples show a marked improvement in kinetics, with the higher Rh coverage (0 V for 60 s) displaying slightly greater enhancement. There are at least two possible explanations for the observed enhancement. The theory, originally proposed by Conway and Jerkiewicz[58], that was already discussed explains the enhancement by the formation of a less stable surface hydride that facilitates hydrogen absorption. An alternative explanation, suggested by Lasia et al. [13, 14], relies on the concept of dual pathways for hydrogen absorption by Pd. One pathway, direct absorption, is fast and the other slower pathway is indirect absorption that proceeds through the surface hydride. This model implies that when Rh is present and the Pd hydride peaks are diminished, most absorption is facilitated by the faster, direct mechanism, while slower, indirect absorption occurs more when the adsorption peaks are clearly observed. Similar behavior has been reported for adsorbed crystal violet[64, 65] and submonolayer Pt coverages[8] on Pd thin films. In both of these examples the hydrogen adsorption waves are suppressed while the rate of absorption and desorption are increased.

A Pd nanofilm with 10 E-ALD cycles of Rh was used to further investigate the electrochemical reactions occurring by scanning to more negative potentials. Figure 5.9 shows 4 different sets of CVs, with different negative potential limits, of the same 15 cycle E-ALD Pd film modified with 10 cycles of E-ALD Rh. The CVs in Figure 5.9 (A) are identical to those shown in Figures 5.7 (purple) and 5.8 (blue) and are included here for comparison. After scanning the Rh modified Pd nanofilm to −0.25 V (Figure 5.9 (B)), two new oxidation peaks appear at −0.23 and −0.22 V, labeled 1 and 2, respectively.

Peak 3 was already identified as desorption of absorbed hydrogen and here we focus on peak 1, which has been assigned to the hydrogen gas oxidation reaction (HOR). As the potential is scanned further negative to −0.275 (C) and −0.3 V (D) the HOR peak shifts to more negative potentials. Rh is a platinum group metal and therefore has a low overvoltage for the hydrogen evolution reaction (HER), making it a good HER catalyst. The E_0 for HER is −0.21 V and the acidic electrolyte (0.1 M H_2SO_4) supplies a high concentration of H^+. Therefore, large amounts of H_2 should be generated by H^+ reduction when scanning negative of the E_0. A low flow rate of 4 mL/min was used during CV and it is reasonable to assume that the pH at the electrode surface increased during the reaction due to substantial loss of H^+. According to the Nernst equation, this pH change would shift the E_0 negatively, making it possible to oxidize any H_2 remaining near the electrode surface when the potential scan is reversed. This hypothesis was tested by increasing the flow rate to its maximum value (17 mL/min.) and observing the effect on the oxidation peak. As expected, the peak almost disappeared entirely because an increased flow rate would decrease the effects of HER on the pH by continually replenishing the acidic electrolyte at the electrode surface and flushing away H_2 generated that could potentially be oxidized.

We suggest here that Peak 2 is an additional feature for desorption of either surface or bulk hydride that arises due to changes in the Pd/Rh surface structure. When large quantities of hydrogen are absorbed, as results from applying more and more negative potentials, expansion of the crystal lattice can cause the surface to buckle. One possible explanation for the appearance of peak 2 is that buckling exposes new surface atoms, which may have different surface hydride energies that catalyze bulk desorption

or allow surface hydride species to desorb at different potentials. This change in surface structure is also evident for a bare Pd E-ALD film that is subjected to more and more negative potentials as shown in Figure 5.10. Scan 1, with the negative potential limit of −0.225 V, has a sharp peak around −0.2 V for bulk hydrogen desorption. However, after scanning negative to −0.25 V, the peak broadens, due to more charge for hydrogen desorption, and develops a shoulder at positive potentials. Scans 3 and 4 have a large, more positive peak at −0.16 V and a shoulder on the negative edge around −0.18 V. The shift in peak positions suggests changes in the Pd film structure and agrees with those shifts seen for the Rh modified Pd nanofilm.

Conclusion

Pd E-ALD nanofilms on polycrystalline Au were used to investigate the effects of various coverages of Rh on the hydrogen adsorption/absorption and desorption features of Pd. CV suggested that all the Rh overlayers examined here substantially enhanced the rate of hydrogen absorption and desorption for bulk Pd. The Rh overlayer formed by deposition at 0 V for 60 s exhibited the greatest improvement.

Rh overlayers formed by 1 to 10 cycles of E-ALD left large areas of exposed Pd, as evidenced by the size and position of the features for Pd surface hydride. In contrast, Rh deposited at 0 V and -0.125 V for various lengths of time appears to have covered the majority of Pd surface sites. In the case of constant potential deposition, only the Rh overlayer formed at 0 V for 60 s still had clearly identifiable peaks for Pd surface hydride formation, though shifted negatively, which suggests a less stable hydride. Although clear peaks were not seen for longer Rh deposition times, faradaic charge was observed in this same potential range, and it was suggested to result from adsorbed hydrogen on

very small areas of exposed Pd surrounded by Rh. Regardless of the validity of this argument, Rh is not capable of hydrogen absorption, which suggests that some Pd surface sites must exist in order to allow hydrogen absorption to occur.

Two theories were presented to explain the observed kinetic improvements with the addition of Rh overlayers. In the first, the mechanism is assumed to involve the surface hydride as an intermediate and enhancement is explained by destabilization of the surface hydride in the presence of Rh, which accelerates hydrogen absorption.[58] The second theory assumes there are two absorption mechanisms with different rates[13, 14] and that Rh reduces the surface hydride coverage, allowing the majority of hydrogen absorption to proceed by the faster, direct mechanism, while the slower, indirect absorption is predominant when the surface hydride coverage is greater as is the case for bare Pd or small Rh coverages.

Acknowledgements

Acknowledgment is made of the support of the National Science Foundation, Division of Materials Research #1006747, as well as Sandia National Laboratories, a multi-program laboratory managed and operated by Sandia Corporation, a wholly owned subsidiary of Lockheed Martin Corporation, for the U.S. Department of Energy's National Nuclear Security Administration under contract DE-AC04-94AL85000.

References

1. Dullaghan, J.A.A.a.C.A., *Electrodeposition of Palladium and Palladium Alloys*, in *Modern Electroplating*, M.S.a.M. Paunovic, Editor. 2000, John Wiley & Sons, Inc.: New York. p. 483-554.
2. Ward, T.L. and T. Dao, *Model of hydrogen permeation behavior in palladium membranes.* Journal of Membrane Science, 1999. **153**(2): p. 211-231.
3. Kay, B.D., C.H.F. Peden, and D.W. Goodman, *Kinetics of Hydrogen Absorption by Pd(110)* Physical Review B, 1986. **34**(2): p. 817-821.
4. Delmelle, R. and J. Proost, *An in situ study of the hydriding kinetics of Pd thin films.* Physical Chemistry Chemical Physics, 2011. **13**(23): p. 11412-11421.
5. Montella, C., *EIS study of hydrogen insertion under restricted diffusion conditions - I. Two-step insertion reaction.* Journal of Electroanalytical Chemistry, 2001. **497**(1-2): p. 3-17.
6. Bockris, J.O., J. McBreen, and L. Nanis, *Hydrogen Evolution and Hydrogen Entry Into A-Iron* Journal of the Electrochemical Society, 1965. **112**(10): p. 1025-&.
7. Gabrielli, C., et al., *Investigation of hydrogen adsorption and absorption in palladium thin films - II. Cyclic voltammetry.* Journal of the Electrochemical Society, 2004. **151**(11): p. A1937-A1942.
8. Bartlett, P.N. and J. Marwan, *The effect of surface species on the rate of H sorption into nanostructured Pd.* Physical Chemistry Chemical Physics, 2004. **6**(11): p. 2895-2898.

9. Chen, J.S., et al., *Hydrogen insertion reaction with restricted diffusion .1. Potential step-EIS theory and review for the direct insertion mechanism.* Journal of Electroanalytical Chemistry, 1996. **406**(1-2): p. 1-13.

10. Bagotskaya, I.A., *Effect of the Solution Composition on the Diffusion Rate of Electrolytic Hydrogen Through Metallic Diaphragms 1. Diffusion of Hydrogen Through Iron Diaphragms I.* Zhurnal Fizicheskoi Khimii, 1962. **36**(12): p. 2667-2673.

11. Frumkin, A.N., *Advances in Electrochemtstry and Electrochemical Engineering*, ed. P. Delahay. Vol. 3. 1963, New York: Intersclence Publishers.

12. Lim, C. and S.I. Pyun, *Impedence Analysis of Hydrogen Absorption Reaction on Pd Membrane-electrode in 0.1 M LiOH Solution Under Permeable Boundary-Conditions* Electrochimica Acta, 1994. **39**(3): p. 363-373.

13. Duncan, H. and A. Lasia, *Mechanism of hydrogen adsorption/ab sorption at thin Pd layers on Au(111).* Electrochimica Acta, 2007. **52**(21): p. 6195-6205.

14. Lasia, A., *On the mechanism of the hydrogen absorption reaction.* Journal of Electroanalytical Chemistry, 2006. **593**(1-2): p. 159-166.

15. Czerwinski, A., et al., *The study of hydrogen sorption in palladium limited volume electrodes (Pd-LVE) I. Acidic solutions.* Journal of Electroanalytical Chemistry, 1999. **471**(2): p. 190-195.

16. Sheridan, L.B.G., D. K.; Stickney, J. L. and Robinson, D. B. , *Formation of Palladium Nanofilms using Electrochemical Atomic Layer Deposition (E-ALD) with Chloride Complexation.* Langmuir, 2013. **Accepted**.

17. Sheridan, L.B., Czerwiniski, J.; Jayaraju, N.; Gebregziabiher, D. K.; Stickney, J. L.; Robinson, D. B. and Soriaga, M. P., *Electrochemical Atomic Layer Deposition (E-ALD) of Palladium Nanofilms by Surface Limited Redox Replacement (SLRR), with EDTA Complexation.* Electrocatalysis, 2012. **3**(2): p. 96-107.

18. Sheridan, L.B.K., Y.G.; Stickney, J. L. and Robinson, D. B. , *Palladium Nanofilms on Au(111) Formed by Electrochemical Atomic Layer Deposition (E-ALD) with Chloride Complexation: Studies using Voltammetry and in-Situ Scanning Tunneling Microscopy.* In preparation, 2013.

19. George, S.M., *Atomic Layer Deposition: An Overview.* Chemical Reviews, 2010. **110**(1): p. 111-131.

20. Stickney, J.L., *Electrochemical Atomic Layer Epitaxy (EC-ALE): Nanoscale Control in the Electrodeposition of Compound Semiconductors*, in *Advances in Electrochemical Science and Engineering*, R.C.A.a.D.M. Kolb, Editor. 2002, Wiley-VCH: Weinheim.

21. Adzic, R.R., *Electrocatalytic Properties of the Surfaces Modified by Foreign Metal Adatoms* Advances in Electrochemistry and Electrochemical Engineering, ed. H.G.a.C.W. Tobias. Vol. 13. 1984, New York: Wiley-Interscience. 159-260.

22. Magnussen, O.M., *Ordered anion adlayers on metal electrode surfaces.* Chemical Reviews, 2002. **102**(3): p. 679-725.

23. Kolb, D.M., *Advances in Electrochemistry and Electrochemical Engineering*, ed. H.G.a.C.W. Tobias. Vol. 11. 1978, New York: John Wiley. 125.

24. Gregory, B.W. and J.L. Stickney, *Electrochemical Atomic Layer Epitaxy (Ecale).* Journal of Electroanalytical Chemistry, 1991. **300**(1-2): p. 543-561.

25. Wade, T.L., et al., *Electrodeposition of InAs.* Electrochemical and Solid State Letters, 1999. **2**(12): p. 616-618.

26. Banga, D.O., et al., *Formation of PbTe nanofilms by electrochemical atomic layer deposition (ALD).* Electrochimica Acta, 2008. **53**(23): p. 6988-6994.

27. Wade, T.L., et al., *Electrochemical formation of a III-V compound semiconductor superlattice: InAs/InSb.* Journal of Electroanalytical Chemistry, 2001. **500**(1-2): p. 322-332.

28. Vaidyanathan, R., et al., *Preliminary studies in the electrodeposition of PbSe/PbTe superlattice thin films via electrochemical atomic layer deposition (ALD).* Langmuir, 2006. **22**(25): p. 10590-10595.

29. Banga, D., et al., *Electrodeposition of CuInSe2 (CIS) via Electrochemical Atomic Layer Deposition (E-ALD).* Langmuir, 2012. **28**(5): p. 3024-3031.

30. Brankovic, S.R., J.X. Wang, and R.R. Adzic, *Metal monolayer deposition by replacement of metal adlayers on electrode surfaces.* Surface Science, 2001. **474**(1-3): p. L173-L179.

31. Mrozek, M.F., Y. Xie, and M.J. Weaver, *Surface-enhanced Raman scattering on uniform platinum-group overlayers: Preparation by redox replacement of underpotential-deposited metals on gold.* Analytical Chemistry, 2001. **73**(24): p. 5953-5960.

32. Vasilic, R. and N. Dimitrov, *Epitaxial growth by monolayer-restricted galvanic displacement.* Electrochemical and Solid State Letters, 2005. **8**(11): p. C173-C176.

33. Kim, Y.G., et al., *Platinum nanofilm formation by EC-ALE via redox replacement of UPD copper: Studies using in-situ scanning tunneling microscopy.* Journal of Physical Chemistry B, 2006. **110**(36): p. 17998-18006.

34. Thambidurai, C., Y.G. Kim, and J.L. Stickney, *Electrodeposition of Ru by atomic layer deposition (ALD).* Electrochimica Acta, 2008. **53**(21): p. 6157-6164.

35. Jayaraju, N., et al., *Electrochemical Atomic Layer Deposition (E-ALD) of Pt Nanofilms Using SLRR Cycles.* Journal of the Electrochemical Society, 2012. **159**(10): p. D616-D622.

36. Gebregziabiher, D.K., et al., *Electrochemical atomic layer deposition of copper nanofilms on ruthenium.* Journal of Crystal Growth, 2010. **312**(8): p. 1271-1276.

37. Thambidurai, C., et al., *E-ALD of Cu Nanofilms on Ru/Ta Wafers Using Surface Limited Redox Replacement.* Journal of the Electrochemical Society, 2010. **157**(8): p. D466-D471.

38. Thambidurai, C., et al., *Copper Nanofilm Formation by Electrochemical ALD.* Journal of the Electrochemical Society, 2009. **156**(8): p. D261-D268.

39. Viyannalage, L.T., R. Vasilic, and N. Dimitrov, *Epitaxial growth of Cu on Au(111) and Ag(111) by surface limited redox replacement - An electrochemical and STM study.* Journal of Physical Chemistry C, 2007. **111**(10): p. 4036-4041.

40. Vasilic, R., L.T. Viyannalage, and N. Dimitrov, *Epitaxial growth of Ag on Au(111) by galvanic displacement of Pb and Tl monolayers.* Journal of the Electrochemical Society, 2006. **153**(9): p. C648-C655.

41. Fayette, M., et al., *From Au to Pt via Surface Limited Redox Replacement of Pb UPD in One-Cell Configuration.* Langmuir, 2011. **27**(9): p. 5650-5658.

42. Jayaraju, N., *Electrochemical atomic layer deposition (E-ALD) of Pt and PtRu nanofilms*, in *Chemistry*. 2010, University of Georgia: Athens.

43. Greeley, J. and M. Mavrikakis, *Surface and subsurface hydrogen: Adsorption properties on transition metals and near-surface alloys.* Journal of Physical Chemistry B, 2005. **109**(8): p. 3460-3471.

44. Lukaszewski, M., K. Hubkowska, and A. Czerwinski, *Electrochemical absorption and oxidation of hydrogen on palladium alloys with platinum, gold and rhodium.* Physical Chemistry Chemical Physics, 2010. **12**(43): p. 14567-14572.

45. Zurowski, A., M. Lukaszewski, and A. Czerwinski, *Electrosorption of hydrogen into palladium-rhodium alloys.* Electrochimica Acta, 2006. **51**(15): p. 3112-3117.

46. Llopis, J.F. and I.M. Tordesillas, *Rhodium*, in *Encyclopedia of electrochemistry of the elements*, A.J. Bard, Editor. 1973, New York: M. Dekker. p. 299-328.

47. Oliveira, R.T.S., et al., *Rh electrodeposition on Pt in acidic medium: a study using cyclic voltammetry and an electrochemical quartz crystal microbalance.* Journal of Electroanalytical Chemistry, 2004. **569**(2): p. 233-240.

48. Gomez, R. and J.M. Feliu, *Rhodium adlayers on Pt(111) monocrystalline surfaces. Electrochemical behavior and electrocatalysis.* Electrochimica Acta, 1998. **44**(6-7): p. 1191-1205.

49. de Dios, F.J.G., R. Gomez, and J.M. Feliu, *Preparation and electrochemical behavior of ordered Rh adlayers on Pt(100) electrodes.* Langmuir, 2005. **21**(16): p. 7439-7448.

50. Langerock, S. and L. Heerman, *Study of the electrodeposition of rhodium on polycrystalline gold electrodes by quartz microbalance and voltammetric techniques.* Journal of the Electrochemical Society, 2004. **151**(3): p. C155-C160.

51. Kibler, L.A., M. Kleinert, and D.M. Kolb, *The initial stages of rhodium deposition on Au(111).* Journal of Electroanalytical Chemistry, 1999. **467**(1-2): p. 249-257.

52. Arbib, M., et al., *Electrochemical nucleation and growth of rhodium on gold substrates.* Journal of Electroanalytical Chemistry, 2001. **510**(1-2): p. 67-77.

53. Wade, T.L., T.A. Sorenson, and J.L. Stickney, *Interfacial Electrochemistry*, ed. A. Wieckowski. 1999, New York: Marcel Dekker.

54. Stickney, J.L., *Electrochemical atomic layer epitaxy*, in *Electroanalytical Chemistry, Vol 21*, A.J.B.a.I. Rubinstein, Editor. 1999, Marcel Dekker, Inc.: New York. p. 75-209.

55. Kibler, L.A., A.M. El-Aziz, and D.M. Kolb, *Electrochemical behaviour of pseudomorphic overlayers: Pd on Au(111).* Journal of Molecular Catalysis a-Chemical, 2003. **199**(1-2): p. 57-63.

56. Sung, Y.E., S. Thomas, and A. Wieckowski, *Characterization of the Rh(111) Electrode by CEELS, AES, LEED, and VOLTAMMETRY - Adsorption of (Bi)Sulfate, Perchlorate and Carbon-monoxide* Journal of Physical Chemistry, 1995. **99**(36): p. 13513-13521.

57. Hoshi, N., K. Kagaya, and Y. Hori, *Voltammograms of the single-crystal electrodes of palladium in aqueous sulfuric acid electrolyte: Pd(S)- n(111) x*

(111) and Pd(S)- n(100) x (111). Journal of Electroanalytical Chemistry, 2000. **485**(1): p. 55-60.

58. Conway, B.E. and G. Jerkiewicz, *Thermodynamic and Electrode Kinetic Factors in Cathodic Hydrogen Sorption Into Metals and Its Relationship to Hydrogen Adsorption and Poisoning.* Journal of Electroanalytical Chemistry, 1993. **357**(1-2): p. 47-66.

59. Fukai, Y., *The metal-hydrogen system basic bulk properties*. Springer series in materials science Vol. 121. 1993, Berlin: Springer-Verlag

60. Taniguchi, M., E.K. Kuzembaev, and K. Tanaka, *A Mimic Model of Pt-Rh Catalyst Prepared by Electrochemical Deposition of Rh on the Pt(100) Surface* Surface Science, 1993. **290**(3): p. L711-L717.

61. Baranows, B., S. Majchrza, and T.B. Flanagan, *High-pressure Investigation of Rhodium-Palladium-Hydrogen System* Journal of Physical Chemistry, 1973. **77**(1): p. 35-39.

62. Sakamoto, Y., N. Ishimaru, and M. Hasebe, *Electrochemical Properties of Some Palladium Alloy Hydride Electrodes* Zeitschrift Fur Physikalische Chemie-International Journal of Research in Physical Chemistry & Chemical Physics, 1994. **183**: p. 319-324.

63. Kobayashi, H., et al., *Nanosize-Induced Hydrogen Storage and Capacity Control in a Non-Hydride-Forming Element: Rhodium.* Journal of the American Chemical Society, 2011. **133**(29): p. 11034-11037.

64. Baldauf, M. and D.M. Kolb, *A Hydrogen Adsorpiton and Absorption Study with Ultrathin Pd Overlayers on Au(111) and Au(100)* Electrochimica Acta, 1993. **38**(15): p. 2145-2153.

65. Birry, L. and A. Lasia, *Effect of crystal violet on the kinetics of H sorption into Pd.* Electrochimica Acta, 2006. **51**(16): p. 3356-3364.

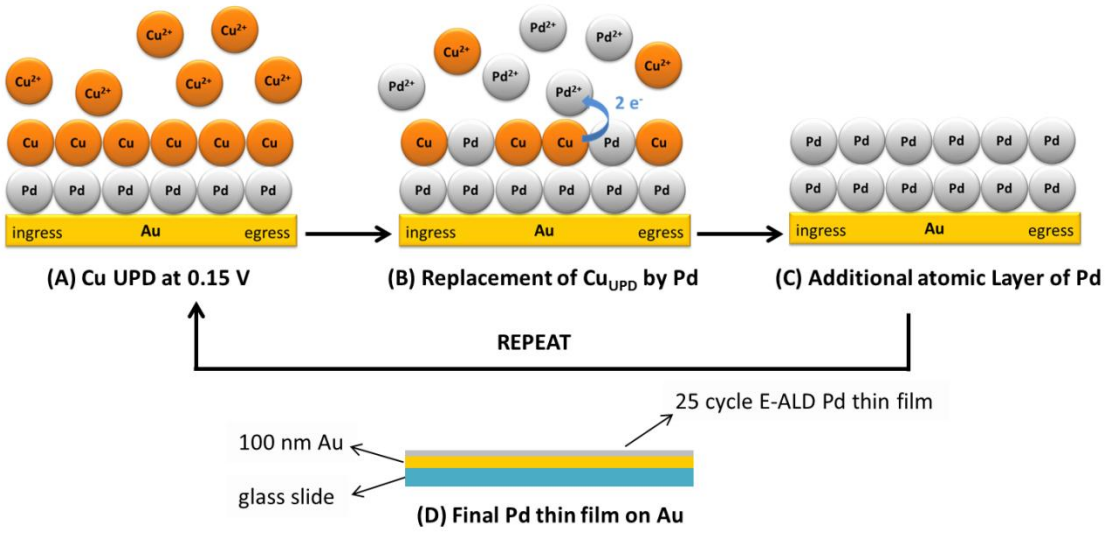

Figure 5.1 Schematic of an E-ALD cycle using SLRR to form a Pd nanofilm on polycrystalline Au. Note that Cu_{UPD} deposited directly on Au is replaced by Pd ions to form the 1st Pd atomic layer.

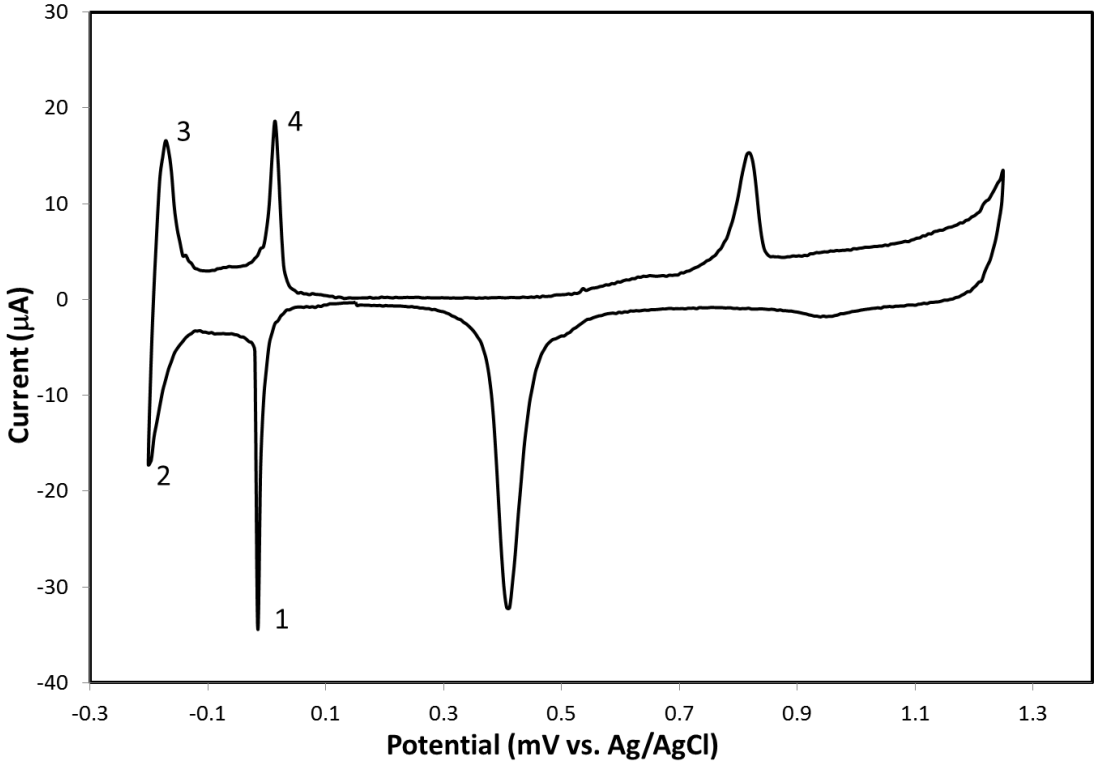

Figure 5.2 CVs of a 15 cycle E-ALD Pd nanofilm on Au(111) in 0.1 M H_2SO_4 at 10 mV/s.

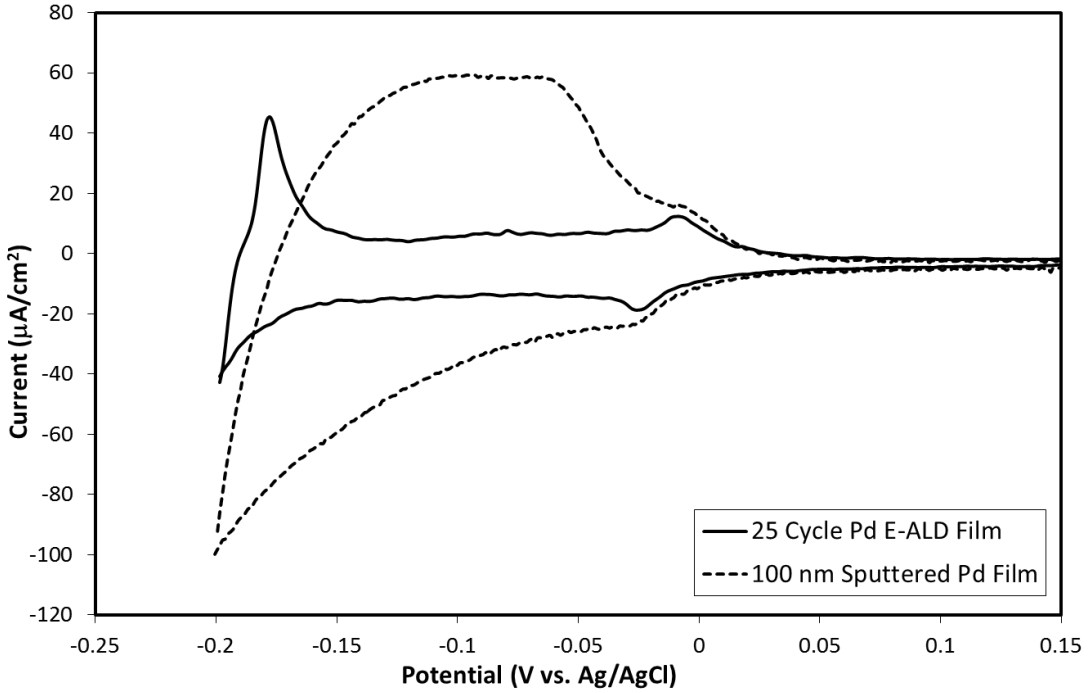

Figure 5.3 CVs of a 25 cycle E-ALD Pd nanofilm on polycrystalline Au (solid line) and a 100 nm sputtered Pd film on Si (dashed line) in 0.1 M H_2SO_4 at 10 mV/s.

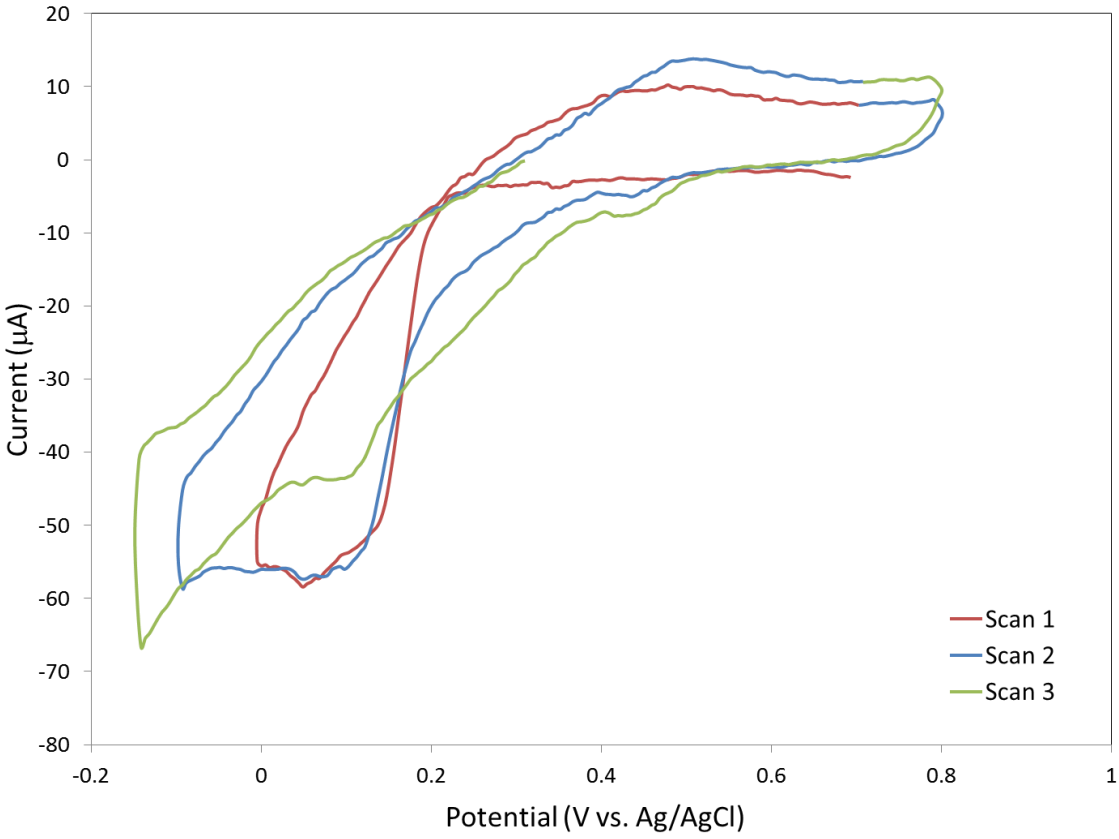

Figure 5.4 CVs polycrystalline Au in 0.1 mM $RhCl_3$ in 10 mM HCl and 0.1 M H_2SO_4 at 10 mV/s.

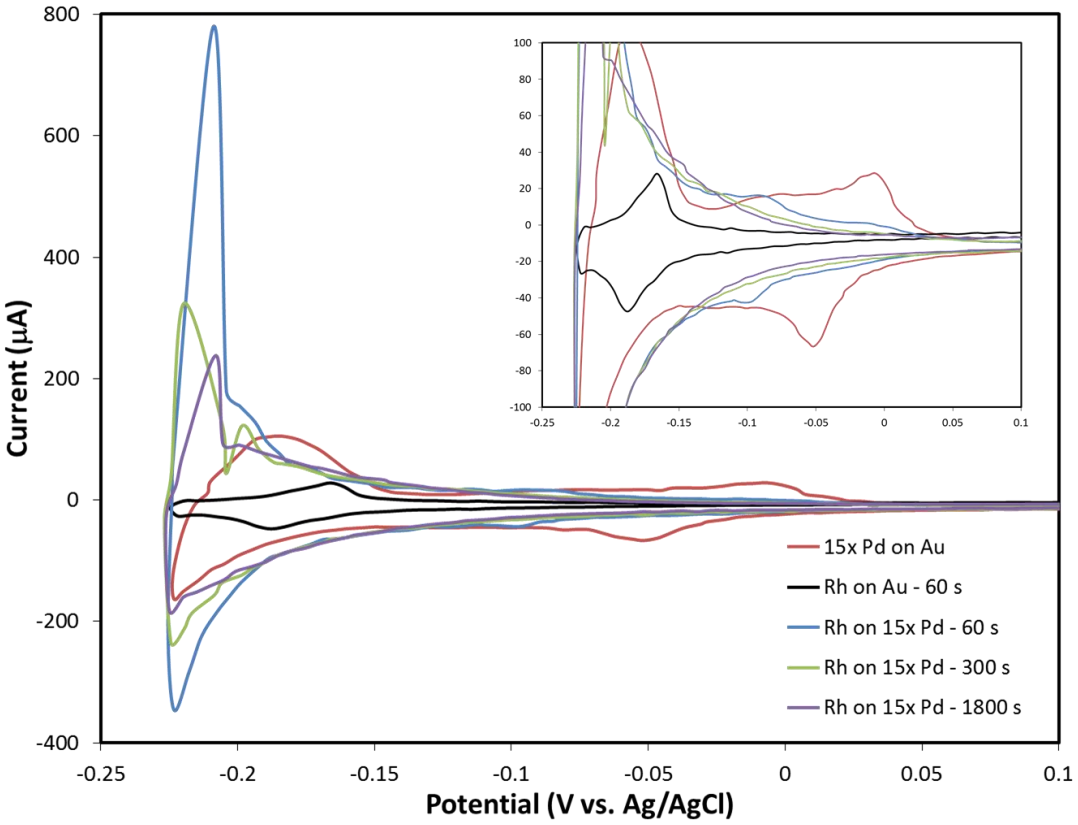

Figure 5.5 CVs of a 15 cycle E-ALD Pd nanofilm on polycrystalline Au before and after Rh modification by constant potential deposition at 0 V for 60, 300 and 1800 s. A CV of Rh deposited on polycrystalline Au at 0 V for 60 s is included for comparison. The electrolyte was 0.1 M H_2SO_4 and the scan rate was 10 mV/s.

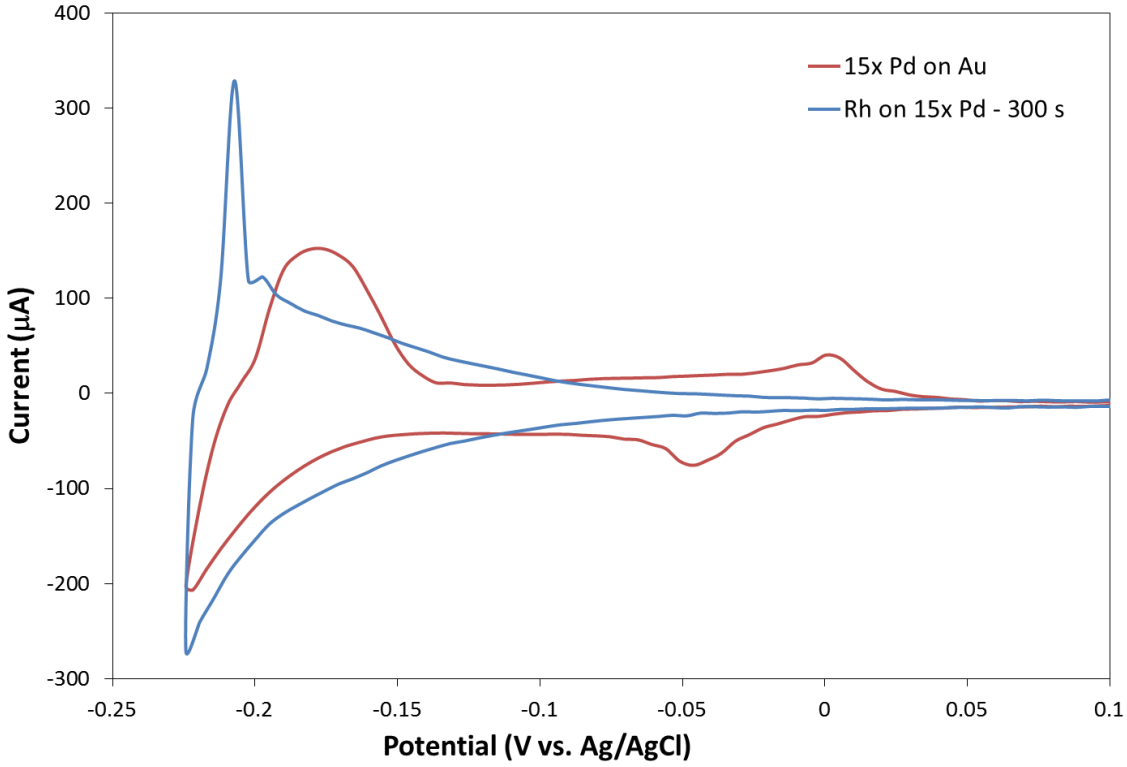

Figure 5.6 CVs of a 15 cycle E-ALD Pd nanofilm on polycrystalline Au before and after Rh modification by constant potential deposition at −0.125 V for 300 s. The electrolyte was 0.1 M H_2SO_4 and the scan rate was 10 mV/s.

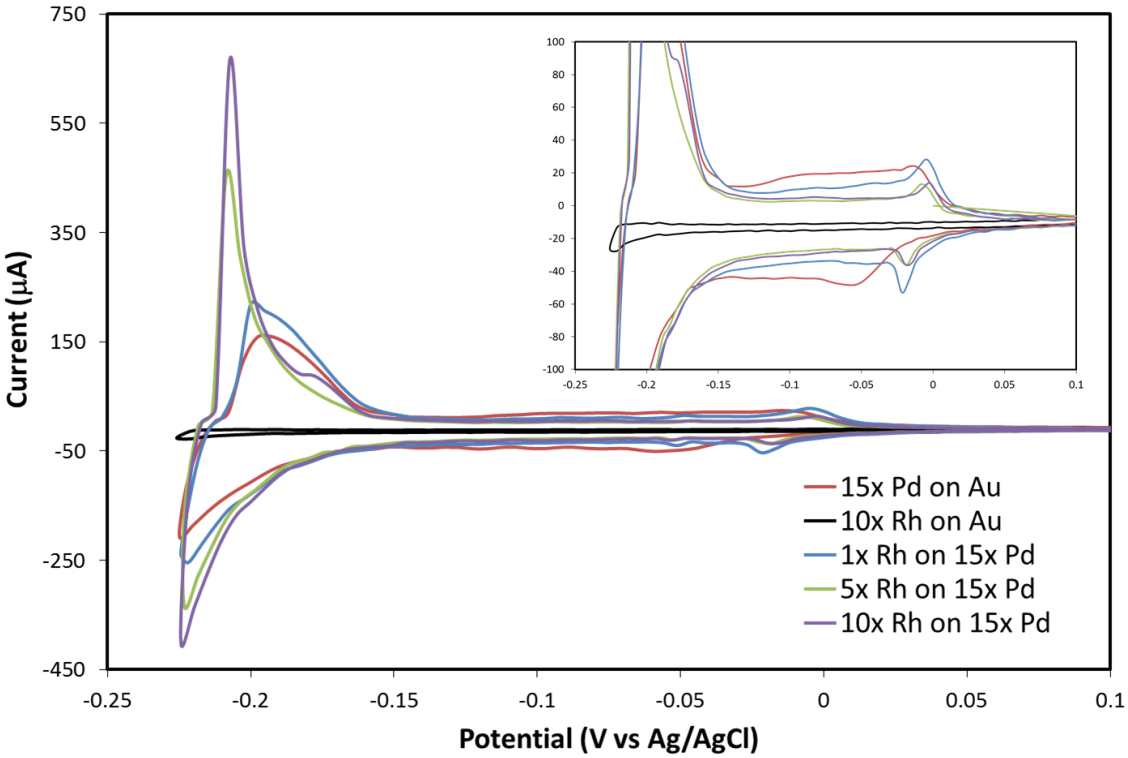

Figure 5.7 CVs of a 15 cycle E-ALD Pd nanofilm on polycrystalline Au before and after Rh modification by 1, 5 and 10 E-ALD cycles of Rh. A CV of 10 E-ALD cycles of Rh deposited on polycrystalline Au is included for comparison. The electrolyte was 0.1 M H_2SO_4 and the scan rate was 10 mV/s.

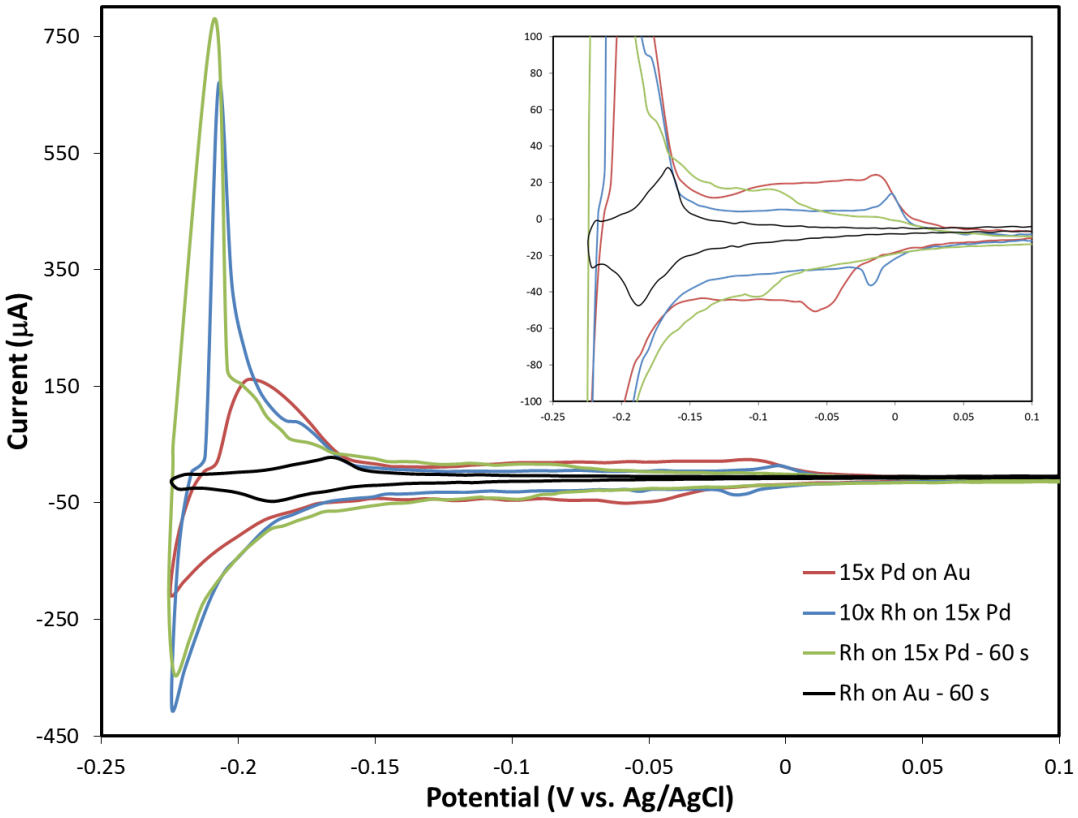

Figure 5.8 CVs of a 15 cycle E-ALD Pd nanofilm on polycrystalline Au before and after Rh modification. 10 E-ALD cycles of Rh on Pd is compared with Rh deposited at 0 V for 60 s. A CV Rh deposited on polycrystalline Au at 0 V for 60 s is included for comparison. The electrolyte was 0.1 M H_2SO_4 and the scan rate was 10 mV/s.

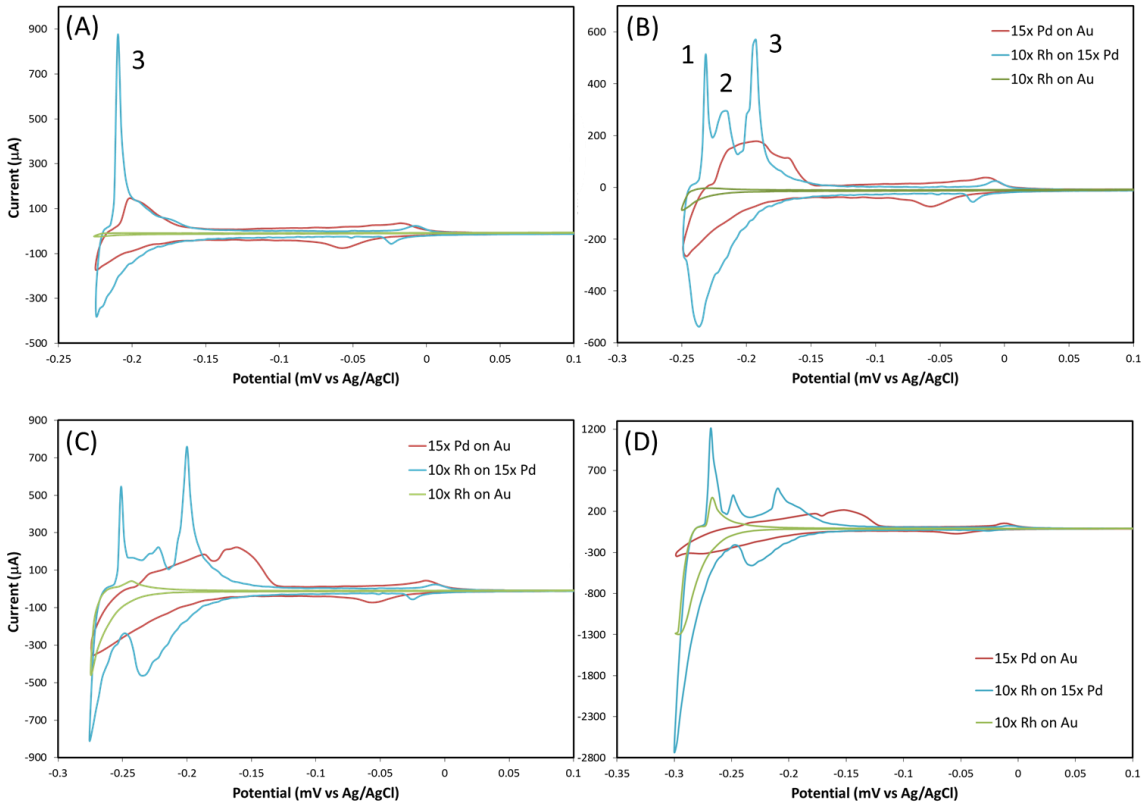

Figure 5.9 CVs of a 15 cycle E-ALD Pd nanofilm on polycrystalline Au before and after Rh modification by 10 E-ALD cycles of Rh with different negative potential limits. A CV of 10 E-ALD cycles of Rh deposited on polycrystalline Au is included for comparison. The electrolyte was 0.1 M H_2SO_4 and the scan rate was 10 mV/s.

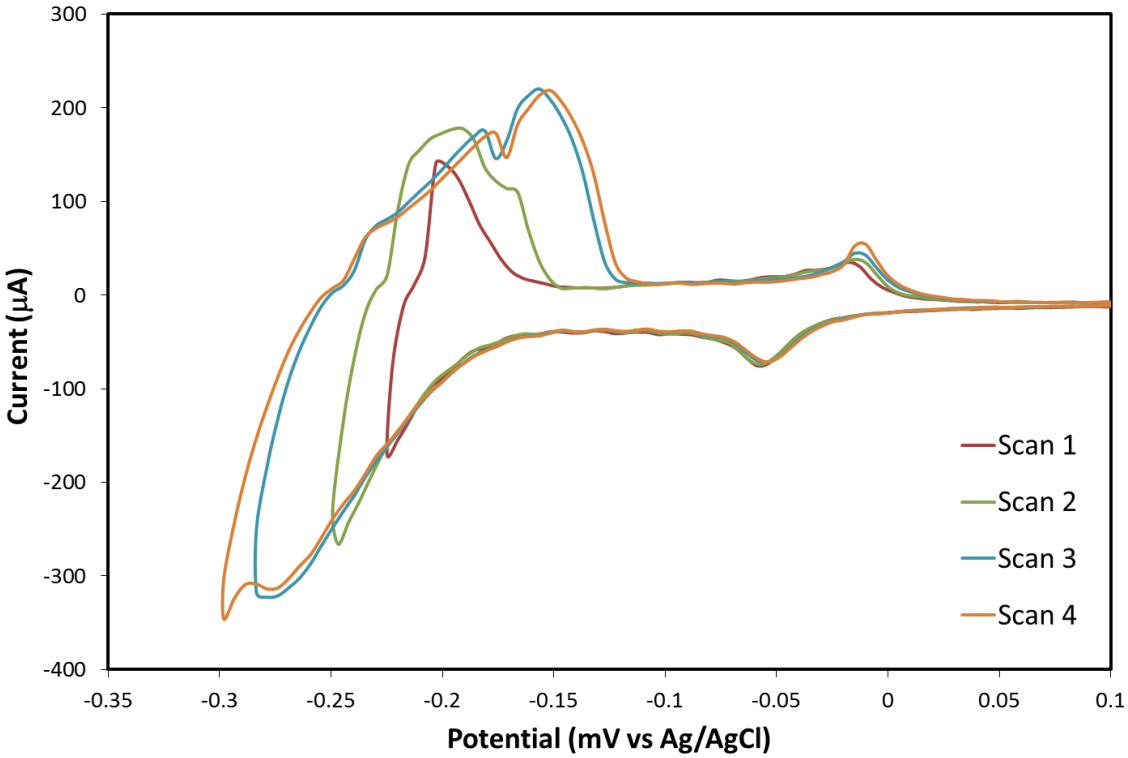

Figure 5.10 CVs of a 15 cycle E-ALD Pd nanofilm on polycrystalline Au with different negative potential limits. The electrolyte was 0.1 M H_2SO_4 and the scan rate was 10 mV/s.

CHAPTER 6

CONCLUSION AND FUTURE STUDIES

The formation and characterization of Pd nanofilms on polycrystalline Au and Au(111) by E-ALD using SLRR was the focus of this dissertation. Chapter 2 discussed the selection of a sacrificial metal and EPMA results showed that Pb was incorporated into the Pd deposits, though Cu was not, establishing that Cu_{UPD} was the suitable choice. Initial results showed that excess Pd was deposited near the flow cell ingress, and film thickness decreased from ingress to egress. This suggested that the SLRR mechanism involved indirect transfer of electrons from a sacrificial metal atom to the depositing metal ion through the electrode as opposed to a direct transfer of electrons from atom to ion. Various concentrations of EDTA, a strong Pd complexing agent, were added to the Pd ion solution to lower the Pd^{2+} activity and slow down the rate of the replacement relative to the rate of introduction of Pd^{2+} solution into the cell. The theory was that differential deposition could be avoided if the Pd^{2+} solution was homogenously distributed throughout the cell before the replacement had proceeded substantially. The resulting films were more uniform, but thinner than expected for an E-ALD film formed using SLRR. Therefore, an alternative complexing agent, Cl^-, was investigated and also found to improve uniformity, but without diminishing film thickness.

The cycle was then optimized, as described in Chapter 3, for Pd ion solutions containing excess Cl^- as a complexing agent. The ideal ratio, found to be $[Pd^{2+}] / [Cl^-] = 8$, was used to form films for further characterization. The Cu coverage per cycle was

consistent from cycle to cycle and the Pd coverage as a function of the number of cycles performed was linear, suggesting a lack of surface roughening and layer-by-layer film growth. The coulometry for Cu_{UPD} was compared with anodic stripping of the resulting Pd films and indicated good exchange efficiency for the replacement at 95 ± 6%. XRD showed the as-deposited films to be polycrystalline with a primary Pd(220) orientation. The Au substrate was also primarily (220), suggesting an epitaxial relationship. Cyclic voltammetry (CV) of a 25 cycle film demonstrated the expected behavior of a thin film Pd electrode and there was no indication of exposed Au.

In Chapter 4 the optimized Pd E-ALD cycle was used to form deposits on Au(111), making electrochemical scanning tunneling microscopy (EC-STM) analysis possible. Wide-area images were taken of the first 3 cycles of deposition and revealed constant morphology from one cycle to the next, while high resolution images showed monoatomic steps, suggestive of layer-by-layer growth. The addition of iodine, a strong adsorbate, was also studied and found to increase Pd atom surface mobility, resulting in larger terraces with improved order, while retaining monoatomic steps. The reactions of Pd with hydrogen were examined for 1-30 cycle Pd nanofilms using CV in 0.1 M H_2SO_4. The underlying Au had a strong influence on the hydrogen adsorption features for deposits formed using less than 5 cycles. The observed features in the absorption region for 1 and 2 cycle films were assigned to the H_2 evolution reaction (HER) and subsequent oxidation of H_2, while absorption/desorption occurred for thicker films, increasing with film thickness. An electrochemical (EC) annealing program, that improved surface ordering, was established. The improved order was evidenced by the increase in

sharpness and reversibility of the hydrogen adsorption/desorption peaks, which closely resembled those of bulk Pd(111).

The effect of Rh overlayers on the rates of hydrogen absorption and desorption were the focus of Chapter 5. E-ALD Pd nanofilms on polycrystalline Au were used as platforms to study how different coverages of Rh influenced the Pd absorption/desorption kinetics. Rh was deposited by constant potential deposition at 0 V for 60, 300 and 1800 s. CV of these Rh overlayers were compared with those formed by 1, 5 and 10 E-ALD cycles of Rh. CV results indicated that all coverages caused enhancement of both hydrogen absorption and desorption of the underlying Pd nanofilm. The Rh overlayer formed by deposition at 0 V for 60 s and that formed by 10 E-ALD cycles were found to provide the greatest improvement, with the latter being slightly superior. Two theories were also suggested and discussed in an attempt to explain the notable effect Rh had on the kinetics. The first theory assumes that the absorption mechanism involves the surface hydride as an intermediate and the presence of Rh destabilizes the surface hydride, which increases the rate of hydrogen absorption.[1] The second theory considers two absorption mechanisms, each with different rates.[2, 3] When Rh is deposited and reduces the surface hydride coverage, the majority of hydrogen absorption is able to proceed by the faster, direct mechanism, while slower, indirect absorption dominates when the Pd surface hydride coverage is greater (i.e. for bare Pd or lower Rh coverages).

Future work will focus on a better understanding of Rh deposition and quantification of the Rh coverage. The amount of exposed Pd has not been determined and is necessary to better understand the mechanism leading to the observed kinetic enhancement. XPS analysis is planned to aid in determining if alloy formation is

occurring and possibly as a method to calibrate the Rh coverage. EC-STM experiments may not be possible because of the irreversibility of Rh deposition. However, it could reveal information about the Rh growth mechanism during both E-ALD and constant potential deposition if it is experimentally plausible. The optimum Rh coverage was not established; therefore, Rh overlayers formed using more than 10 cycles need to be investigated, as do shorter Rh deposition times at 0 V. Attempts to deposit enough Rh to completely terminate hydrogen absorption into the underlying Pd were unsuccessful. Establishing this critical thickness may aid in understanding the absorption mechanism in the presence of Rh. Finally, there is also interest in studying other metal overlayers on Pd to determine their effects on hydrogen absorption/desorption kinetics. Pt, Cu, Ru and Re are all metals of interest.

References

1. Conway, B.E. and G. Jerkiewicz, *Thermodynamic and Electrode Kinetic Factors in Cathodic Hydrogen Sorption Into Metals and Its Relationship to Hydrogen Adsorption and Poisoning.* Journal of Electroanalytical Chemistry, 1993. **357**(1-2): p. 47-66.
2. Duncan, H. and A. Lasia, *Mechanism of hydrogen adsorption/ab sorption at thin Pd layers on Au(111).* Electrochimica Acta, 2007. **52**(21): p. 6195-6205.
3. Lasia, A., *On the mechanism of the hydrogen absorption reaction.* Journal of Electroanalytical Chemistry, 2006. **593**(1-2): p. 159-166.